EVALUATION OF STRESS INTENSITY FACTOR FOR AN INFINITE HOLLOW CYLINDER CONTAINING A CRACK AND TWO RIGID INCLUSIONS BY FINITE ELEMENT ANALYSIS

by

Erkan ÖTERKUŞ

A Dissertation Submitted to the

Graduate School in Partial Fulfillment of the

Requirements for the Degree of

MASTER OF SCIENCE

Department: Mechanical Engineering

Major: Mechanical Engineering

Izmir Institute of Technology

Izmir, Turkey

December, 2002

We approve the thesis of **Erkan ÖTERKUŞ**

Date of Signature

25.12.2002

....
....

Assist. Prof. Dr. H. Seçil Altundağ ARTEM
Supervisor
Department of Mechanical Engineering

25.12.2002

....
....

Assoc. Prof. Dr. Barış ÖZERDEM
Department of Mechanical Engineering

25.12.2002

....
....

Assoc. Prof. Dr. Mustafa GÜDEN
Department of Mechanical Engineering

25.12.2002

....
....

Assist. Prof. Dr. Engin AKTAŞ
Department of Civil Engineering

25.12.2002

....
....

Assist. Prof. Dr. M. Evren TOYGAR
Department of Mechanical Engineering

25.12.2002

....
....

Assoc. Prof. Dr. Barış ÖZERDEM
Head of Department of Mechanical Engineering

ACKNOWLEDGEMENTS

ABSTRACT

A numerical implementation based on the finite element method for the infinite cracked hollow cylinder under the action of axisymmetric tensile loads at infinity is considered in this study. The infinite cylinder contains a ring-shaped crack of width (b – a) at the symmetry plane z = 0, and two rigid inclusions of width (d – c) located symmetrically on both sides of the crack. Material of the cylinder is assumed to be linearly elastic and isotropic.

The proposed model uses efficiently the capabilities of a commercially available finite element analysis program, ANSYS, to determine the stress intensity factors at the crack tips. In the finite element analysis, six-noded triangular elements were used to model the square-root stress singularity at the crack tips. In order to get the stress intensity factors, the displacement extrapolation method was used.

The numerical results for various crack and inclusion configurations are obtained and compared with the analytical results in order to verify Artem's study. When the inclusions are far away from the crack, the interaction among them vanishes. In this case, the numerical and analytical results are in good agreement. On the other hand, when the inclusions get closer to the crack, a discrepancy has been occurred within the acceptable limits.

ÖZ

Bu çalışmada sonsuzda eksenel çekmeye maruz çatlamış bir tüp probleminin sonlu elemanlar metodu kullanılarak sayısal çözümlemesi yapılmıştır. Tüpte z = 0 düzleminde eni (b – a) olan halka biçiminde bir çatlak ve bu düzlemin iki tarafında simetrik olarak bulunan ve enleri (d – c) olan halka biçiminde iki rijit enklüzyon bulunmaktadır. Tüp malzemesinin lineer elastik ve izotrop olduğu varsayılmaktadır.

Çatlak uçlarındaki gerilme şiddeti katsayılarını sayısal olarak hesaplamak için oluşturulan model ANSYS sonlu elemanlar analiz programını kullanmıştır. Sonlu elemanlar analizinde çatlak uçlarındaki tekilliğin modellenmesinde altı düğüm noktalı üçgen elemanlardan faydalanıldı. Gerilme şiddeti katsayılarının hesaplanmasında yer değiştirme ekstrapolasyon metodu kullanıldı.

Çeşitli çatlak ve enklüzyon konfigürasyonları için sayısal sonuçlar elde edildi. Bu sonuçlar Artem'in analitik sonuçlarının doğruluğunun araştırılmasında kullanıldı. Enklüzyonlar ve çatlak birbirlerinden yeterince uzak olduğunda aralarındaki etkileşim kaybolur. Bu durumda sayısal ve analitik sonuçlar tam bir uyum gösterir. Ancak, enklüzyonlar çatlağa yaklaştığında kabul edilebilir sınırlar dahilinde farklılıklar oluşmuştur.

TABLE OF CONTENTS

LIST OF FIGURES

LIST OF TABLES

CHAPTER 1

INTRODUCTION

The construction of modern structures with improved mechanical properties demands for the development of preventive design methodologies to account for their operating environment, especially under extreme loading conditions or in the presence of defects. Among them, the most severe are crack-like defects which cause changes in structural characteristics thus producing unpredictable, even catastrophic, structural response [1]. The name of the field that deals with these subjects is fracture mechanics and the evaluation of stress intensity factors (SIFs) is an important part of fracture mechanics. Different methods exist in evaluation process including experimental, theoretical and numerical methods.

In certain problems, such experimental techniques as photoelasticity, moire interferometry and the method of caustics may be very effective in estimating the stress intensity factors.

Theoretical methods are essential for solving crack problems for two reasons. First, they provide the correct form of singularities and asymptotic results that may be needed to analyze and interpret the experimental results and to use for improving the accuracy of purely numerical solutions. Secondly, they provide accurate solutions for relatively simple part/crack geometries and for certain idealized material behavior that could be used as benchmarks for numerical and approximate procedures.

However, in practical applications, the geometry of the medium is seldom simple and realistic material models seldom lead to analytically tractable formulations. It is therefore necessary to develop purely numerical methods that can accommodate complicated part/crack geometries and material models. The finite element method (FEM) appears to be ideal for this purpose and is widely used in fracture mechanics.

From the engineering mechanics approach, many studies on the evaluation of the stress intensity factors by finite element method can be found in the literature. Tarafder, *et.al* [2] evaluated SIFs by FEM for longitudinally cracked cylindirical components experiencing arbitrary stress variation across the wall thickness. Shih and Chen [3] calculated the stress intensity factors of an elliptical crack front embedded with a round bar by using ANSYS, a commercial finite element analysis program. Three dimensional

finite element analysis was employed by Shankar and Wu [4] to determine stress intensity factors for cracks in the weld line. Stress intensity factors of assumed notch cracks and through thickness cracks in tensile shear and modified coach peel specimens were determined by the finite element method in the study of Pan and Sheppard [5]. Finite element analyses were carried out by Banks-Sills and Eliasi [6] in order to determine the stress intensity factor as a function of crack length for the case in which the cannon barrel contains two symmetrically located cracks.

However, the stress intensity factor evaluation by using the finite element method in the analyses involving the combination of different type of defects in the form of cracks, holes, or inclusions are limited. In a study of Sergeev, et al. [7] the FEM is used to determine the stress intensity factors in a composite longeron web with an arbitrarily oriented straight crack near a hole. Xiao, et al. [8] calculated the stress intensity factors for a ring-shaped crack surrounded by spherical inclusions by FEM. In a study of Xiao and Bai [9] about a circular piezoelectric inhomogeneity interacting with a nearby crack, the SIFs are obtained by using ANSYS. In another study of Xiao and Bai [10], numerical investigation by FEM on the interaction between a coated piezoelectric fiber-shaped sensor and a nearby crack was carried out. Xiao and Chen [11] calculated the stress intensity factor for a Griffith crack interacting with a coated inclusion by using FEM.

In this study, the stress intensity factors are evaluated for the problem of an infinite hollow cylinder containing a crack and two rigid inclusions by finite element analysis using ANSYS. This study is complementary to that of Artem's work [12]. The results of this study have been compared with those of Artem's to verify her accuracy, because the mathematical difficulties in the analytical study which may arise in a hollow cylinder containing flaws like cracks and rigid inclusions cause to make mistakes during the derivation procedures. Firstly, in order to verify the finite element model, the results of Erdol and Erdogan [13] for a hollow cylinder with no inclusion were compared with the results of the finite element analysis. In the finite element modelling, six-noded quarter point triangular elements were used to model the square-root stress singularity at the crack tips. In order to get the stress intensity factors, the displacement extrapolation method was used.

CHAPTER 2

STRESS INTENSITY FACTORS

Fracture is a problem that society has faced for as long as there have been man-made structures. The problem may actually be worse today than in previous centuries, because more can go wrong in our complex technological society. Fortunately, advances in the field of fracture mechanics have helped to offset some of the potential dangers posed by increasing technological complexity [14].

In linear fracture mechanics analysis, determination of the stress intensity factor (SIF) is always a major consideration and has to be evaluated.

2.1 Introduction

In a general sense the stress intensity factor is the counterpart of stress concentration factor in notched solids [15]. In the tension test of an isotropic homogeneous bar of constant cross-sectional area A, the stress σ is assumed to be uniformly distributed over the cross section, provided the section is sufficiently far removed from the ends of the bar, where the load may be applied in a nonuniform manner (Figure 2.1).
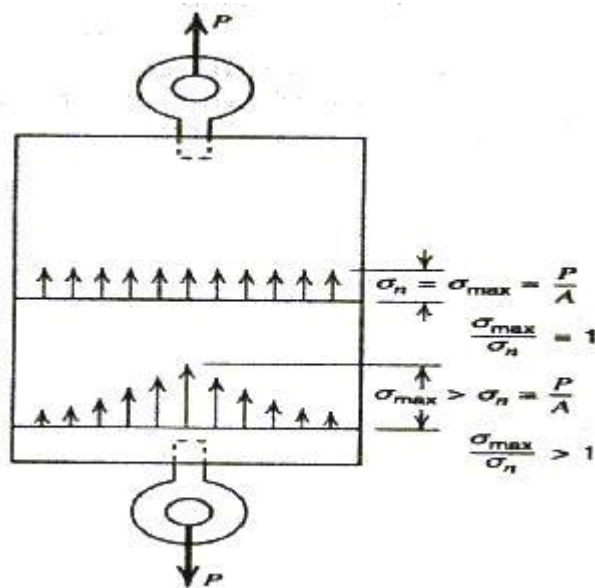
Figure 2.1. Stress distribution in an isotropic homogenous bar under tension [16].

At the end sections, ordinarily the stress distribution is not uniform. Nonuniformity of stress may also occur because of geometric changes (holes or notches) in the cross section of a specimen (Figures 2.2 and 2.3).
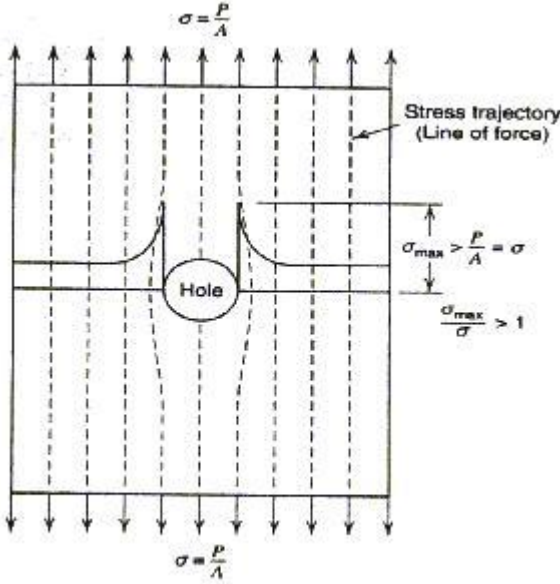
Figure 2.2. Stress distribution of a specimen when a hole occurs [16].
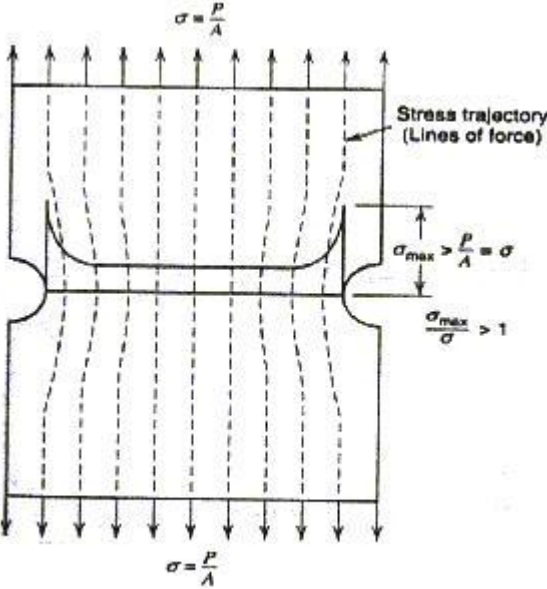
Figure 2.3. Stress distribution of a specimen when notches occur [16].

4

This nonuniformity in stress distribution may result in a maximum stress σ_{max} at a section that is considerably larger than the average stress ($\sigma_n = P/A$, where P is the total tension load.).

The ratio K defined as

$$K = \frac{\sigma_{max}}{\sigma_n} \qquad (2.1)$$

is called the "stress concentration factor" for the section (point); the more abrupt the cross-sectional area transition in the tension specimen, the larger the stress concentration factor (Figure 2.4).
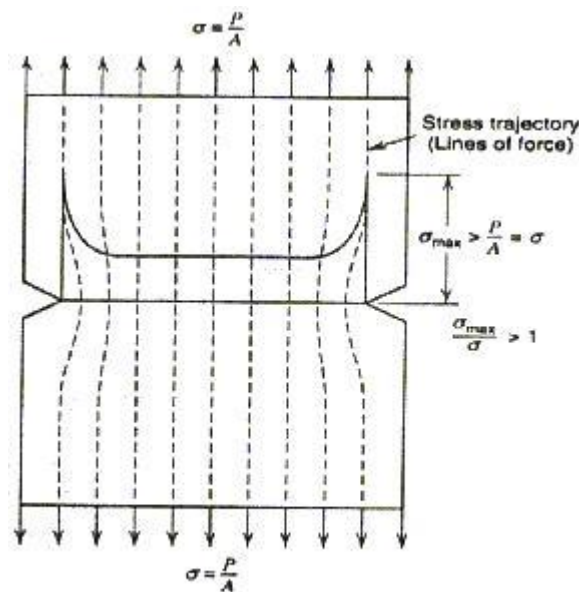
Figure 2.4. Stress concentrations where the cross-sectional area decreases [16].

A pictorial representation of stress trajectories (Figures 2.1, 2.2, 2.3 and 2.4) is often employed as an approximate model in the physics of solids to explain the strain (stress) in the neighborhood of a geometrical discontinuity (crack, dislocation, etc.) in a solid. This representation is based on the analogy between magnetic lines of forces and stress trajectories. For example, analogous to magnetic lines of forces, the stress trajectories, whose paths must lie in the material, cluster together in passing around a geometric hole or discontinuity. In doing so, the average spacing between the lines of force is reduced and, therefore, there results a stress concentration (stress gradient) or an increase in local stress (more lines of force squeezed into the same area). To expand this idea further, consider a geometrical

5

discontinuity (crack) and sketch the hypothetical local arrangement of atoms around the tip of the crack (Figure 2.5).
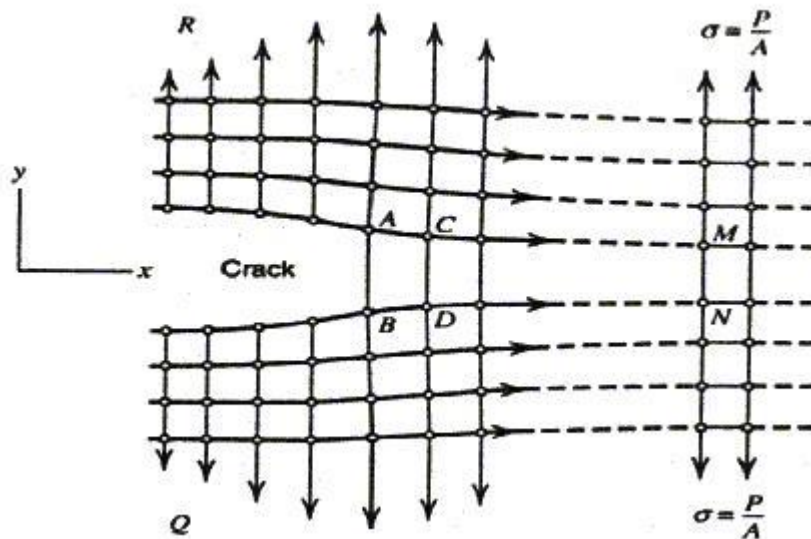
Figure 2.5. Atomic model of crack in solid [16].

The lines of force may be considered to be transmitted from one row of atoms to another. Therefore, the transmission of force around the tip of the crack (say, a small crack in an infinite plate) entails heavy loading and straining of the bonds (AB, CD, AC, etc.). Smaller loads and strains are carried by bonds away from the crack (the strain of bond MN is much less than that of AB). For bonds sufficiently far from AB, for example, bond MN, the associated stress is essentially $\sigma = P/A$. The conceptual model of Figure 2.5 leads to the conclusion that for bond AB to be extended, bonds AC and BD also must be extended. Hence, the uniaxial loading of the plate causes the region around the crack tip to have not only a high tensile strain in the y direction but also a high tensile strain in the x direction. The concept of lines of force also suggests a redistribution of strain energy from regions above or below the crack (regions R and Q in Figure 2.5) to the highly strained region at the crack tip (see also Figures 2.1, 2.2, 2.3 and 2.4). Also because of distortion of rectangular elements in Figure 2.5, high shear stresses exist in the neighborhood of a stress concentration.

As an example, consider the case of an infinite plate or sheet with a small circular hole of radius a under uniaxial tension σ (Figure 2.6). With respect to polar coordinates (r, θ), the plane stress components at any point P are given by the formulas

6

$$\sigma_{rr} = \frac{\sigma}{2}\left(1 - \frac{a^2}{r^2}\right) + \frac{\sigma}{2}\left(1 - \frac{a^2}{r^2}\right)\left(1 - \frac{3a^2}{r^2}\right)\cos2\theta$$

$$\sigma_{\theta\theta} = \frac{\sigma}{2}\left(1 + \frac{a^2}{r^2}\right) - \frac{\sigma}{2}\left(1 + \frac{3a^4}{r^4}\right)\cos2\theta$$

$$\sigma_{r\theta} = -\frac{\sigma}{2}\left(1 - \frac{a^2}{r^2}\right)\left(1 + \frac{3a^2}{r^2}\right)\sin2\theta \qquad\qquad (2.2a\text{-}c)$$
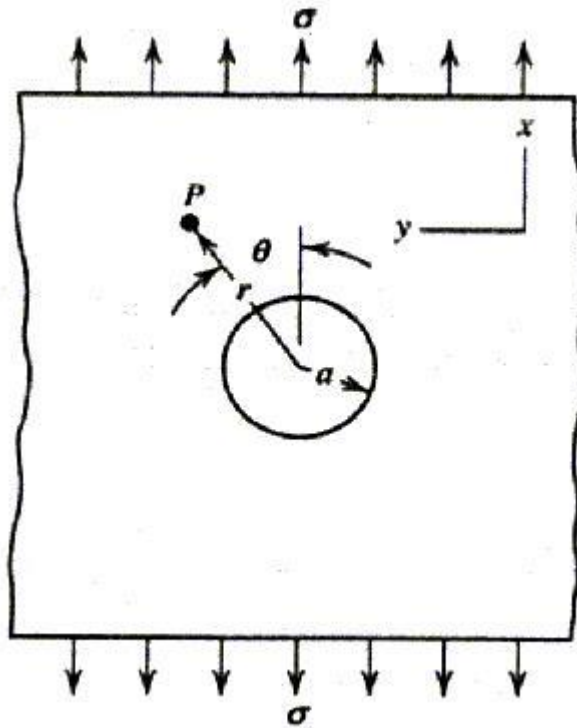
Figure 2.6. Infinite plate with a small circular hole [16].

It is noted that the stress state given by Equations 2.2 satisfies the boundary conditions

at $r = a$, $\sigma_{rr} = \sigma_{r\theta} = 0$ for all θ

and

$r = \infty$

$\sigma_{xx} = \sigma_{rr} = \sigma$, $\sigma_{xy} = \sigma_{r\theta} = 0$ *for* $\theta = 0$, π *and* $\sigma_{yy} = \sigma_{rr} = 0$, $\sigma_{xy} = \sigma_{r\theta} = 0$ *for* $\theta = \pi/2$, $3\pi/2$.

For $r = a$, $\sigma_{\theta\theta} = \sigma(1 - 2\cos2\theta)$ (2.3a-c)

Hence, for $\theta = \pi/2$, $3\pi/2$, $\sigma_{\theta\theta}$ attains its maximum value of $\sigma_{\theta\theta(max)} = 3\sigma$. For $\theta = 0$, π, $\sigma_{\theta\theta}$ attains a compressive value $-\sigma$. Thus, $\sigma_{\theta\theta}$ attains a maximum tensile value of

three times the uniformly distributed stress σ, at the hole $r = a$ for $\theta = \pi/2, 3\pi/2$ (Figure 2.7). This value (3σ) is the largest normal stress that occurs in the plate. Hence, the stress concenteration factor at the hole is 3 [16].

In the case of notches, the maximum stress at the notch root is given by

$$\sigma = K\sigma_n = \frac{A}{\sqrt{\rho}}\sigma_n \tag{2.4}$$

where K is the (dimensionless) stress concentration factor, A is a constant, ρ is the notch radius, and σ_n is a nominal stress representing the magnitude of external roots. Note that as $\rho \rightarrow 0$, σ tends to infinity. In this case it is said that the (theoretical) stress state at the notch root is singular and the asymptotic examination would show that the magnitude of the stresses are of the form $\sigma_{ij} \sim k/r^\alpha$, $(0 < \alpha < 1)$, where r is the distance from the notch root and k is a constant. It is seen that the constants α (the power) and k (the strength) fully describe the nature of stress singularity at the notch root. In the special case when the notch becomes a crack, the strength of the stress singularity k is known as the stress intensity factor. Even though in homogenous materials α is always real, in nonhomogenous wedges α can be complex.
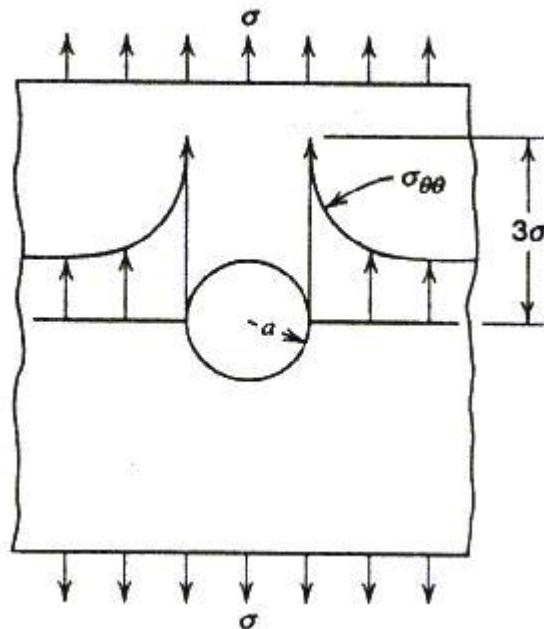
Figure 2.7. $\sigma_{\theta\theta}$ distribution for $\theta = \pi/2, 3\pi/2$ [16].

As it stands, the concept is really useless on two grounds: (a) in practice the notch radius cannot be zero, and (b) due to local inelastic deformations or yielding there would always be

some stress relaxation and redistribution eliminating the possibility of infinite stress. These shaky foundations to some extent explains the reasons for the slow acceptance of the stress intensity factor as a pyhsically relevant parameter when it was introduced in the 1950s. The concept, however, is closely associated with the phenomenon of brittle fracture and, despite its peculiar dimension ($Nm^{3/2}$) for a primary correlation parameter of a very important physical phenomenon, it seems to have found almost universal acceptance and very wide use [15].

2.2 Fracture Mechanics: Development and Practical Applications

In designing structural or machine components an important step is the identification of the most likely mode of failure and the application of a suitable failure criterion. Fracture characterized as the formation of new surfaces in the material is one such mode of mechanical failure. At the most basic level the essential feature of the process is breaking of interatomic bonds in the solid. From a macroscopic standpoint, however, fracture may be viewed as the rupture separation of the structural component into two or more pieces due to the propagation of cracks. In between the process involves the nucleation, growth and coalescence of microvoids and cracks in the material. Thus, in studying the fracture of solids ideally one would have to consider such widely diverse factors as the microscopic phenomena taking place at various length scales, and the macroscopic effects regarding the loading, environmental conditions, and the geometry of the medium. Due to this highly complex nature of the phenomenon, at the present time there seems to be no single theory dealing satisfactorily with all its relevant aspects. Quite naturally, then, the theories developed to study the fracture of solids tend to treat the subject generally from one of three points of view, namely microscopic or atomic, microstructural, and macroscopic or continuum mechanics.

From the standpoint of engineering applications, it has been the macroscopic theories based on the notions of continuum solid mechanics and classical thermodynamics that have provided the quantitative working tools in dealing with the fracture of structural materials. In the macroscopic approach to fracture, it is generally assumed that the material contains some flaws which may act as fracture nuclei and that the medium is a homogeneous continuum in the sense that the size of a dominant flaw is large in comparison with the characteristic microstructural dimension of the material. The problem is, then, to study the influence of the applied loads, the flaw geometry, environmental conditions and material behavior on the fracture process in the solid - a subject which has come to be known as fracture mechanics.

The early strength theories of solids were based on maximum stress. However, it appears that the so-called `size effect', which plays a rather important role in fracture, was known before the introduction of the concept of stress to study the strength of solids. In one of his sketch books, Leonardo da Vinci describes his experiments on breaking iron wires and how the weight required to break the wire increases as its length is cut in half in successive tests. Similar results were observed by Lloyd and by Le Blanc in the 1830s, again on iron bars and wires. In 1858, Karmarsch gave an empirical expression for the load bearing capacity of metal wires which had the form $\sigma_u = A + (B/d)$, where A and B are constants, d is the wire diameter and σ_u is the breaking stress.

In a remarkable, but little-known, article, Wieghardt essentially provided the solution for a linear elastic wedge subjected to an arbitrary concentrated force P applied to one of the wedge boundaries. The solution includes the analysis of the asymptotic behavior of the stress state near the wedge apex and the special case of the crack problem in considerable detail. This appears to be the first elasticity solution in which the existence of stress singularity was recognized, its correct form of $r^{-\alpha}$ was obtained (r being the distance from the wedge apex), and the dependence of α on the wedge angle and on the symmetry of loading was demonstrated. In the crack problem, after obtaining the solution, the leading terms having the form $1/\sqrt{r}$ in the asymptotic expansion were separated and the correct angular distributions were given.

Wieghardt then went on to state that: we will now use these equations (for the stresses) to provide answers to more questions one might pose regarding the strength of our crack against the action of the force P. One may ask: given the strength parameters of our elastic material, what is the magnitude of P necessary for material fracture? And, furthermore, at which place and in which direction will the fracture initiate?

Thus, since he did not question the validity of the maximum stress criterion for fracture, Wieghardt was faced with a paradox. At the crack tip, the stress becomes infinite for any arbitrarily small P and yet the experience shows that the material fractures only if P is raised to a critical value. He tried to resolve the paradox by stating, that: since an elastic material does not rupture at a single point but rather fractures over a small section, one might argue that cracking occurs not due to specific stresses (or deformations) but due to a resultant over a small section.

Since the stresses are integrable, the resultant would always be finite. Thus, after essentially side-stepping the first question, he observes that, if it occurs at all, the fracture will

initiate at the crack tip. He then proceeds to examine the direction of fracture initiation by using the then accepted hypotheses of maximum shear stress or maximum tensile stress. Thus, Wieghardt's work leaves the impression that the fracture criterion would consist of the comparison of an average stress in a `small section' around the crack tip with the theoretical strength of the solid.

Another important scientist that should be cited in fracture mechanics is Griffith.The starting point of his studies was the current knowledge based on ample observations in glass and metal wires, rods, and plates that there is an approximately two orders of magnitude difference between theoretical strength and bulk strength of solids, and his conclusion, based again on observations, that various forms of imperfections, defects and scratches are primarily responsible for this discrepancy. The obvious approach would then be to calculate the correct values of the maximum stresses around these defects and compare them with the theoretical strength of the material. This Griffith did by simulating the defects with an elliptical hole, the solution for which was previously given by Inglis. The results showed that the calculated maximum stress is independent of the absolute size of the flaw and depends only on the ratio of the semiaxes of the ellipse. These findings were in apparent conflict with the test results and led Griffith to conclude that "maximum stress" may not be an appropriate strength criterion and an alternative theory was needed [17].

The basic idea of Griffith's theory is that, similar to liquids, the surface of a solid possesses surface tension, and that when a crack in the solid propagates, the increase in the externally added or internally released energy is balanced by the increase in the surface tension energy. In an elastic solid such as that considered by Griffith if U and V, respectively, refer to the work of the external forces and the elastic energy and if γ refers to the specific surface tension energy of the solid, then Griffith's energy balance theory may be expressed as

$$\frac{d}{dA}(U - V) = \gamma \tag{2.5}$$

where A is the surface area of the crack. For example, by using the solution

$$\sigma_{yy}(x,0) = \frac{\sigma_0|x|}{\left(x^2 - a^2\right)^{1/2}}, \qquad \sigma_{xy}(x,0) = 0, \qquad \left(|x| > a\right) \tag{2.6}$$

$$v(x,0) = \frac{1 + \kappa}{4\mu}\sigma_0\left(a^2 - x^2\right)^{1/2}, \qquad \left(|x| < a\right) \tag{2.7}$$

for an infinite plane that is under uniform tension σ_0 in y direction and which contains a through crack of length 2a along the x axis, it may be shown that for the fixed grip case (more specifically, if the crack is introduced after loading and then fixing the grips) the total strain energy (per unit thickness) is

$$V = \frac{1}{2}\frac{\sigma_0^2}{E}v_0 - \frac{1+\kappa}{8\mu}\pi\sigma_0^2 a^2 \qquad (2.8)$$

where v_0 is the total volume (per unit thickness), μ is the shear modulus, and $\kappa = 4 - 3\nu$ for plane strain and $\kappa = (3 - \nu)/(1 + \nu)$ for plane stress, ν being the Poisson's ratio. If we now observe that for fixed grip case $dU = 0$ and $dA = 4da$ (where da is the extension of the crack at each end), from Equations 2.5 and 2.8 it follows that

$$\frac{1+\kappa}{8\mu}\pi\sigma_0^2 a = 2\gamma \qquad (2.9)$$

Note that $(1+\kappa)/8\mu$ is 1/E for the plane stress and $(1-\nu^2)/E$ for the plane strain case. In the case of crack extension under "fixed load" both dU and dV increase and it can be shown that d(U-V)/dA is still given by Equation 2.9. Aside from the minor error pointed out by Sack and Orowan, Equation 2.9 is essentially the energy balance equation obtained by Griffith. In Equation 2.9 the left-hand side is the energy available for fracture and the right-hand side represents the resistance of the solid to fracture propagation.

The next important development on the subject was Sneddon's work on the plane and the axisymmetric crack problems. By using Westergaard's solution for the plane strain crack problem, and by solving the (axisymmetric) penny-shaped crack problem through the use of Hankel transforms, Sneddon obtained the correct asymptotic behavior of stresses in the small neighborhood of the crack front and showed that the asymptotic expressions for the components of the stress in the two cases differ only by a numerical factor $(2/\pi)$. For the case of an infinite elastic solid under uniform axial tension σ_0 and containing a penny-shaped crack of radius a he also obtained the following energy balance equation.

$$\frac{1-\nu^2}{E}\frac{4}{\pi}\sigma_0^2 a = 2\gamma \qquad (2.10)$$

which differs from (the plane-strain version of) Equation 2.9 only by a factor $(2/\pi)^2$. However, by (incorrectly) stating that $\sigma_{\theta\theta}$ in the penny-shaped crack has no analogue in the plane-strain case, he failed to recognize the importance of his finding and did not generalize

his results. As pointed out later by Irwin, in the penny-shaped crack problem the stress state around the crack front is, of course, one of plane strain, and the isolation of the "numerical factor" referred to by Sneddon is the key to generalizing the crack problems. It should be pointed out that the energy balance relation Equation 2.5 is only a necessary condition for crack growth. From the physical meaning of the terms in Equation 2.5 it is clear that the stability of (quasi-static) fracture propagation may be determined from

$$\frac{d}{dA}\left[\frac{d}{dA}(U-V)-\gamma\right]\begin{cases} >0: \text{unstable} \quad \text{fracture} \\ <0: \text{stable} \qquad \text{fracture} \\ =0: \text{neutral} \quad \text{equilibrium} \end{cases} \tag{2.11}$$

Since the practical fracture resistance of structural solids was observed to be orders of magnitude higher than the corresponding surface tension energy γ, Griffith's work was more or less ignored by the engineering community until the late 1940s. The revival of the theory came about after the X-ray work indicated that even in materials that were fracturing in "purely brittle" manner, there were extensive plastic deformations on the fracture mechanics. This led Irwin and Orowan (independently) to propose that in the energy balance theory the rate of plastic work at the crack front should also be considered as a dissipative energy component. In the early 1950s Irwin made two important contributions. First, he observed that in a fracturing elastic solid if the characteristics size of the zone of large plastic deformations or energy dissipation around the crack front is very small compared to the length parameter of the crack, then it is reasonable to assume that the energy (U-V) "pumped" into the fracture zone will come from the elastic bulk of the solid and therefore will not be critically dependent on the details of the stress state very near the crack front, and the stress state in the elastic bulk of the solid will not differ from a purely elastic crack solution to any significant extent. The importance of this observation lies in the fact that one may now be justified in calculating the energy (U-V) available for fracture from a purely elastic solution.

Irwin's second contribution was his recognition of the universality of the asymptotic stress and displacement fields around the crack tip of his interpretation of the fixed-grip strain energy release rate (which involves the strain energy distribution in the entire solid) in terms of the rate of crack closure that can be calculated by using the asymptotic expressions for the crack surface displacements and corresponding "cleavege" stresses only. He introduced a constant ς (after Griffith) and observed that the symmetric crack solutions given by

Westergaard and Sneddon may be generalized to include asymptotic expressions for all crack problems having the plane of the crack as the plane of symmetry and for small values of the distance r from the crack tip the cleavege stress and the crack surface displacement in the plane of the crack may be expressed as

$$\sigma_{yy} \cong \left(\frac{8\mu}{1+\kappa}\frac{\varsigma}{\pi}\right)^{1/2}\frac{1}{\sqrt{2r}} \ , \ v \cong 2\left(\frac{1+\kappa}{8\mu}\frac{\varsigma}{\pi}\right)^{1/2}\sqrt{2r} \tag{2.12}$$

For small crack extension da he then proceeded to calculate the strain energy release through the crack-closure energy as follows

$$d(U-V) = 2\int_0^{da}\frac{1}{2}\sigma_{yy}(r)\,v\,(da-r)dr = \varsigma da \tag{2.13}$$

or

$$\frac{d}{da}(U-V) = \varsigma \tag{2.14}$$

Thus, from Equations 2.12 and 2.14 it is seen that the energy available for fracture per unit crack extension may be directly related to the coefficient of the singular term in the expression of the stress state at the crack tip. Irwin called the coefficient $(8\mu \div (1+\kappa)\times \varsigma \div \pi)^{1/2}$ which appears in the asymptotic expression of the stress the "stress intensity factor".

Subsequently, by using Westergaard's solution Irwin showed that the stress and displacement states in the close neighborhood of the smooth integral boundary of a plane crack in a linearly elastic solid under most general loading conditions may be expressed in terms of three stress intensity factors k_1, k_2 and k_3 associated with the symmetric opening, in-plane or forward shear, and antiplane shear modes of deformation, respectively (Figure 2.8).
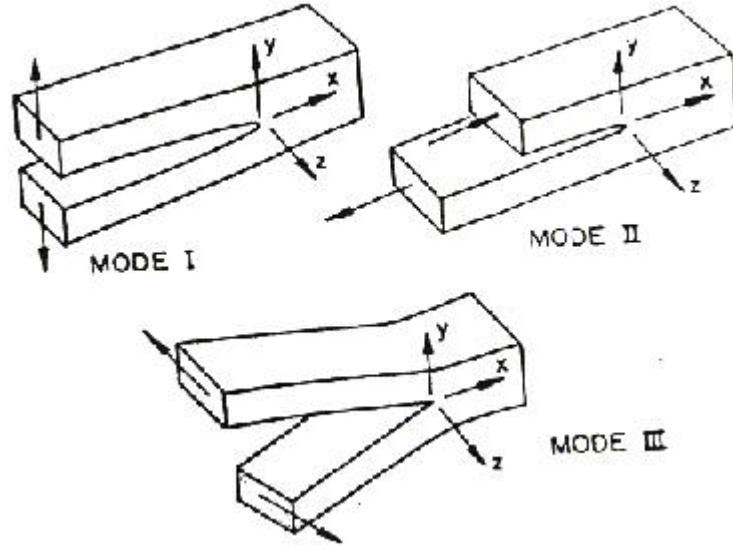
Figure 2.8. Modes I, II, and III crack surface displacements [15].

These asymptotic stress and displacement components may be expressed as follows:

$$\sigma_{xx} \cong \frac{k_1}{\sqrt{2r}}\cos\frac{\theta}{2}\left(1-\sin\frac{\theta}{2}\sin\frac{3\theta}{2}\right)-\frac{k_2}{\sqrt{2r}}\sin\frac{\theta}{2}\left(2+\cos\frac{\theta}{2}\cos\frac{3\theta}{2}\right),$$

$$\sigma_{yy} \cong \frac{k_1}{\sqrt{2r}}\cos\frac{\theta}{2}\left(1+\sin\frac{\theta}{2}\sin\frac{3\theta}{2}\right)+\frac{k_2}{\sqrt{2r}}\sin\frac{\theta}{2}\cos\frac{\theta}{2}\cos\frac{3\theta}{2},$$

$$\sigma_{xy} \cong \frac{k_1}{\sqrt{2r}}\cos\frac{\theta}{2}\sin\frac{\theta}{2}\cos\frac{\theta}{2}+\frac{k_2}{\sqrt{2r}}\cos\frac{\theta}{2}\left(1-\sin\frac{\theta}{2}\sin\frac{3\theta}{2}\right),$$

$$\sigma_{zz} \cong \begin{cases} 0 & ,\text{for plane stress} \\ v\left(\sigma_{xx}+\sigma_{yy}\right), & \text{for plane strain} \end{cases} \qquad (2.15a\text{-}d)$$

$$u \cong \frac{k_1}{8\mu}\sqrt{2r}\left[(2\kappa-1)\cos\frac{\theta}{2}-\cos\frac{3\theta}{2}\right]+\frac{k_2}{8\mu}\sqrt{2r}\left[(2\kappa+3)\sin\frac{\theta}{2}+\sin\frac{3\theta}{2}\right],$$

$$v \cong \frac{k_1}{8\mu}\sqrt{2r}\left[(2\kappa+1)\sin\frac{\theta}{2}-\sin\frac{3\theta}{2}\right]+\frac{k_2}{8\mu}\sqrt{2r}\left[(2\kappa-3)\cos\frac{\theta}{2}+\cos\frac{3\theta}{2}\right], \quad (2.16a,\ b)$$

$$\sigma_{xz} \cong -\frac{k_3}{\sqrt{2r}}\sin\frac{\theta}{2},$$

15

$$\sigma_{yz} \cong \frac{k_3}{\sqrt{2r}} \cos \frac{\theta}{2}, \tag{2.17a, b}$$

$$w \cong \frac{k_3}{\mu} \sqrt{2r} \sin \frac{\theta}{2}, \tag{2.18}$$

where xz is the plane of the crack, the axis z is tangent to the crack border, and r, θ are the polar coordinates in the xy plane (Figure 2.8).

From Equations 2.12 and 2.15b it is seen that the strain energy release rate ς defined by Equation 2.14 is related to the Mode I stress intensity factor k_1 as follows:

$$k_1 = \left(\frac{8\mu}{1+\kappa} \frac{\varsigma}{\pi} \right)^{1/2}, \quad \text{or} \quad \varsigma = \frac{1+\kappa}{8\mu} k_1 2\pi \tag{2.19}$$

If the elasticity solution of the crack problem is available, the stress intensity factors may be evaluated at any point on the crack border from the asymptotic behavior of the stresses (in the plane of the crack) or crack surface displacements by using the Equations 2.15-2.18 for $\theta = 0$ or $\theta = \pi$.

Consideration of such factors as material anisotropy, nonhomogenity, and nonlinearity, and dynamic (or inertia) effects would clearly influence the asymptotic expressions given by Equations 2.15-2.18.

In the type of "brittle" or "low energy" fracture under consideration it was observed that the plastic deformations are confined to a small region around the crack front. To establish a simple "fracture criterion", one may thus assume that (a) the characteristic size of the "energy dissipation" or "fracture process" zone around the growing crack front is "small" compared to the length parameter of the crack, and (b) the size and shape of the dissipation zone remain relatively constant as the crack extends. Based on these assumptions one may then make the hypothesis that, in solids undergoing essentially brittle fracture, under given environmental conditions, the resistance of the material to the fracture, more precisely, the energy needed to create a unit fracture surface is a material constant. In Mode I fracture, from Equation 2.14 we recall that the energy available for unit fracture surface is ς (which is now referred to as ς_I for Mode I). Correspondingly Irwin designated the material's critical resistance parameter by ς_{IC} which he called the "fracture toughness" of the material. ς_{IC} is also known as the "specific fracture energy" or the "critical strain energy release rate". Referring to Equation 2.19, it is

now seen that (under Mode I conditions) the necessary condition for fracture may be expressed as

$$\varsigma_I = \frac{1+\kappa}{8\mu} k_I^2 \pi = \varsigma_{IC} \tag{2.20}$$

and, since ς_{IC} is constant, $\partial\varsigma_I/\partial a$ determines the fracture stability, where a is a length parameter characterizing the fracture area (see Equations 2.11 and 2.14).

Mainly because of the validity of the hypothesis regarding the fracture toughness ς_{IC} being practically constant, in applications the simple fracture criterion expressed by Equation 2.20 has been extremely successful. The parameter ς_{IC} is determined experimentally by following certain procedures established by the American Society for Testing Materials. From Equation 2.20 one may see that the next step in the evaluation of a fracture criterion applicable to structures that behave in a brittle manner was inevitable. Since ς_{IC} is a measured constant and k_I is the only calculated quantity, it was natural to reduce the criterion to a simpler form by defining the critical value of the stress intensity factor as the material constant. At this point also a slight change in notation took place as a result of absorbing the coefficient π in Equation 2.20 into (the definiton of) the stress intensity factor, namely $\pi k_I^2 = K_I^2$, K_I being the new stress intensity factor. The definition of Modes I, II, and III stress intensity factors is:

$$K_I = \lim_{x \to a} \sqrt{2\pi(x-a)}\sigma_{yy}(x,0,0,) \text{ , etc.} \tag{2.21}$$

The corresponding critical value of K_I which represents the fracture resistance of the material and which is obtained from standardized experiments is denoted by K_{IC} and is called the "critical stress intensity factor". Note that K_{IC} is related to the fracture toughness ς_{IC} by

$$K_{IC} = \left(\frac{8\mu}{1+\kappa}\varsigma_{IC}\right)^{1/2} \tag{2.22}$$

and the fracture criterion Equation 2.20 becomes

$$K_I = K_{IC}. \tag{2.23}$$

Again, since K_{IC} is constant, for unstable fracture one must have $\partial K_I/\partial a > 0$, a being a length parameter of the crack. An additional change in terminology seems to be referring to K_{IC} as the "fracture toughness" of the material. This improper usage, too, appears to be embedded

permanently in the fracture literature. If the conditions leading to the simple fracture criterion Equation 2.23 are satisfied the field, fracture mechanics, is sometimes referred as the "linear elastic fracture mechanics" (LEFM).

In addition, to the direct application of Equation 2.23 to static or quasi-static fracture problems, it is also used (by properly modifying K_I and K_{IC}) in such other problems as impact loading and dynamic fracture propagation. In impact loading, K_{IC} is simply replaced by K_{ID} which is obtained from standardized impact tests. In dynamic crack propagation problems, K_I can be, in most cases, calculated as a function of time and is still the most effective factor representing the crack-structure geometry and the applied load [15].

2.3 Methods of Solution

There are several kinds of methods of solutions of crack problems leading to the calculation of the stress intensity factors such as; complex potentials, integral transforms, singular integral equations, alternating method and finite element method.

2.3.1. Complex Potentials

Applicable to only two dimensional problems, the complex potentials were first introduced by Goursat to represent the biharmonic function. Expressing the displacements in terms of two holomorphoic functions φ and ψ as

$$2\mu(u + iv) = \kappa\varphi(z) - z\overline{\varphi}'(\overline{z}) - \overline{\psi}(\overline{z}) \tag{2.24}$$

and observing that in the mixed boundary value problem which represents the plane containing the number of cracks along (a_k, b_k), (k=1,2,...), a_k and b_k are branch of points, the complex potentials, for example, in the neighborhood of the end point $z = b_k$ may be expressed as

$$\varphi'(z) = \frac{F_{1k}(z)}{(z - b_k)^{1/2}} + G_{1k}(z), \quad \psi'(z) = \frac{F_{2k}(z)}{(z - b_k)^{1/2}} + G_{2k}(z), \tag{2.25}$$

where the functions F_{jk} and G_{jk}, $(j=1,2,...)$ are holomorphic near and at b_k. It can be further shown that the asymptotic stress distribution Equation 2.15 directly follows from Equation 2.25 and the stress intensity factors may be determined from

$$k_1 - ik_2 = \lim_{z \to b_k} 2\sqrt{2(z - b_k)}\varphi'(z) \qquad (2.26)$$

The method of complex potentials provides perhaps the simplest and most rigorous method for solving the crack problems and for analyzing the singular behavior of the solution. The serious shortcoming of the method is that it is restricted to two-dimensional elastostatic problems for (generally) infinite domains.

There are a number of techniques used in the solution of two-dimensional crack problems which are also based on the application of complex potentials. Among these the method of conformal-mapping, Laurent series expansion, boundary collocation method, and certain applications of the Wiener-Hopf method can be mentioned.

2.3.2. Integral Transforms

The integral transform is one of the most widely used methods in the formulation of the boundary value problems in mechanics. If the problem is a mixed boundary value problem the formulation would invariably lead to a pair of dual integral equations. Specifically, the crack problems for an elastic plane or an infinite strip containing a line crack, plane infinite wedge with a radial crack, and an elastic cylinder with an infinite or finite radius containing an axisymmetric crack may easily be reduced to dual integral equations by using Fourier, Mellin, and Hankel transforms, respectively. The dual integral equations may than be reduced to an Abel's (integral) equation which may turn be either solved in closed form or reduced to a Fredholm integral equation.

2.3.3. Singular Integral Equations

Dual integral equations, dual series equations, or dual series-integral equations arising from the formulation of the crack problems may be reduced to a singular integral equation (with a Cauchy-type singularity) in a straightforward manner. The crack problems can also be formulated in terms of a (system of) singular integral equation(s) directly by using the related

Green's functions (e.g., dislocation and concentrated load solutions) and technique of superposition. The method has clear advantages in problems involving unusual stress singularities . It also lends itself to relatively simple numerical treatment.

2.3.4. The Alternating Method

The method is also known as Schwarz algorithm or successive approximations. It is developed for regions with several contours (e.g., a crack and a bounding surface) and is based on the idea that by solving the problem successively for the region with one contour at a time and varying (or correlating) the boundary conditions at each step, a useful approximate solution may be obtained after a sufficient number of steps.

2.3.5. Finite Element Method

For apparent reasons this is one of the most widely used methods in practice to calculate the stress intensity factors. In the so-called indirect method the stress intensity factor is obtained through extrapolation of curve fitting to the values of a stress or a displacement component calculated at certain interior locations. In the direct method, special crack-tip elements are used and the stress intensity factors are directly calculated. The special elements developed for this purpose seem to be quite numerous among which one may mention the circular core element, the enriched element, the singular triangle, the quarter-point element, and specialized hybrid elements. In all these techniques the basic idea is to design the elements adjacent to the crack tip in such a way that the displacements are forced to vary according to the asymptotic distributions given by Equation 2.16. The properly calculated local amplitudes would then give k_1 and k_2. This method will be investigated in detail in the following chapters.

There are, of course, other methods solve the crack problems and to determine the stress intensity factors among which one may mention the methods of weight functions, boundary integral equations, curvilinear coordinates, and finite differences. One may also note that in certain problems such experimental techniques as the method of caustics and photoelasticity may prove to be quite effective in estimating the stress intensity factors [15].

CHAPTER 3

FINITE ELEMENT METHOD

3.1 Numerical Methods

There are many practical engineering problems for which we cannot obtain exact solutions. This inability to obtain an exact solution may be attributed to either the complex nature of governing differential equations or the difficulties that arise from dealing with the boundary and initial conditions. To deal with such problems, we resort to numerical approximations. In contrast to analytical solutions, which show the exact behavior of a system at any point within the system, numerical solutions approximate exact solutions at discrete points, called nodes. The first step of any numerical procedure is discretization. This process divides the medium of interest into a number of small subregions and nodes. There are two common classes of numerical methods: (1) finite difference methods and (2) finite element methods. With finite difference methods, the differential equation is written for each node, and the derivatives are replaced by difference equations. This approach results in a set of simultaneous linear equations. Although finite difference methods are easy to understand and employ simple problems, they become difficult to apply to problems with complex geometries or complex boundary conditions. This situation is also true for problems with nonisotropic material properties.

In contrast, the finite element method uses integral formulations rather than difference equations to create a system of algebraic equations. Moreover, an approximate continuous function is assumed to represent the solution for each element. The complete solution is then generated by connecting or assembling the individual solutions, allowing for continuity at the interelemental boundaries [18]. The finite element method will be investigated in detail in the following paragraphs.

3.2 Finite Element Method

The finite element method is a numerical procedure for analyzing structures and continua. Usually the problem addressed is too complicated to be solved satisfactorily

by classical analytical methods. The problem may concern stress analysis, heat conduction, or any of several other areas. The finite element procedure produces many simultaneous algebraic equations, which are generated and solved on a digital computer. Finite element calculations are performed on personal computers, mainframes, and all sizes between. Results are rarely exact. However, errors are decreased by processing more equations, and results accurate enough for engineering purposes are obtainable at reasonable cost.

The finite element method originated as a method of stress analysis [19]. It is used to analyze both linear and nonlinear systems. Nonlinear analysis includes material yielding, creep or cracking; aeroelastic response; buckling and postbuckling response; contact and friction; etc. The finite element method is used for both static and dynamic analyses. In its most general form, the method is not restricted to structural (or mechanical) systems [16]. Today finite elements are also used to analyze problems of heat transfer, fluid flow, lubrication, electric and magnetic fields, and many others. Problems that previously were utterly intractable are now solved routinely. Finite element procedures are used in the design of buildings, electric motors, heat engines, ships, airframes, and spacecraft. Manufacturing companies and large design offices typically have one or more large finite element programs in-house. Smaller companies usually have access to a large program through a commercial computing center or use a smaller program on a personal computer.
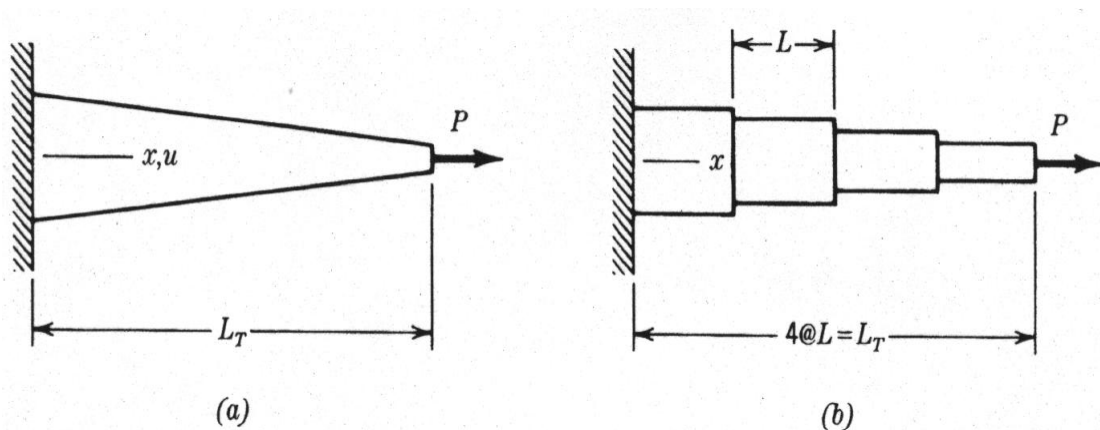
Figure 3.1. **(a)** A tapered bar under end load P. **(b)** A model built of four uniform (nontapered) elements of equal length [19].

Figure 3.1 shows a very simple problem that illustrates discretization, a basic finite element concept. Imagine that the displacement of the right end of the bar is required. The classical approach is to write the differential equation of the continuously tapered bar, solve this equation for axial displacement u as a function of x, and finally substitute $x = L_T$ to find the required end displacement. The finite element approach to this problem does not begin with differential equation. Instead, the bar is discretized by modeling it as a series of finite elements, each uniform but of a different cross-sectional area A (Figure 3.1(b)). In each element, u varies linearly with x; therefore, for $0 < x < L_T$, u is a piecewise-smooth function of x. The elongation of each element can be determined from the elementary formula PL/AE. The end displacement, at $x = L_T$, is the sum of the element elongations. Accuracy improves as more elements are used.

In the foregoing example, and in general, the finite element method models a structure as an assemblage of small parts (elements). Each element is of simple geometry and therefore is much easier to analyze than the actual structure. In essence, a complicated solution by a model that consists of piecewise-continuous simple solutions is approximated. Elements are called "finite" to distinguish them from differential elements in calculus.
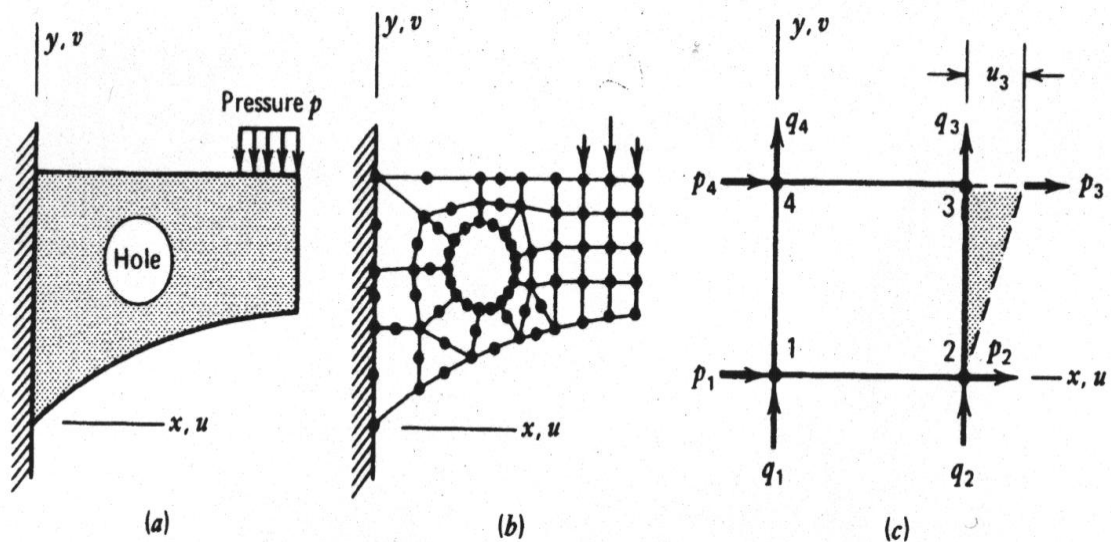
Figure 3.2. (a) A plane structure of arbitrary shape. **(b)** A possible finite element model of the structure. **(c)** A plane rectangular element showing nodal forces p_i and q_i. The dashed line shows the deformation mode associated with x-direction displacement of node 3 [19].

Figure 3.2(a) shows a plane structure. Displacements and stresses caused by pressure p are required. The finite element model, Figure 3.2(b), consists of plane areas, some triangular and some quadrilateral (if done properly, there is no difficulty in combining the different element types). Black dots, called nodes or node points, indicate where elements are connected to one another. In this model each node has two degrees of freedom (d.o.f.): that is, each node can displace in both the x direction and the y direction. Thus, if there are n nodes in Figure 3.2(b), there are 2n d.o.f. in the model. (In the real structure there are infinitely many d.o.f. because the structure has infinitely many particles.) Algebraic equations that describe the finite element model are solved to determine the d.o.f. Use of only 2n d.o.f. in analysis is similar to use of the first 2n terms of a convergent infinite series.

It can be seen that in going from Figure 3.2(a) to 3.2(b) the distributed pressure p has been converted to concentrated forces at nodes.

From Fig. 3.2 it may appear that discretization is accomplished simply by sawing the continuum into pieces and then pinning the pieces together again at node points. But such a model would not deform like the continuum. Under load, strain concentrations would appear at the nodes, and the elements would tend to overlap or separate along the saw cuts. Clearly, the actual structure does not behave in this way, so the elements must be restricted in their deformation patterns. For example, if elements are allowed to have only such deformation modes as will keep edges straight (Figure 3.2(c)), then adjacent elements will neither overlap nor separate. In this way the basic requirement is satisfied that deformations of a continuous medium must be compatible.

An important ingredient in a finite element analysis is the behavior of the individual elements. A few good elements may produce better results than many poorer elements. It can be seen that several element types are possible by considering Figure 3.3. Function φ, which might represent any of several physical quantities, varies smoothly in the actual structure. A finite element model typically yields a piecewise-smooth representation of φ. Between elements there may be jumps in the x and y derivatives of φ. Within each element φ is a smooth function that is usually represented by a simple polynomial. What shall the polynomial be? For the triangular element, the linear polynomial

$$\varphi = a_1 + a_2 x + a_3 y \qquad\qquad (3.1)$$

is appropriate, where the a_i are constants. These constants can be expressed in terms of φ_1, φ_2, and φ_3, which are the values of φ at the three nodes. Triangles model the actual φ by a surface of flat triangular facets. For the four-node quadrilateral, the "bilinear" function

$$\varphi = a_1 + a_2 x + a_3 y + a_4 xy \qquad (3.2)$$

is appropriate. The eight node quadrilateral in Figure 3.3 has eight a_i in its polynomial expansion and can represent a parabolic surface.
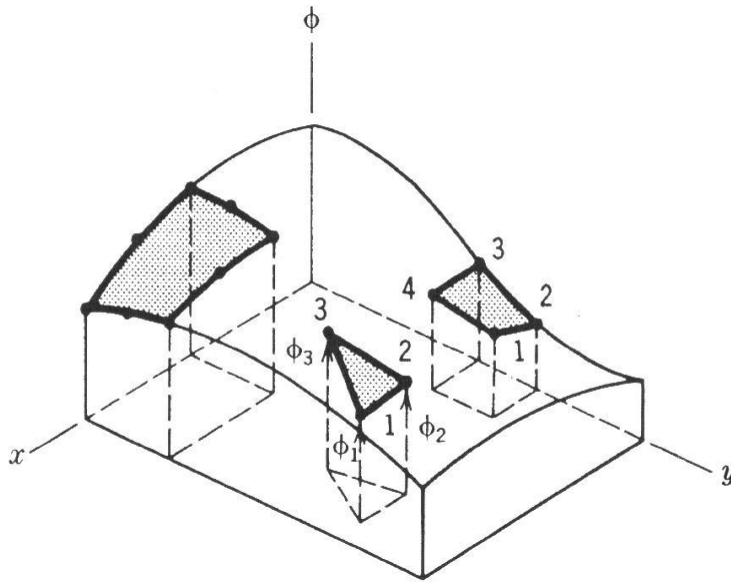
Figure 3.3. A function of $\varphi = \varphi(x, y)$ that varies smoothly over a rectangular region in the xy plane, and typical elements that might be used to approximate it [19].

Equations 3.1 and 3.2 are interpolations of function φ in terms of the position (x,y) within an element. That is, when the a_i have been determined in terms of nodal values φ_i, Equations 3.1 and 3.2 define φ within an element in terms of the φ_i and the coordinates. Clearly, if the mesh of elements is not too coarse and if the φ_i happened to be exact, then φ away from nodes would be a good approximation. Nodal values φ_i are close to exact if the mesh is not too coarse and if the element properties are properly formulated.

How can the user decide which element to use? Unfortunately, the answer is not simple. An element that is good in one problem area may be poor in another. Even in a specific problem area an element may behave well or badly, depending on the particular geometry, loading and boundary conditions.

The "finite element method" is a method of piecewise approximation in which the approximating function φ is formed by connecting simple functions, each defined over a small region (element). And a "finite element" is a region in space in which a function φ is interpolated from nodal values of φ on the boundary of the region in such a way that interelement continuity of φ tends to be maintained in the assemblage.

A finite element analysis typically involves the following steps. Steps 1, 4, and 5 require decisions by the analyst and provide input data for the computer program. Steps 2, 3, 6 and 7 are carried out automatically by the computer program.

1. Divide the structure or continuum into finite elements. Mesh generation programs, called preprocessors, help the user in doing this work.

2. Formulate the properties of each element. In stress analysis, this means determining nodal loads associated with all element deformation states that are allowed.

3. Assemble elements to obtain the finite element model of the structure.

4. Apply the known loads: nodal forces and/or moments in stress analysis.

5. In stress analysis, specify how the structure is supported. This step involves setting several nodal displacements to known values (which often are zero).

6. Solve simultaneous linear algebraic equations to determine nodal d.o.f (nodal displacements in stress analysis).

7. In stress analysis, calculate element strains from the nodal d.o.f and the element displacement field interpolation, and finally calculate stresses from strains. Output interpretation programs, called postprocessors, help the user sort the output and display it in graphical form.

The power of the finite element method resides principally in its versatility. The method can be applied to various physical problems. The body analyzed can have arbitrary shape, loads, and support conditions. The mesh can mix elements of different types, shapes, and physical properties. This great versatility is contained within a single computer program. User-prepared input data controls the selection of problem type, geometry, boundary conditions, element selection, and so on.

Another attractive feature of finite elements is the close physical resemblance between the actual structure and its finite element model. The model is not simply an abstraction. This seems especially true in structural mechanics, and may account for the finite element method having its origin there.

The finite element method also has disadvantages. A specific numerical result is found for a specific problem: a finite element analysis provides no closed-form solution that permits analytically study of the effects of changing various parameters. A computer, a reliable program, and intelligent use are essential. A general purpose program has extensive documentation, which cannot be ignored. Experience and good engineering judgement are needed in order to define a good model. Many input data are required and volumnious output must be sorted and understood [19].

3.2.1 Historical Background of the Finite Element Method

The idea representing a given domain as a collection of discrete parts is not unique to the finite element method. It was recorded that ancient mathematicians estimated the value of π by noting that the perimeter of a polygon inscribed in a circle approximates the circumference of the latter. They predicted the value of π to accuracies of almost 40 significant digits by representing the circle as a polygon of a finitely large number of sides [20].

Beginning in 1906, researchers suggested a "lattice analogy" for stress analysis. The continuum was replaced by a regular pattern of elastic bars. Properties of the bars were chosen in a way that caused displacements of the joints to approximate displacements of points in the continuum. The method sought to capitalize on well-known methods of structural analysis.

Courant appears to have been the first to propose the finite element method as we know it today. In a 1941 mathematics lecture, published in 1943, he used the principle of stationary potential energy and piecewise polynomial interpolation over triangular subregions to study the Saint-Venant torsion problem. Courants's work was ignored until engineers had independently developed it.

None of the foregoing work was of much practical value at the time because there were no computers available to generate and solve large sets of simultaneous algebraic equations. It is no accident that the development of finite elements coincided with major advances in digital computers and programming languages.

By 1953 engineers had written stiffness equations in matrix format and solved the equations with digital computers. Most of this work took place in the aerospace industry. At the time, a large problem was one with 100 d.o.f. In 1953, at the Boeing Airplane Company, Turner suggested that triangular plane stress elements be used to model the skin of a delta wing. This work, published almost simultaneously with similar work done in England, marks the beginning of widespread use of finite elements. Much of this early work went unrecognized because of company policies against publication.

The name "finite element method" was coined by Clough in 1960. The practical value of the method was soon obvious. New elements for stress analysis applications were developed, largely by intuition and physical argument. In 1963 the finite element method gained respectability when it was recognized as having a sound mathematical foundation: it can be regarded as the solution of a variational problem by minimization of a functional. Thus the method was seen as applicable to all field problems that can be cast in a variational form. Papers about the application of finite elements to problems of heat conduction and seepage flow appeared in 1965.

Large general-purpose finite element computer programs emerged during the late 1960s and early 1970s. Examples include ANSYS, ASKA, and NASTRAN. Each of these programs included several kinds of elements and could perform static, dynamic, and heat transfer analysis. Additional capabilities were soon added. Also added were preprocessors (for data input) and postprocessors (for results evaluation). These processors rely on graphics and make it easier, faster, and cheaper to do finite element analysis. Graphics development became intensive in the early 1980s as hardware and software for interactive graphics became available and affordable.

A general-purpose finite element program typically contains over 100000 lines of code and usually resides on a mainframe or a supermicrocomputer. However, in the mid-1980s, adaptations of general-purpose programs began to appear on personal computers. Hundreds of analysis and analysis-related programs are now available, large and small, general and narrow, cheap and expensive, for lease or for purchase.

Ten papers about finite elements were published in 1961, 134 in 1966, and 844 in 1971. By 1976, two decades after engineering applications began, the cumulative total publications about finite elements exceeded 7000. By 1986, the total was about 20000 [19].

3.2.2 Sources of Error

There are three sources of error in the finite element method: errors due to approximation of the domain (discretization error), errors due to approximation of the element behavior (formulation error), and errors due to use of finite precision arithmetic.

Discretization error is due to the approximation of the domain with a finite number of elements of fixed geometry. For instance, consider the analysis of a rectangular plate with a centrally located hole (Figure 3.4(a)). Due to symmetry, it is sufficient to model only-one quarter of the plate. If the region is subdivided into triangular elements (a triangular mesh or grid), the circular hole is approximated by a series of straight lines. If a few large traingles are used in a coarse mesh, (Figure 3.4(b)), greater discretization error results than if a large number of small elements are used in a fine mesh, (Figure 3.4(c)). Other geometric shapes may be chosen for the elements. For example, with quadrilateral elements that can represent curved sides, the circuler hole is more accurately approximated (Figure 3.4(d)). Hence, discretization error may be reduced by grid refinement. The grid can be refined by using more elements of the same type but of smaller size (h-refinement) or by using elements of a different type (p-refinement).

Formulation error results from the use of finite elements that do not precisely describe the behavior of continuum. For instance, a particular element might be formulated on the assumption that displacements vary linearly over the domain. Such an element would contain no formulation error when used to model a prismatic bar under constant tensile load; in this case, the assumed displacement matches the actual displacement. If the same bar were subjected to uniformly distributed body force, then the actual displacements vary quadratically and formulation error would exist. Formulation error can be minimized by proper selection element type and appropriate grid refinement. Numerical error is a consequence of round-off during floating-point computations and the error associated with numerical integration procedures. This source of error is dependent on the order in which computations are performed in the program and the use of double or extended precision variables and functions. The use of bandwith minimization can help control numerical error. Generally, in a well-designed finite element program, numerical error is small relative to formulation error [16].
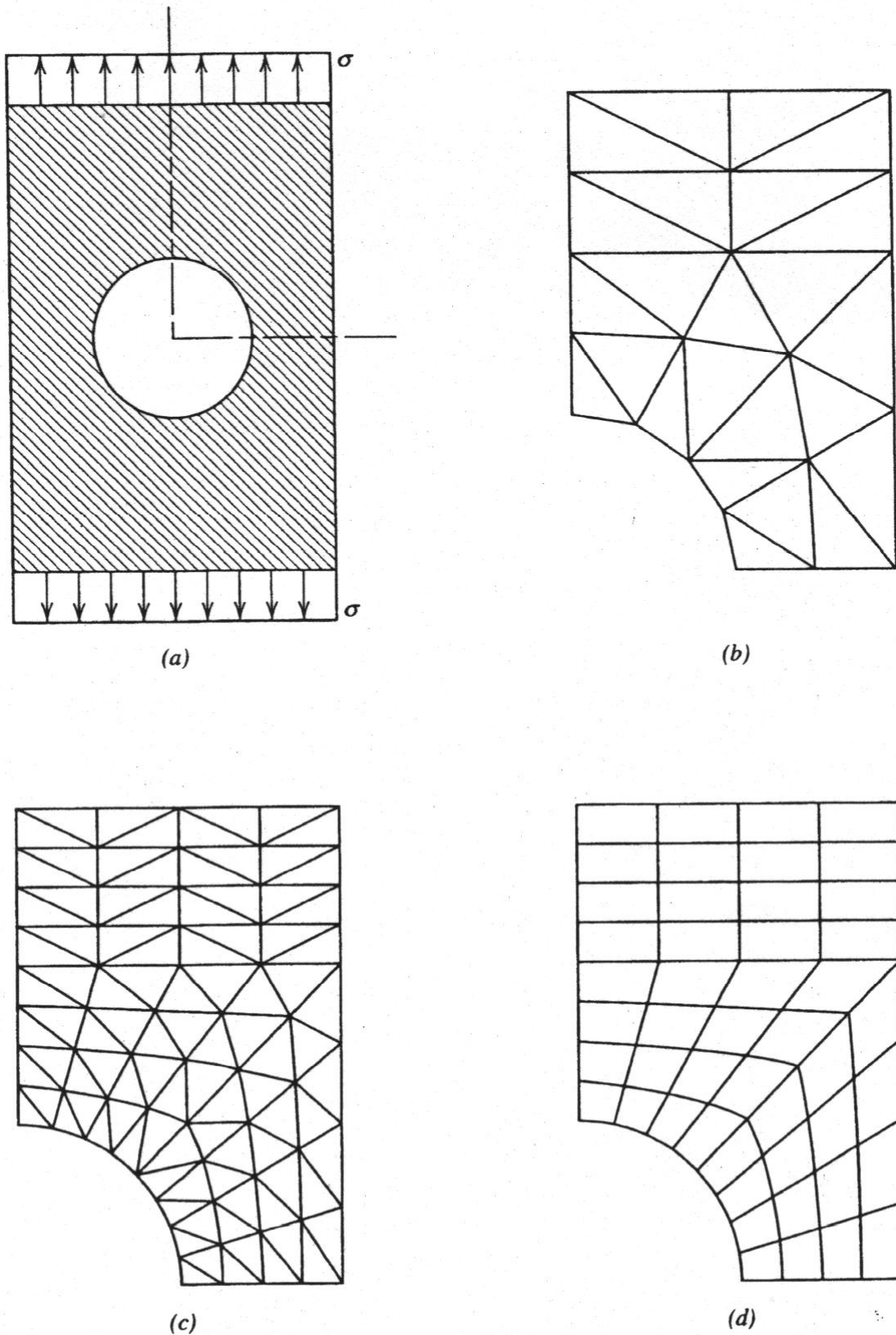
Figure 3.4. Finite element models of plate with centrally located hole. **(a)** Plate geometry and loading. **(b)** Coarse mesh of triangles. **(c)** Fine mesh of triangles. **(d)** Mesh of quadrilaterals with curved edges [16].

Add to these, powerful programs cannot be used without training. Their results cannot be trusted if users have no knowledge of their internal workings and little understanding of the physical theories on which they are based. An error caused by misunderstanding or oversight is not correctible by mesh refinement or by use of a more powerful computer. Some authorities have suggested that users be "qualified", somewhat in the manner of practitioners having be licensed before engaging in a profession in which the potential for damage to the public is substantial. Although the finite element method can make a good engineer better, it can make a poor engineer more dangerous.

Computed results must in some way be judged or compared with expectations. Alternative results, useful for comparison, might be obtained from a different computer program that relies on a different analytical basis, from a simplified model amenable to hand calculation, from the behavior of similar structures already built, and from experiment. Experiment may be expensive and has its own pitfalls, but is desirable if the analytical process is pushed beyond previous experience and established practice [19].

CHAPTER 4

ANALYTICAL STUDY

The axisymmetric problem for the hollow cylindrical bar shown in Figure 4.1 solved analytically by Artem [12]. The cylinder with inner and outer radii A and B is subjected to uniformly distributed axial tension of intensity p_0 at infinity. The infinite hollow cylinder contains a ring-shaped crack of width (b-*a*) at the symmetry plane z=0 and two ring-shaped rigid inclusions of width (d-c) at z=± L planes.
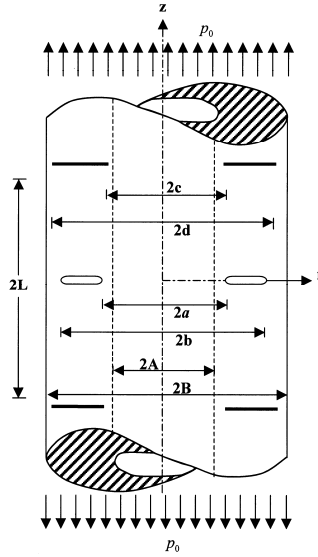
Figure 4.1. Geometry of the problem [12].

Along the rigid inclusions with negligible thickness displacements are constant and continuous whereas stresses have jumps. The surfaces of the crack are free of tractions. Therefore, the field equations of axisymmetric elasticity problem must be solved together with the following boundary conditions:

$$\sigma_z(r,0) = 0, \qquad\qquad (a<\text{r}<\text{b}), \qquad\qquad (4.1a)$$

$$w(r,0) = 0, \qquad\qquad (\text{A}<\text{r}<a, \ \ b<\text{r}<\text{B}) \quad (4.1b)$$

$$\sigma_z(r,\pm\infty) = p_0, \qquad\qquad (\text{A}<\text{r}<\text{B}), \qquad\qquad (4.2a,b)$$

$$u(r,\pm L) = 0, \quad w(r,\pm L) = const., \qquad (c<\text{r}<d), \qquad\qquad (4.3a\text{-}d)$$

$$\sigma_r(A,z) = 0, \quad \tau_{rz}(A,z) = 0, \qquad (\text{-}\infty<\text{z}<\infty), \qquad (4.4a,b)$$

$$\sigma_r(B, z) = 0, \quad \tau_{rz}(B, z) = 0, \qquad (-\infty < z < \infty), \qquad (4.5a,b)$$

where u and w are the r- and z-components of the displacement vector.

Solution for the problem shown in Figure 4.1 may be obtained conveniently by considering 1) problem of an infinite hollow cylinder subjected to loads at infinity with no crack or inclusions, and 2) problem of an infinite hollow cylinder containing a ring-shaped crack at z=0 and two ring-shaped rigid inclusions at z=± L (perturbation problem) shown in Figure 4.2. The external load is the negative of the stresses and displacements at locations of the crack and the inclusions obtained from the first problem.
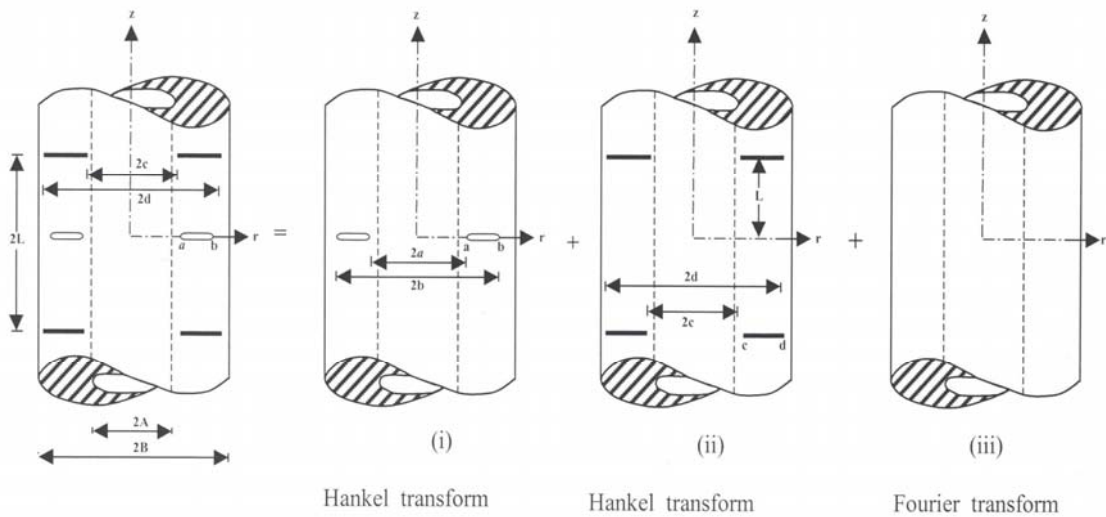
Figure 4.2. The informal superposition scheme (perturbation problem) [12].

Solution of the first problem is relatively simple and straight forward. Therefore in this study, the second problem will be treated in detail. General expressions for the displacement and stress components for perturbation problem are obtained by solving the field equations using Fourier and Hankel transform techniques. Applying the boundary conditions on stress free inner and outer lateral surfaces of the cylinder, on crack and on rigid inclusions a system of three singular integral equations with kernels having Cauchy-type singularity in terms of crack surface displacement derivative and normal and shear stress jumps on rigid inclusions are obtained (see [12] for details)

$$\frac{2\mu}{\pi(\kappa+1)}\int_a^b f(t)\left[\frac{2}{t-r}+2M_1(r,t)+tN_{11}(r,t)\right]dt + \frac{1}{\kappa+1}\int_c^d h(t)t\left[T_1(r,t)-\frac{2}{\pi}N_{12}(r,t)\right]dt$$

$$+\frac{1}{\kappa+1}\int_c^d g(t)t\left[T_2(r,t)-\frac{2}{\pi}N_{13}(r,t)\right]dt = -p_0, \qquad (a<r<b)$$

$$\frac{1}{\kappa+1}\int_a^b f(t)t\left[T_3(r,t)+\frac{2}{\pi}N_{21}(r,t)\right]dt$$

$$+\frac{1}{2\mu(\kappa+1)}\int_c^d h(t)\left[tT_4(r,t)+\frac{\kappa}{\pi}M_2(r,t)+\frac{\kappa}{\pi}\frac{1}{t-r}-\frac{4}{\pi}tN_{22}(r,t)\right]dt$$

$$+\frac{1}{2\mu(\kappa+1)}\int_c^d g(t)t\left[T_5(r,t)-\frac{4}{\pi}N_{23}(r,t)\right]dt = 0, \qquad (c<r<d)$$

$$\frac{1}{\kappa+1}\int_a^b f(t)t\left[T_6(r,t)+\frac{2}{\pi}N_{31}(r,t)\right]dt - \frac{1}{2\mu(\kappa+1)}\int_c^d h(t)t\left[T_7(r,t)+\frac{4}{\pi}N_{32}(r,t)\right]dt$$

$$+\frac{1}{2\mu(\kappa+1)}\int_c^d g(t)\left[tT_8(r,t)+\frac{\kappa}{\pi}M_3(r,t)+\frac{\kappa}{\pi}\frac{1}{t-r}-\frac{4}{\pi}tN_{33}(r,t)\right]dt = 2\varepsilon_0,$$

$$(c<r<d) \qquad (4.6a\text{-}c)$$

where

$$M_i(r,t)=\frac{M_i^*(r,t)-1}{t-r} \qquad (i=1-3), \qquad (4.7)$$

and

$$M_1^*(r,t)=\begin{cases} \dfrac{2(t-r)}{r}K\left(\dfrac{t}{r}\right)+\dfrac{2r}{t+r}E\left(\dfrac{t}{r}\right) & (r\rangle t), \\[4mm] \dfrac{2t}{t+r}E\left(\dfrac{r}{t}\right) & (r\langle t), \end{cases}$$

$$M_2^*(r,t)=\begin{cases} \dfrac{2t}{t+r}E\left(\dfrac{t}{r}\right) & (r\rangle t), \\[4mm] -\dfrac{2}{r}(t-r)K\left(\dfrac{r}{t}\right)+\dfrac{2t^2/r}{(t+r)}E\left(\dfrac{r}{t}\right) & (r\langle t), \end{cases}$$

$$M_3{}^*(r,t) = \begin{cases} \dfrac{2(t-r)}{r}K\left(\dfrac{t}{r}\right) + \dfrac{2r}{t+r}E\left(\dfrac{t}{r}\right) & (r \rangle t), \\[4mm] \dfrac{2t}{t+r}E\left(\dfrac{r}{t}\right) & (r \langle t), \end{cases}$$

(4.8a-c)

in which K and E are the complete elliptic integrals of the first and the second kinds, respectively.

Then, these integrals are converted into series by the use of Gauss-Lobatto integration formula so that a system of linear algebraic equations is obtained. This system is solved numerically. After the numerical solution obtained, the stress intensity factors at crack tips are determined.

CHAPTER 5

FINITE ELEMENT SOLUTION BY ANSYS

In order to evaluate stress intensity factors at the crack tips in this study, a finite element analysis program, ANSYS, is used. ANSYS is a comprehensive general-purpose finite element computer program that contains over 100000 lines of code. ANSYS is capable of performing static, dynamic, heat transfer, fluid flow, and electromagnetism analyses. ANSYS has been a leading finite element analysis program for well over 20 years. The current version of ANSYS has a completely new look, with multiple windows incorporating Graphical User Interface (GUI), pull down menus, dialog boxes, and a tool bar. Today, ANSYS is in use in many engineering fields, including aerospace, automotive, electronics, and nuclear [18]. With the help of GUI, one can do his work by pushing commands on the window. Also, one can write a program in ANSYS Parametric Design Language (APDL) and then run it without pushing the buttons. APDL allows one to build his model in terms of parameters (variables), which in turn allows one to make design changes easily [21]. Actually these two ways are same in the basis, but the main difference is that the pushing task automatically writes the command line of task in APDL language in the former and one can see what he has done at the same time on the computer screen. Add to these, ANSYS has no limits on the number of the nodes, elements, or degrees of freedom. And also it should be noted that ANSYS uses dynamic memory allocation and the parameters managing the memory usage have been left to their default values [22].

5.1 Introduction

When one runs the program, he can see an empty interface on the computer screen. At the beginning, one should decide which unit system will be used in the analysis. In this study, SI unit system is used and this task can be done only by writing the command:

/units,si

on the command line. The next step is to select the type of the analysis of the problem such as structural, thermal and ANSYS fluid. Here, one will define the type and then the program will filter the interface, means that commands on the GUI in the following steps are related with the type of the analysis which is defined. The type of the analysis of this study is "structural" and this task can be done on the GUI by the way shown below:

Preferences > Structural

5.2 Preprocessing part

The first step of the finite element method starts with preprocessing. In the preprocessing part, one can select the type of elements, define the material properties, build the model, give attributes to the model and mesh the model. The first step is to select the element type which is Plane2 in this study (Figure 5.1). Plane2 is a six-node triangular structural-solid element. The element has quadratic displacement behavior with two degrees of freedom at each node, translation in the nodal x- and y- directions. Surface pressure loads may be applied to element faces. Output data include nodal displacements and element data, such as directional stresses and principal stresses [18].

Preprocessor > Add/Edit/Delete..... > Add > Structural Solid > Triangle 6node 2

After selecting the type of the element, the next step is to define its properties such as plane stress, plane strain, axisymmetric or plane stress with thickness. In this study, the analysis of an axisymmetric cylinder subjected to axisymmetric loading is considered, so axisymmetric condition can be used.
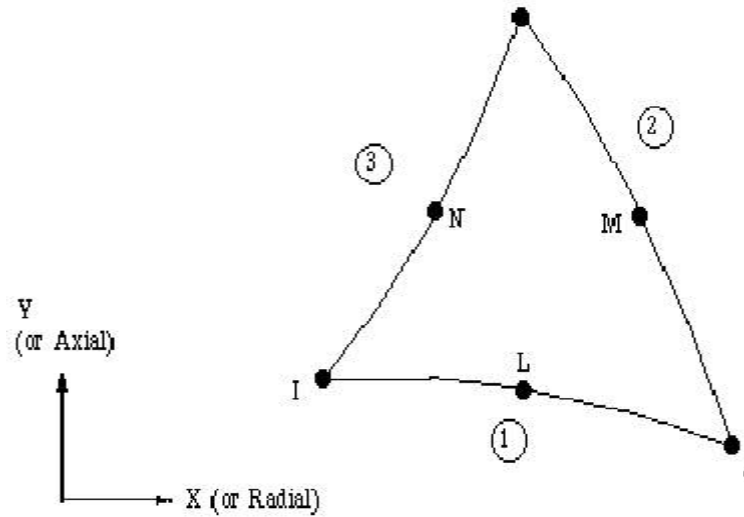
Figure 5.1. Plane2 2D 6-Node Triangular Structural Solid Element of ANSYS [23].

Problems involving three-dimensional axisymmetric solids or solids of revolution, subjected to axisymmetric loading, reduce to simple two-dimensional problems. Because of total symmetry about the z axis, as seen in Figure 5.2, all deformations and stresses are independent of the rotational angle θ. Thus, the problem needs to be looked as a two-dimensional problem in rz, defined on the revolving area (Figure 5.2(b)). Gravity forces can be considered if acting in the z direction.
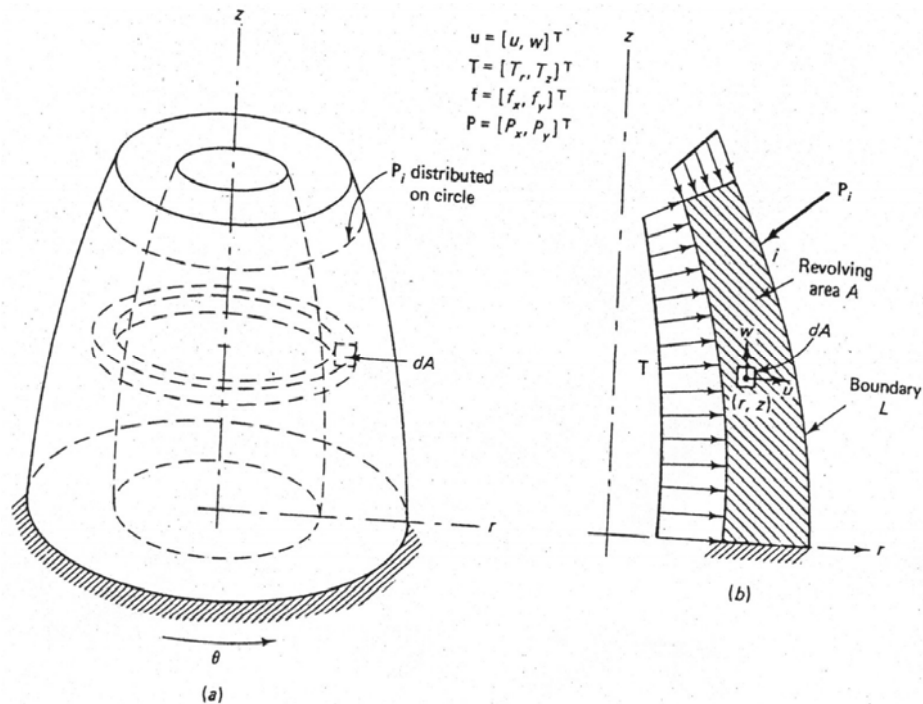
Figure 5.2. Axisymmetric problem [24].
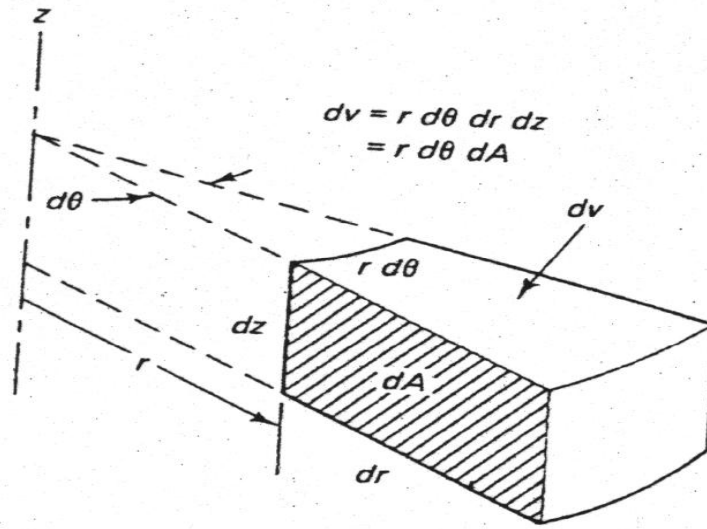
Figure 5.3 Elemental Volume [24].

Considering the elemental volume shown in Figure 5.3, the potential energy can be written in the form

$$\Pi = \frac{1}{2}\int_0^{2\pi}\int_A \boldsymbol{\sigma}^T \boldsymbol{\varepsilon} r dA d\theta - \int_0^{2\pi}\int_A \mathbf{u}^T \mathbf{f} r dA d\theta - \int_0^{2\pi}\int_L \mathbf{u}^T \mathbf{T} r dl d\theta - \sum_i \mathbf{u}_i^T \mathbf{P}_i \qquad (5.1)$$

where $rdld\theta$ is the elemental surface area, and the point load $\mathbf{P}_i$ represents a line load distributed around a circle, as shown in Figure 5.2.

All variables in the integrals are independent of θ. Thus, Equation 5.1 can be written as

$$\Pi = 2\pi\left(\frac{1}{2}\int_A \boldsymbol{\sigma}^T \boldsymbol{\varepsilon} r dA - \int_A \mathbf{u}^T \mathbf{f} r dA - \int_L \mathbf{u}^T \mathbf{T} r dl\right) - \sum_i \mathbf{u}_i^T \mathbf{P}_i \qquad (5.2)$$

where

$$\mathbf{u} = \left[u, w\right]^T \qquad (5.3)$$

$$\mathbf{f} = \left[f_r, f_z\right]^T \qquad (5.4)$$

$$\mathbf{T} = \left[T_r, T_z\right]^T \qquad (5.5)$$

From Figure 5.4, the relationship between strains ε and the displacements $\mathbf{u}$ can be written as

$$\varepsilon = \left[\varepsilon_r, \varepsilon_z, \gamma_{rz}, \varepsilon_\theta\right] \qquad (5.6)$$

$$u = \left[\frac{\partial u}{\partial r}, \frac{\partial w}{\partial z}, \frac{\partial u}{\partial z} + \frac{\partial w}{\partial r}, \frac{u}{r}\right]^T \qquad (5.7)$$
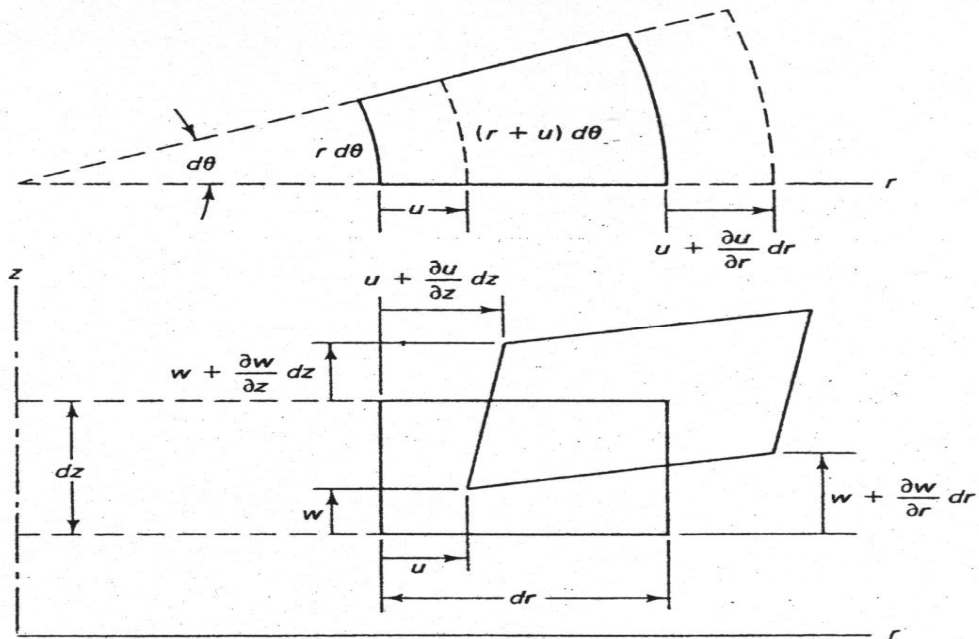
Figure 5.4. Deformation of elemental volume [24].

The stress vector is correspondingly defined as

$$\sigma = \left[\sigma_r, \sigma_z, \tau_{rz}, \sigma_\theta\right]^T \qquad (5.8)$$

The stress-strain relations are given in the form shown below:

$$\sigma = \mathbf{D}\varepsilon \qquad (5.9)$$

where the (4×4) matrix $\mathbf{D}$ is [24]:

$$\mathbf{D} = \frac{E(1-\upsilon)}{(1+\upsilon)(1-2\upsilon)}
\begin{bmatrix}
1 & \dfrac{\upsilon}{1-\upsilon} & 0 & \dfrac{\upsilon}{1-\upsilon} \\
\dfrac{\upsilon}{1-\upsilon} & 1 & 0 & \dfrac{\upsilon}{1-\upsilon} \\
0 & 0 & \dfrac{1-2\upsilon}{2(1-\upsilon)} & 0 \\
\dfrac{\upsilon}{1-\upsilon} & \dfrac{\upsilon}{1-\upsilon} & 0 & 1
\end{bmatrix} \qquad (5.10)$$

To use the axisymmetric conditions has some advantages, such as simplicity in modelling, less RAM requirements and higher solution speed than a 3-D model. Because of these advantages, the element type is selected as a 2-D axisymmetric element and defined by the following command:

Preprocessor > Add/Edit/Delete..... > Options > Element Behavior – Axisymmetric

The next step is to define the material properties. More than one material property can be defined by giving different material numbers to them. In structural analysis, Elastic Modulus, Poisson's ratio and/or Shear Modulus are needed to be defined:

Preprocessor > Material Props > Isotropic

The material properties in this study are taken as:

Whole cylinder without rigid inclusion: Elastic Modulus (E) : 200×10^9 N/m^2

Poisson's ratio (v)   : 0.3

Rigid Inclusion   : Elastic Modulus (E) : 2×10^{18} N/m^2

Poisson's ratio (v)   : 1×10^{-9}

Rigid inclusion means that the material embedded inside another material is unmovable, so the all displacements of the rigid inclusion is zero. Thus, the strain is also zero and according to the Hooke's law $(\sigma = E\varepsilon)$, this zero value of the strain leads the elastic modulus of the rigid inclusion to a value of infinity. In a numerical approach, the infinity can be defined as to get a very big value with respect to the other values. In other words, in order to achieve the infinity condition, the ratio of the elastic moduluses of the rigid inclusion/matrix should be very big. After defining the material properties, the model can be built by using appropriate commands. As it is mentioned before, the axisymmetric condition is used in this analysis, so a 2-D model can be built in order to do the finite element analysis of the problem. The cross sectional area of the whole problem has a rectangular shape and due to symmetry about x-axis, it will be sufficient to consider half of the 2-D rectangular cross-sectional area. Because of the special conditions, the geometry is divided into four smaller rectangles (Figure 5.5).
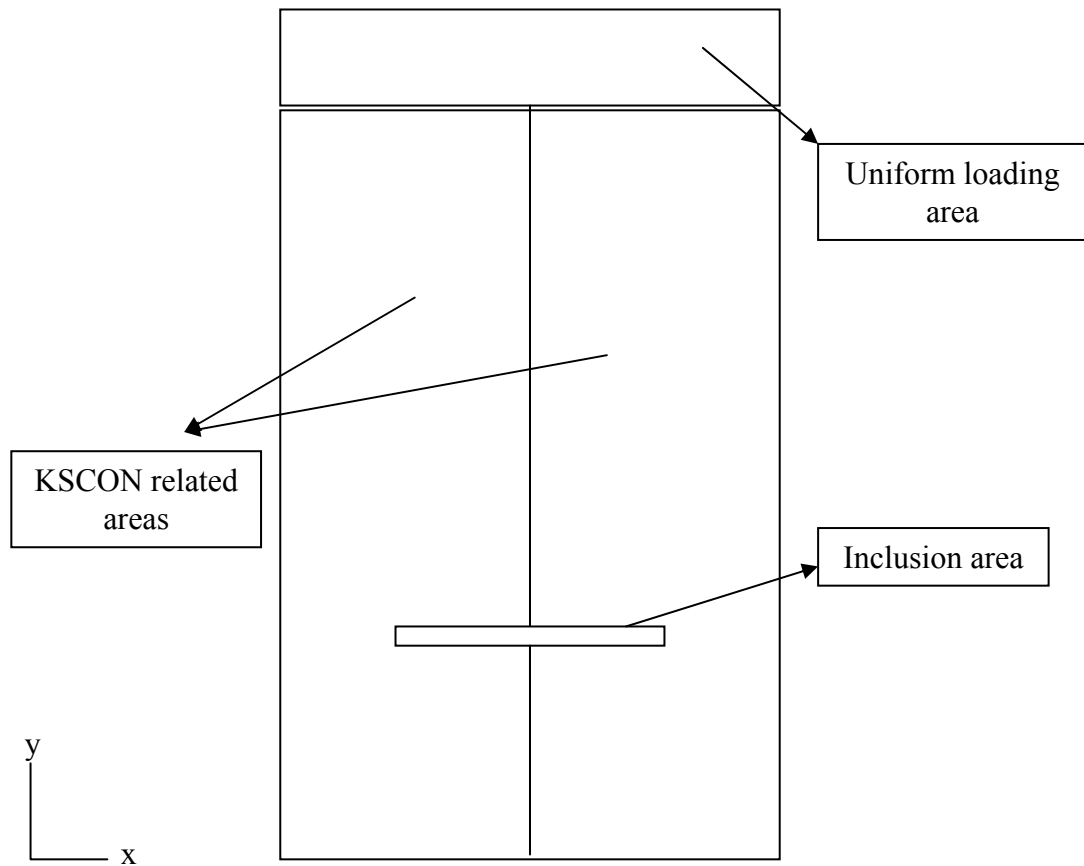
Figure 5.5 2-D Model of the problem

Two similar rectangular areas are formed because of the unique useness of command KSCON, which is used for obtaining singular elements at the crack tips in an area. In this study, there are two crack tips. Inside these two rectangles, there is another small rectangular area, which represents the rigid inclusion. In the analytical study, the inclusion's thickness is assumed to be negligible. So, a rectangle with a small thickness with respect to the height of the whole body is assumed as a negligible dimension. The last rectangle located at the upper part of the two bigger ones is built in order to apply uniform pressure to the line at the upper part of this rectangle. The main problem of building the model is to decide the way of how to build, such as by using the command that directly forms a rectangle or by forming keypoints at the critical points of the structure first and then the rectangles with these keypoints. The best way is the second one. Because in order to use the KSCON command, it is required to define a keypoint at the crack tip. So, the first step in construction of the geometry is to define the keypoints:

Preprocessor > Create > Keypoints > In Active CS

One can define more than one keypoint by giving different numbers. In this study, sixteen keypoints are defined. The next step is to build the required geometry by connecting the keypoints by lines:

Preprocessor > Create > Arbitrary > Through KPs

After building the four different parts of the whole model (Figure 5.5), it is required to transform these four seperate parts into a unique part by glueing them:

Preprocessor > Operate > Glue > Areas > Pick All

After modelling the problem, it is needed to define the attributes, such as material number, real constant set number, element type number and element coordinate system, of the different parts of the whole model. This task can be achieved by clicking the related areas and then making appropriate changes in the table on the screen, especially the material number and element type number. In this study, only one element type is defined, so there is no need to deal with it, but on the other hand two materials with different numbers are defined, such as 1 and 2, for the whole body without rigid inclusion and the rigid inclusion, so it is required to attribute these materials to the related areas:

Preprocessor > Define > Picked Areas

The next step is to mesh the whole model, in other words discretization of the whole model takes place. The first step is to define the required properties of KSCON command in order to form singular elements at the crack tips (Figure 5.6). If a special element is introduced in order to consider the singularity of the stress-strain in the vicinity of the crack tip a more accurate solution can be obtained. This is the way that an accurate stress intensity factor value can be obtained with a rather coarse mesh [25]:

Preprocessor > Size Cntrls > Concentrat KPs > Create
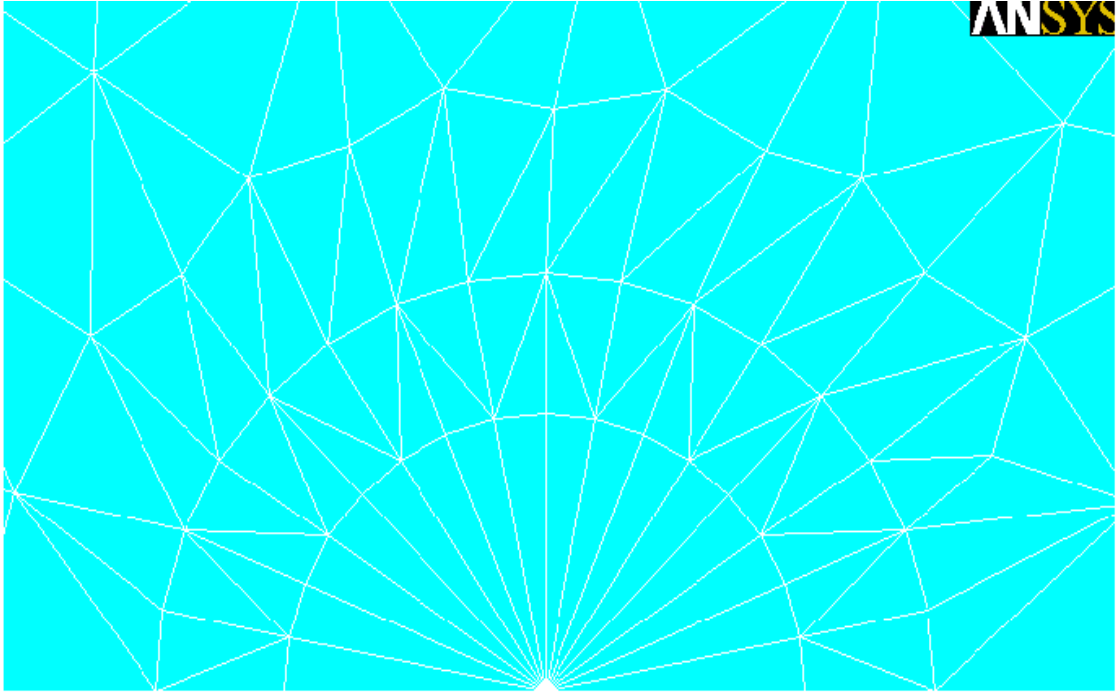
Figure 5.6. Mesh generation at the crack tip.

After clicking the commands repectively, it is required to pick the keypoint at the one of the crack tip. Then a table appears on the screen. In this table, the number of the keypoint at the crack tip, radius of 1st row of elements, radius ratio (2nd row/1st), number of elements around circumference values are needed to be defined. In order to efficiently model the $\sqrt{r}$ type variation of displacements near the crack tip (r being the distance from the crack tip), quarter-point elements (QPEs) have been used to mesh the region surrounding the tip. QPEs were introduced by Barsoum and Henshell and Shaw and are essentially six-noded triangular elements with their mid-side nodes shifted to quarter-point positions. It has been shown that, depending on the mesh and crack configuration, there exists an optimum size of QPE, smaller or larger QPEs compromise the accuracy of results. Murti and Valliappan have suggested that the optimum size of QPE is 15-25% of the crack length. However for deeply cracked configurations, due to constraint of the length of the remaining ligament, QPEs of such sizes cannot be used. An alternative strategy in these situations is to use smaller QPEs surrounded by a layer of transitional elements (TEs), which are 1.5244 times larger than the QPEs. The TEs stabilize the accuracy of calculated SIFs to within acceptable errors for QPEs smaller than the optimum [2]. On the other hand, ANSYS guidelines recommend that the radius of 1st row of elements should be "crack length/8" or smaller and in the circumferential

direction, there should be roughly one element every 30 or 40 degrees. In this study, the maximum radius used is "crack length/10" or less, the number of elements is 16, so roughly every 11-12 degrees there is one singular element and radius ratio is taken as 0.5. Add to these, despite the offer of Murti and Vallipan about the optimum radius of 1st row of elements, it is seen that the value of this radius doesn't affect the results significantly. On the other hand, the number of elements is the most important and effective parameter, so a high number of elements at the crack tip should be taken. The KSCON command can be used once in an area, so if there is more than one critical point needed singular elements, there should be a number of areas at least the number of critical points. And also it should be noted that KSCON command is restricted to the 2-D analyses. So, if a 3-D analysis is done, then the macro FRACT is used to create SOLID95 crack tip element from the SOLID 45 model using a weighted midside node position (quarter point location) [25].

After defining the required properties of singular elements, the next step is to define mesh size properties of the other lines in the model in order to obtain a fine meshed model which is commonly used in this study:

Preprocessor > MeshTool > Lines > Set

After picking lines which one wants to modify the mesh size properties, it is needed to give the value of the required "element edge length" or "number of element divisions". For a finer meshed model, smaller values should be given. In this study, "number of element divisions" is modified as giving appropriate values according to experiences gained before. There is another parameter as "spacing ratio" on this table which has a default value of "1". If one changes this value, lengths of the meshes on lines increase or decrease linearly. This is generally an important property in the finite element method, which is needed to use coarser meshing far from the critical points. But, in this study the model is a bit complex, and there are more than one critical point, such as crack tips and inclusions. So, the default value is used without any change. It is seen that when the results are compared with changed and unchanged spacing ratio, they are similar.

The next step after modifying the default values of meshing parameters is to mesh the model:

Preprocessor > MeshTool > Mesh > Pick All

After picking the required commands for meshing, the meshed model of the whole geometry (Figure 5.7) is obtained and the model is discretized into a high number of elements. Meshing is the last step of the preprocessor part.
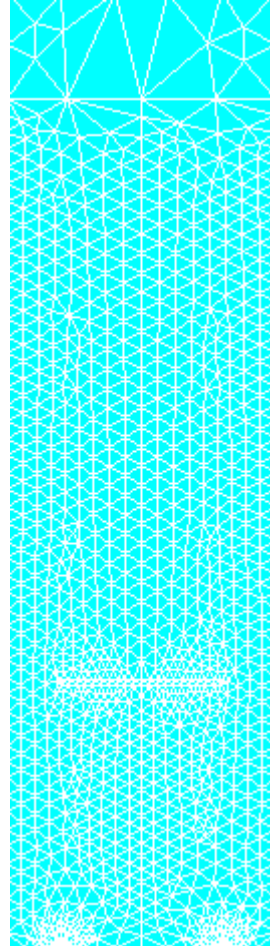
Figure 5.7. The meshed model of the whole geometry.

5.3 Solution part

In the solution part, boundary conditions are applied. First step of the solution part is to define the type of analysis such as static, modal, harmonic, transient, spectrum, eigen buckling and substracting. In this study, there is a static loading so that static analysis is defined as the type of the analysis. It is not necessary to define by picking the command for static analysis because it is the default analysis type:

Solution > Analysis Type > New Analysis > Static

First step of applying boundary conditions is to constrain translation of nodes where needed. In this study, UY degree of freedom of the nodes at the base line except the nodes on the crack line is constrained because of the symmetry condition according to x-axis:

Solution > Apply > Structural > Displacement > On Keypoints

After picking the commands respectively and then picking the keypoints at the left or right crack tip and corner of the base line , it is needed to fill the table on the interface.

In this table "DOFs to be constrained", "Displacement Value" and "Expand Displacement to nodes" data can be defined. For this study, in order to constrain the UY degrees of freedom of nodes due to the symmetry about the x-axis, from the choice of "DOFs to be constrained" UY is selected, then "Displacement value" is given as 0, and lastly "Expand Displacement to nodes" is modifies as "Yes", means that all the nodes between the selected keypoints are also selected and constrained as the given values at the same table. Thus, all nodes between keypoints at the crack tips and corners at the base line are constrained as unmovable in the y-direction. In other words, at z = 0, the nodes on the r axis remain constant in the z-direction except the nodes on the crack line. Add to this, this constrained condition lets us to obtain a crack when a tensile load applied at the upper part of the model or a pressure exerted at the crack line.

The next step is to apply pressure at the upper line of the model:

Solution > Apply > Pressure > On Lines

After picking to the related line, it is needed to give the pressure value. There are two blanks in the table for "Pressure Value" and "Optional pressure at J end". If there is a uniform load distribution, only "Pressure Value" data is sufficient, but for a linear load distribution, the value of "Optional pressure at J end" is needed. J end is the right corner of the line. In this study, there is a uniform load distribution and a pressure value of 100 MPa is taken. According to the 2-D problem, a load having a unit of N/m is used and the load exerted defines the pressure value 100 MPa by using the formula shown below:

$$\text{Load (N/m)} = \text{Pressure (N/m}^2) \times (\text{outer radius (m)} - \text{inner radius (m)}) \qquad (5.11)$$

Another keypoint here is the sign of the value for the pressure value. "+" defines a compressive load and "-" defines a tensile load.

In Figure 5.8, applied boundary conditions on the model can be seen:
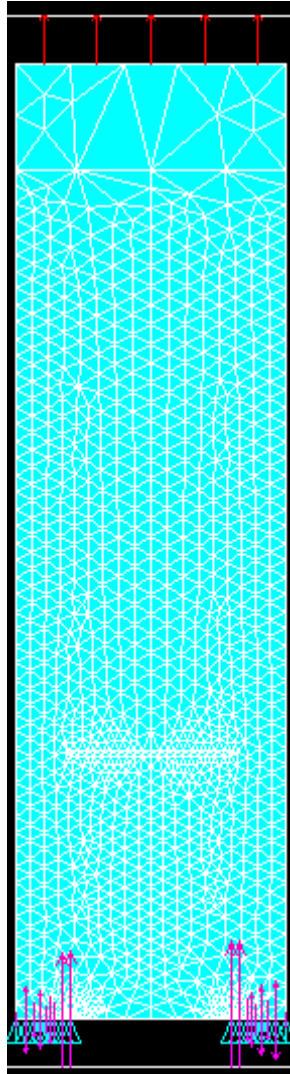
F**igure 5.8.** Boundary conditions of the problem.

The last step in the solution part is to start the solution process of matrices and equations which are formed by the given data from the beginning of the analysis to this step:

Solution > Solve > Current LS > OK

5.4 Postprocessing part

The last step of the analysis is the postprocessing part where the results from the analysis are obtained. In this study, the results of SIFs at the two crack tips and stress distribution inside the model have special importance. Calculation of SIFs at the crack tips can be accomplished in the Postprocessing part of the ANSYS by KCALC command with the displacement extrapolation method. There are also different methods such as the J-integral via the domain integral method [26], modified crack closure technique [27], virtual crack extension method [5]. The analysis uses a fit of the nodal displacements in the vicinity of the crack. The actual displacements at and near a crack for linear elastic materials are:

$$u = \frac{K_I}{4G}\sqrt{\frac{r}{2\pi}}\left((2\kappa-1)\cos\frac{\theta}{2} - \cos\frac{3\theta}{2}\right) - \frac{K_{II}}{4G}\sqrt{\frac{r}{2\pi}}\left((2\kappa+3)\sin\frac{\theta}{2} + \sin\frac{3\theta}{2}\right) + O(r) \quad (5.12)$$

$$v = \frac{K_I}{4G}\sqrt{\frac{r}{2\pi}}\left((2\kappa-1)\sin\frac{\theta}{2} - \sin\frac{3\theta}{2}\right) - \frac{K_{II}}{4G}\sqrt{\frac{r}{2\pi}}\left((2\kappa+3)\cos\frac{\theta}{2} + \cos\frac{3\theta}{2}\right) + O(r) \quad (5.13)$$

$$w = \frac{2K_{III}}{G}\sqrt{\frac{r}{2\pi}}\sin\frac{\theta}{2} + O(r) \quad (5.14)$$

where:

u,v,w = displacements in a local Cartesian coordinate system as shown in Figure 5.9.

r, θ = coordinates in a local cylindirical coordinate system also shown in Figure 5.9.

G = shear modulus

K_I, K_{II}, K_{III} = stress intensity factors relating to deformation shapes shown in Figure 5.10.

$\kappa = 3 - 4v$ if plane strain or axisymmetric

$\kappa = \dfrac{3-v}{1+v}$ if plane stress

v = Poisson's ratio

$O(r)$ = terms of order r or higher
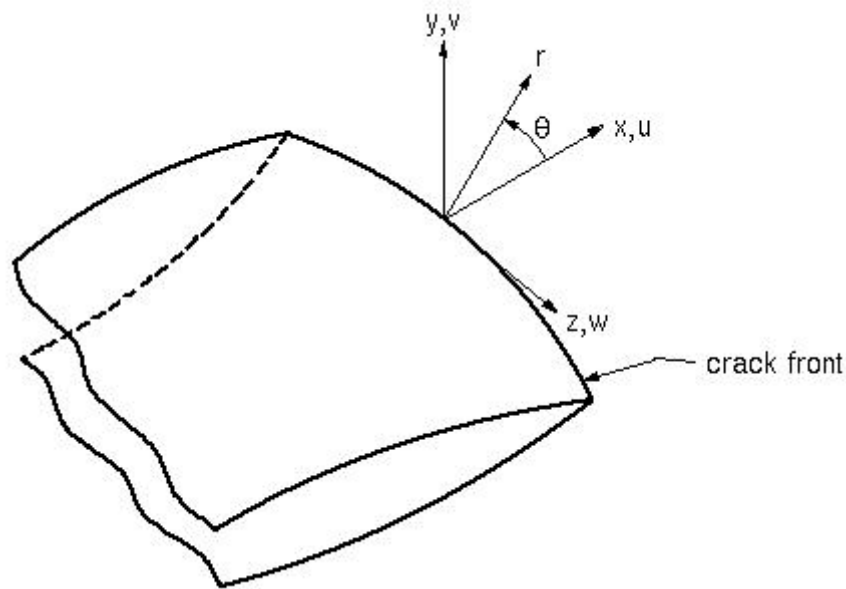
Figure 5.9. Local coordinates measured from a 3-D crack front [28].
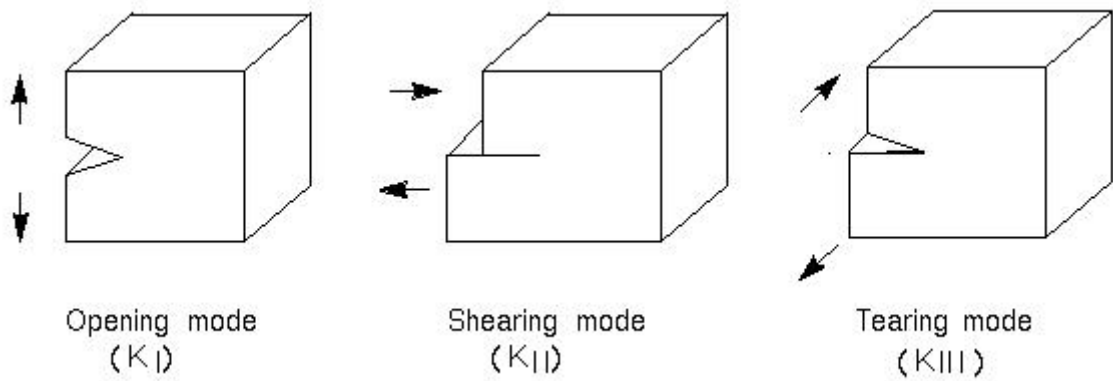
Figure 5.10. The three basic modes of fracture [28].

Evaluating Equations 5.12-5.14 at $\theta = \pm 180°$ and dropping the higher order terms yields:

$$u = +\frac{K_{II}}{2G}\sqrt{\frac{r}{2\pi}}(1 + \kappa) \qquad (5.15)$$

$$v = +\frac{K_I}{2G}\sqrt{\frac{r}{2\pi}}(1 + \kappa) \qquad (5.16)$$

$$w = +\frac{2K_{III}}{G}\sqrt{\frac{r}{2\pi}}$$ (5.17)

For models symmetric about the crack plane(half-crack model,Figure 5.11(a)), Equations 5.15-5.17 can be reorganized to give:

$$K_I = \sqrt{2\pi}\,\frac{2G}{1+\kappa}\frac{|v|}{\sqrt{r}}$$ (5.18)

$$K_{II} = \sqrt{2\pi}\,\frac{2G}{1+\kappa}\frac{|u|}{\sqrt{r}}$$ (5.19)

$$K_{III} = \sqrt{2\pi}\,\frac{2G}{1+\kappa}\frac{|w|}{\sqrt{r}}$$ (5.20)
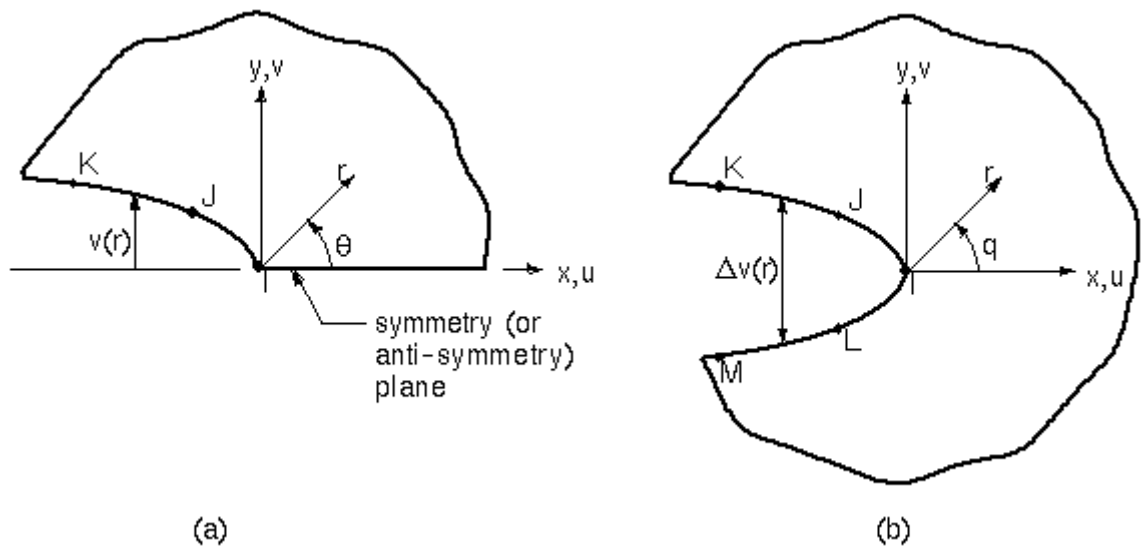
Figure 5.11. Nodes used for approximate crack-tip displacements: **(a)** Half model **(b)** Full model

and for case of no symmetry (full-crack model, Figure 5.11(b)),

$$K_I = \sqrt{2\pi} \frac{G}{1+\kappa} \frac{|\Delta v|}{\sqrt{r}} \qquad (5.21)$$

$$K_{II} = \sqrt{2\pi} \frac{G}{1+\kappa} \frac{|\Delta u|}{\sqrt{r}} \qquad (5.22)$$

$$K_{III} = \sqrt{2\pi} \frac{G}{1+\kappa} \frac{|\Delta w|}{\sqrt{r}} \qquad (5.23)$$

where Δv, Δu, and Δw are the motions of one crack face with respect to the other. As the above six equations are similar, consider only the first one further. The final factor is $\frac{|v|}{\sqrt{r}}$ which needs to be evaluated based on the nodal displacements and locations. As shown in Figure 5.11(a), three points are available. v is normalized so that v at node I is zero. Then A and be determined so that

$$\frac{|v|}{\sqrt{r}} = A + Br \qquad (5.24)$$

at points J and K. Next, let r approaches 0:

$$\lim_{r \to 0} \frac{|v|}{\sqrt{r}} = A \qquad (5.25)$$

Thus, Equation 5.18 becomes

$$K_I = \sqrt{2\pi} \frac{2GA}{1+\kappa} \qquad (5.26)$$

Equations 5.19-5.23 are also fit in the same manner [28].As shown above, the KSCON command can calculate the mixed-mode stress intensity factors K_I, $K_{II,}$ and K_{III}. This

command is limited to linear elastic problems with a homogenous, isotropic material near the crack region because the equations used in calculation process is related to the linear elastic fracture mechanics. In order to use KCALC command properly, it is firstly desired to define a local crack-tip coordinate system, with X parallel to the crack face and Y perpendicular to the crack face. This can be done by the following way:

Workplane > Local Coordinate Systems > Create Local CS > At Specified Location+

After the sequence of picking the crack tip and OK twice forms a local coordinate system at that crack tip. Then, it is desired to define a path along the crack face. The first node on the path should be the crack-tip node. For a half crack model, two additional nodes are required, both along the crack face. For a full-crack model, where both crack faces are included, four additional nodes are required: two along one crack face and two along the other:

General Postproc > Path Operations > Define Path > By nodes

Now, the crack face is defined to the program. The third and next step is to calculate the K_I, $K_{II,}$ and K_{III}:

General Postproc > Nodal Calcs > Stress Int Factr

After picking these commands respectively, it is required to give some properties about the problem, such as the displacement extrapolation is based on whether plane strain, axisymmetric or plane stress condition; material number for extrapolation; and lastly model type of the crack whether half-symmetric, half-asymmetric or full.

In this study, firstly, a local coordinate system is defined at the one of the crack tip. Secondly, by picking the nodes at the crack tip and two neighbour nodes at the right side of the left crack tip or left side of the right crack tip, respectively, a half crack model is defined. Thirdly, in order to calculate K_I, $K_{II,}$ and K_{III} at that crack tips, default values such as plane strain, "1" for the material number and half-symmetric boundary conditions are used.

The stress distribution and displacements for the problem can also be obtained:

General Postproc > Plot Results > Nodal Solu...

It can easily be seen that, there is an intensification at the crack tips and the tips of the inclusions. In this case, it is clear that the regular stress distribution of the whole body is disturbed by the effect of the crack and inclusions. (See Appendix B)

As mentioned before, instead of using the graphical user interface, APDL can be used in all steps of the analysis. In this study, until the step of attributing material properties to the related areas, a log file written in APDL language is used. So, the repeating steps in all analyses are done very fastly and parameters are changed very easily. A sample log file used in this study is given in Appendix C.

Add to these, a convergence test [10] should be done in order to get accurate results and prevent from more time consuming than the optimum analysis. This test can be done by increasing the number of meshes and doing the same analysis, then comparing the results with each other. With the increasing number of mesh, the differences between the results become smaller, so the minimum number where the constantancy starts is the optimum mesh number of the analysis. In this study, it is not need to do such a test in every analysis, because there is not a significant difference between the results whether the coarse or fine mesh used.

Another important point of this study is how the infinity condition of the height of the solid is achieved. This task is achieved by doing the same analysis and increasing the height of the geometry. Then, the results are compared with each other and when the discrepancy between them are insignificant, it can be said that the condition of infinity for the height of the geometry is obtained.

CHAPTER 6

RESULTS AND DISCUSSION

The cracked infinite hollow cylinder with two rigid inclusions is completely defined by the dimensionless parameters L/A, a/A, b/A, c/A, d/A, Poisson's ratio ν and $p_0/2\mu$. Distances are normalized with A, the inner radius of the cylinder. The stress intensity factors at the crack tips are normalized in the form given below:

$$\bar{k}_{1a} = k_{1a}/\left(p_0\sqrt{(b-a)/2}\right) \qquad\qquad \bar{k}_{1b} = k_{1b}/\left(p_0\sqrt{(b-a)/2}\right)$$

Due to the dependency of the whole geometric parameters on A, the results of the finite element analysis by the use of ANSYS for different values of A are obtained. As it is mentioned before, in all analyses the applied tensile load is taken as 100 MPa. In the following figures,in some cases discrepencies have been occurred. For the dispacement extrapolation method, the differences around 5% can be assumed as in acceptable limits. In order to verify the accuracy of the model, the analytical results of the study of Erdol and Erdogan [13] are compared with the finite element analysis results (Figures 6.1-6.3). It can easily be seen in these figures that there is a good agreement between numerical and analytical results, so the model is proved to be reliable for further analyses.
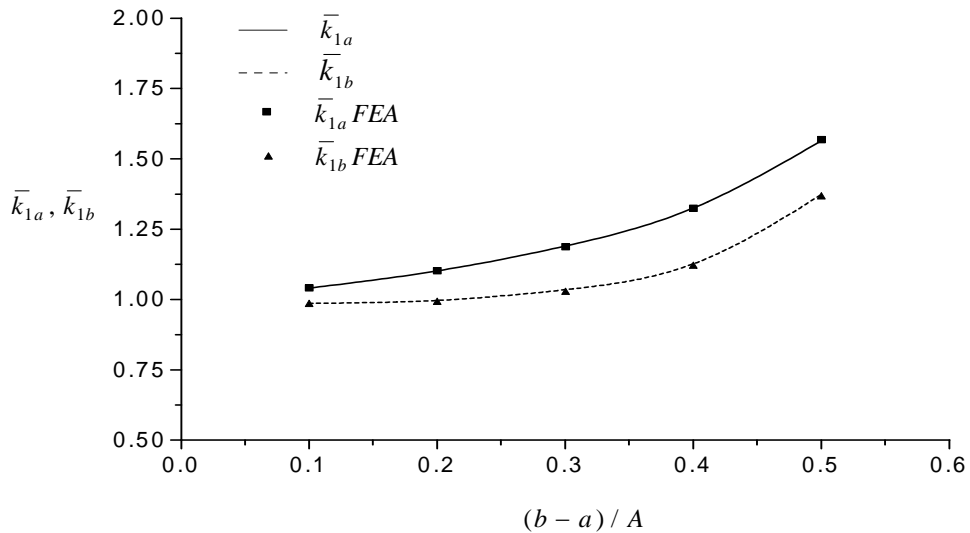
Figure 6.1. Variation of Normalized Stress Intensity Factors $\bar{k}_{1a}$, $\bar{k}_{1b}$ when A=0.2B, a = 0.4B, $\nu = 0.3$.
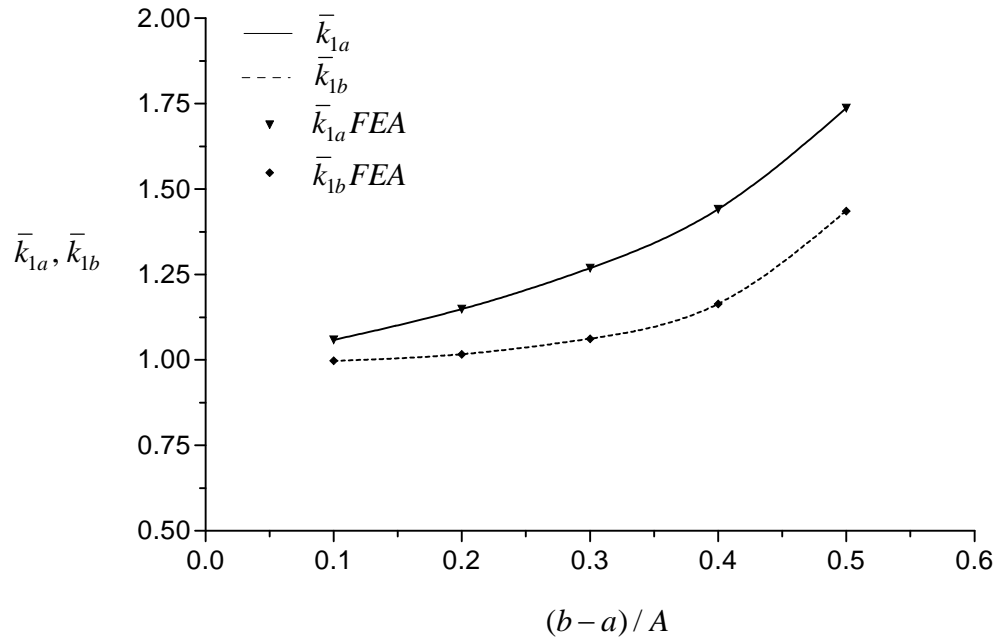
Figure 6.2. Variation of Normalized Stress Intensity Factors $\bar{k}_{1a}$, $\bar{k}_{1b}$ when A=0.3B, a $= 0.4$B, $\nu = 0.3$.
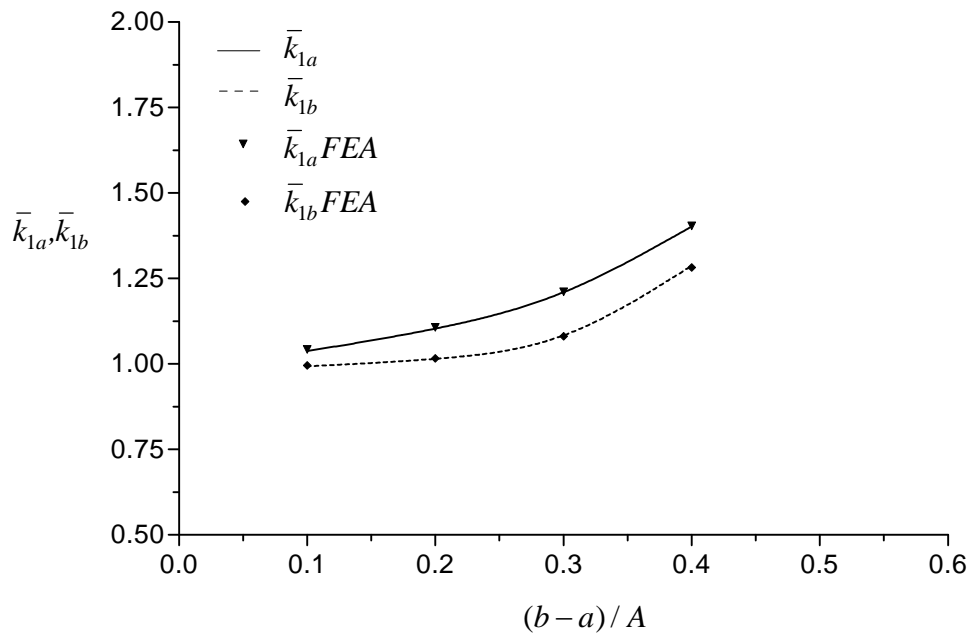
Figure 6.3. Variation of Normalized Stress Intensity Factors $\bar{k}_{1a}$, $\bar{k}_{1b}$ when A=0.3B, a $= 0.5$B, $\nu = 0.3$.

Figure 6.4 shows variation of normalized stress intensity factors $\bar{k}_{1a}$ and $\bar{k}_{1b}$ with $(b - a)/A$ when $L = 0.25A$ and $d - c = 0.15A$. Stress intensity factors $\bar{k}_{1a}$ and $\bar{k}_{1b}$ increase as crack width increases. In this figure, the distance between the rigid inclusions and the crack is small and it can easily be seen that the analytical and numerical results are in good agreement.
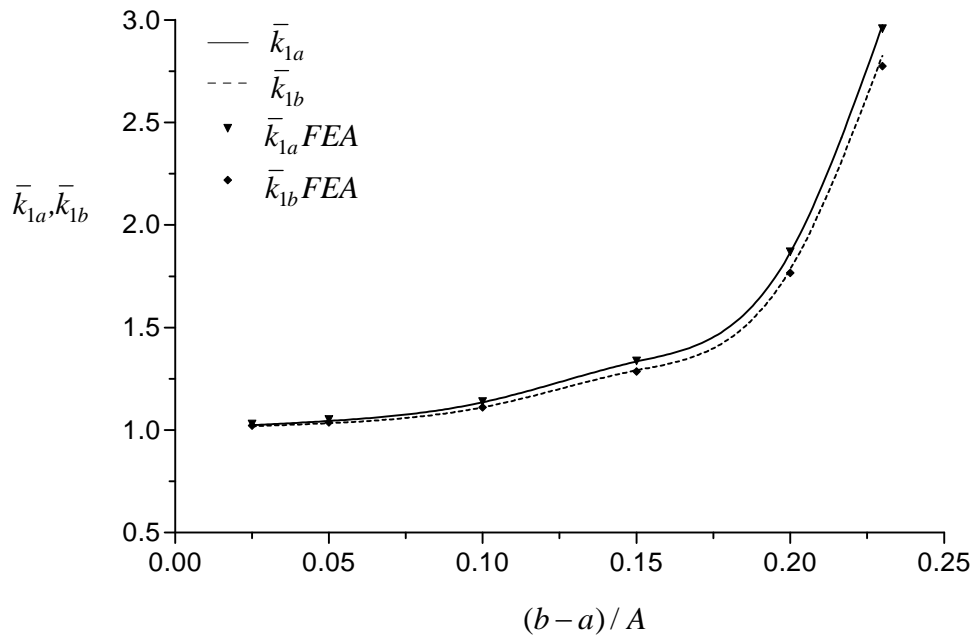
Figure 6.4. Variation of Normalized Stress Intensity Factors $\bar{k}_{1a}$, $\bar{k}_{1b}$ when B =1.25A, L = 0.25A, d - c = 0.15A, a + b = c + d = 2.25A, ν = 0.3.

Figures 6.5-6.7 show variations of normalized stress intensity factors $\bar{k}_{1a}$ and $\bar{k}_{1b}$ with $(d - c)/A$ when $L = 0.5A$ and $b - a = 0.15A$ for different ν values; 0.2, 0.3, 0.4, respectively. The inclusions and the crack are close to each other. As it is seen from these figures $\bar{k}_{1a}$ decreases whereas $\bar{k}_{1b}$ increases with increasing inclusion widths, and there are acceptable differences between numerical and analytical results. The differences increase with increasing ν values.
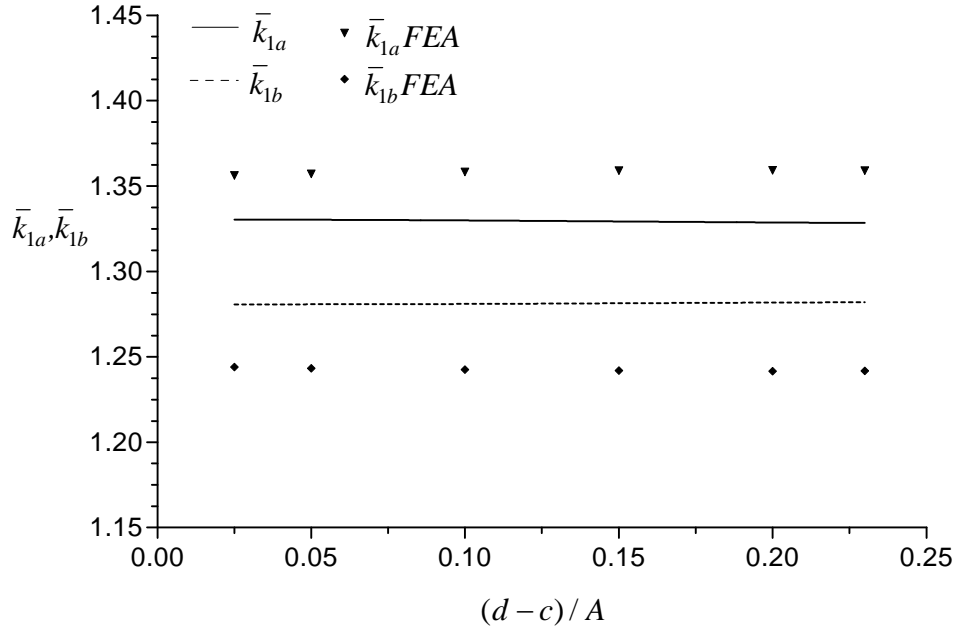
Figure 6.5. Variation of Normalized Stress Intensity Factors $\bar{k}_{1a}$, $\bar{k}_{1b}$ when B =1.25A, L = 0.5A, b - a = 0.15A, a + b = c + d = 2.25A, ν = 0.2.
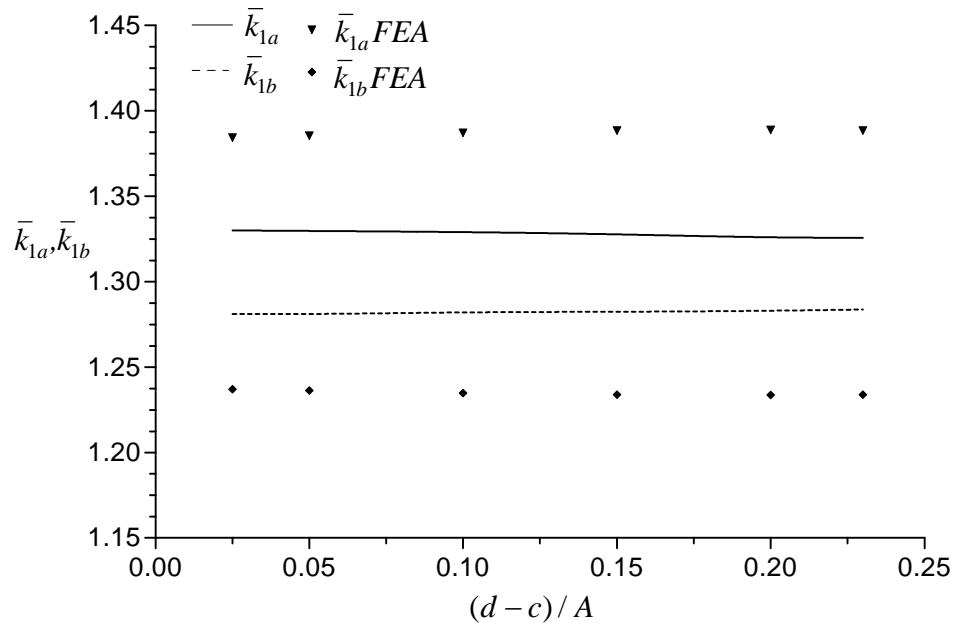
Figure 6.6. Variation of Normalized Stress Intensity Factors $\bar{k}_{1a}$, $\bar{k}_{1b}$ when B =1.25A, L = 0.5A, b - a = 0.15A, a + b = c + d = 2.25A, ν = 0.3.
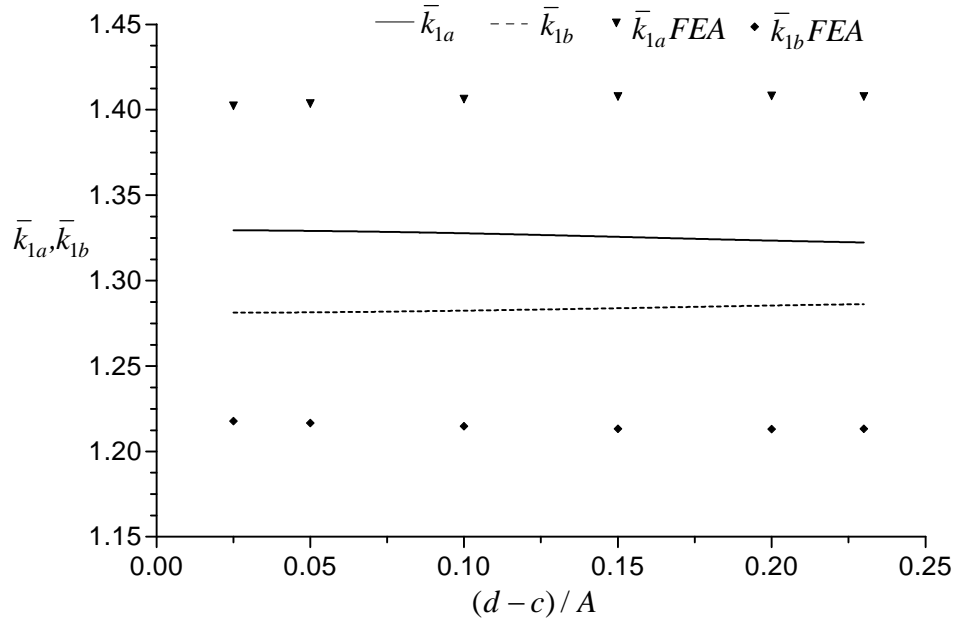
Figure 6.7. Variation of Normalized Stress Intensity Factors $\bar{k}_{1a}$, $\bar{k}_{1b}$ when B =1.25A, L = 0.5A, b - a = 0.15A, a + b = c + d = 2.25A, ν = 0.4.

Figure 6.8-6.10 shows variations of normalized stress intensity factors $\bar{k}_{1a}$ and $\bar{k}_{1b}$ with (d – c)/A when L =4.0A and b - a = 0.15A for different ν values.
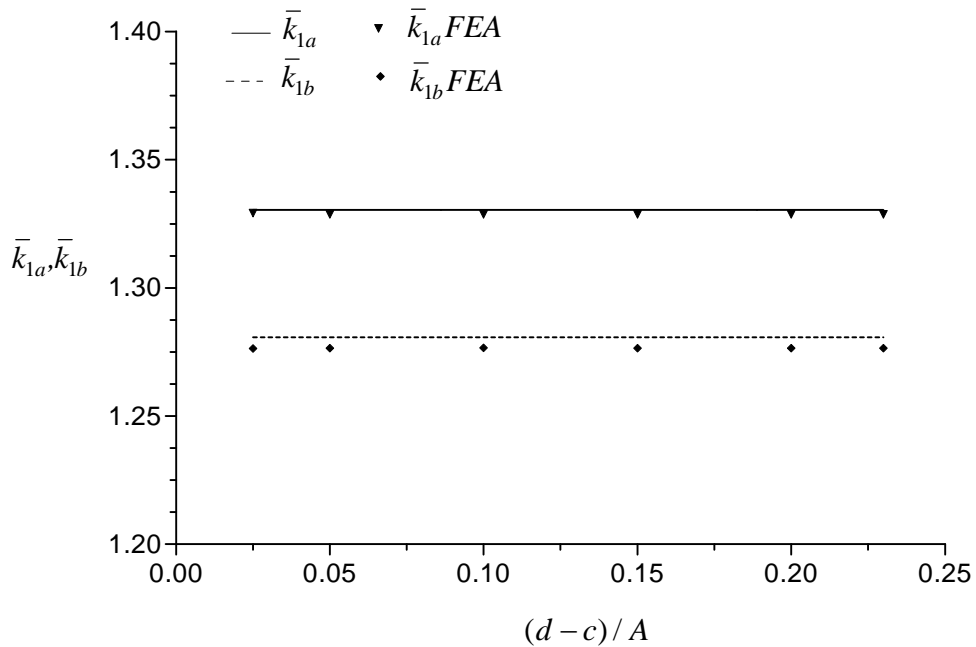
Figure 6.8. Variation of Normalized Stress Intensity Factors $\bar{k}_{1a}$, $\bar{k}_{1b}$ when B =1.25A, L = 4.0A, b - a = 0.15A, a + b = c + d = 2.25A, ν = 0.2.

In these figures, $\bar{k}_{1a}$ and $\bar{k}_{1b}$ remains constant with increasing inclusion widths, the analytical and numerical values coincide well with each other.
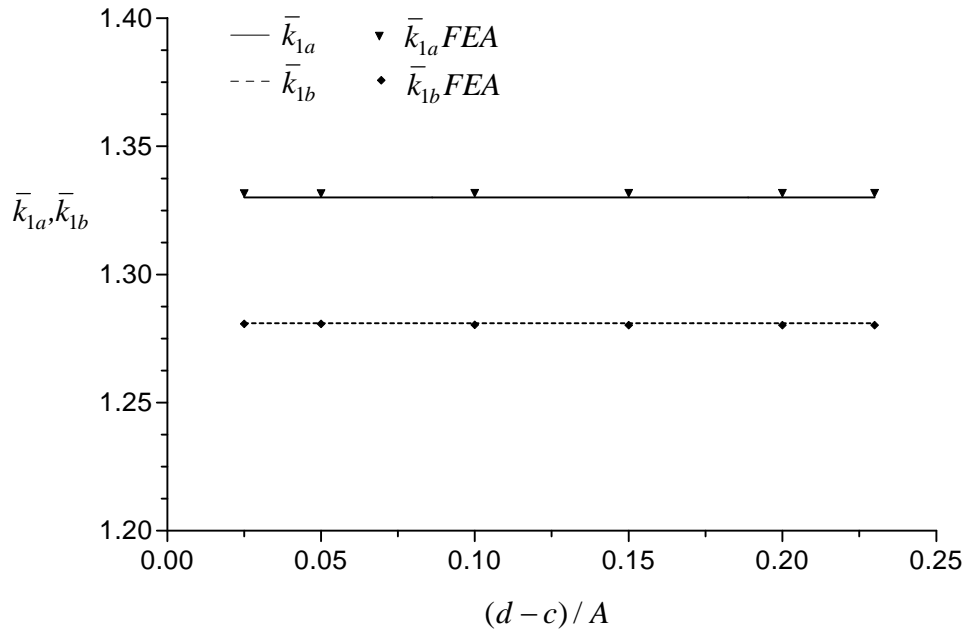
Figure 6.9. Variation of Normalized Stress Intensity Factors $\bar{k}_{1a}$, $\bar{k}_{1b}$ when B =1.25A,

L = 4.0A, b - a = 0.15A, a + b = c + d = 2.25A, ν = 0.3.
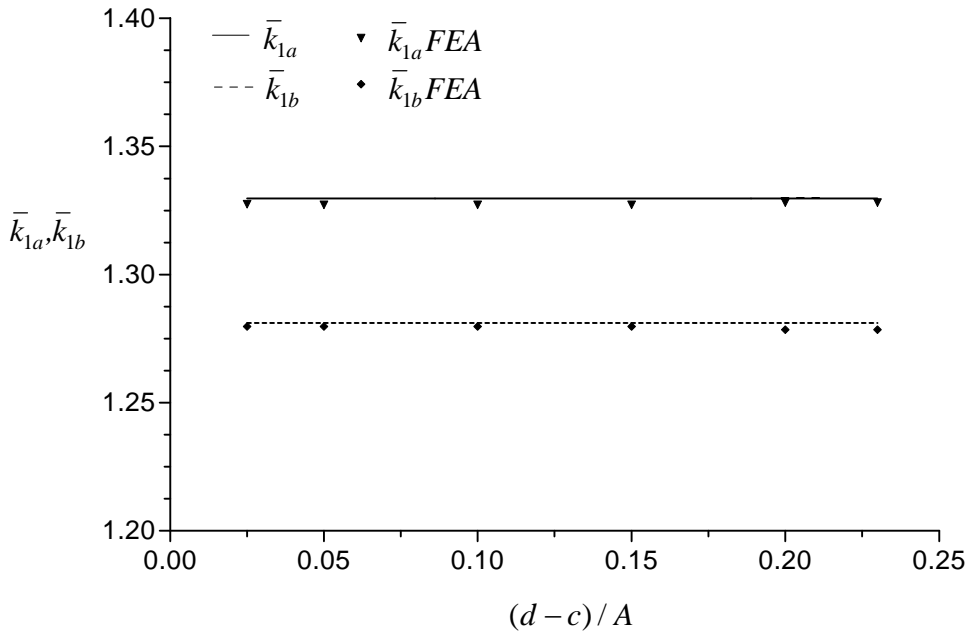
Figure 6.10. Variation of Normalized Stress Intensity Factors $\bar{k}_{1a}$, $\bar{k}_{1b}$ when B =1.25A,

L = 4.0A, b - a = 0.15A, a + b = c + d = 2.25A, ν = 0.4.

Figures 6.11-6.13 show variations of normalized stress intensity factors at the crack tips $\bar{k}_{1a}$ and $\bar{k}_{1b}$ with (d – c)/A when L = 0.5A and b - a = 0.15A for different ν values; 0.2, 0.3, 0.4, respectively. The inclusions and the crack are close to each other. The difference between these figures and Figures 6.5-6.7 is the thickness of the hollow cylinder. There are acceptable differences between numerical and analytical results. The differences increase with increasing ν and width of the rigid inclusion values. As it is seen from these figures $\bar{k}_{1a}$ decreases whereas $\bar{k}_{1b}$ increases with increasing inclusion widths for analytical results, but on the other hand numerical results behave reversely to the analytical results.
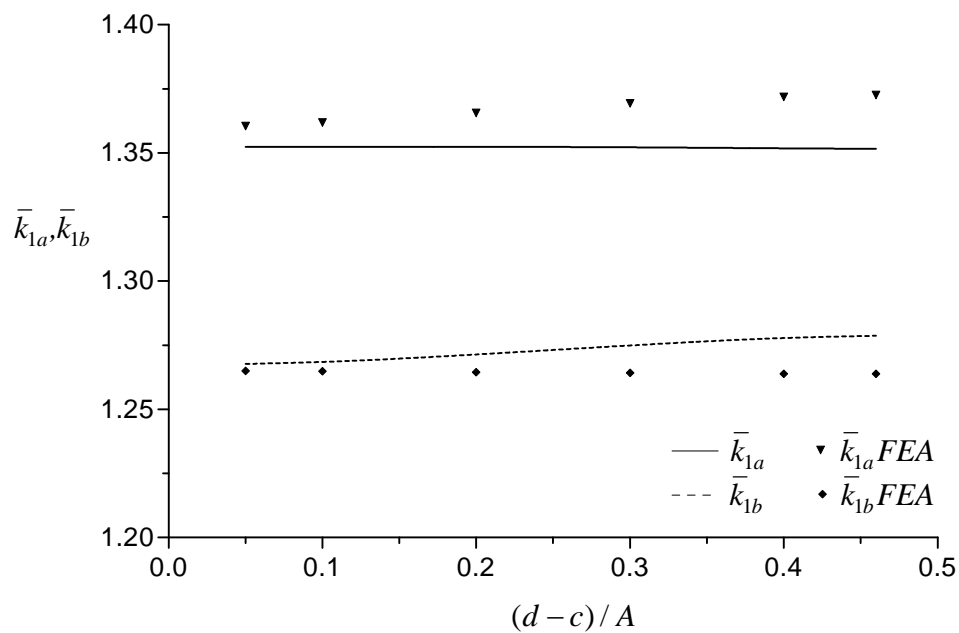
Figure 6.11. Variation of Normalized Stress Intensity Factors $\bar{k}_{1a}$, $\bar{k}_{1b}$ when B =1.5A, L = 0.5A, b - a = 0.3A, a + b = c + d = 2.5A, ν = 0.2.
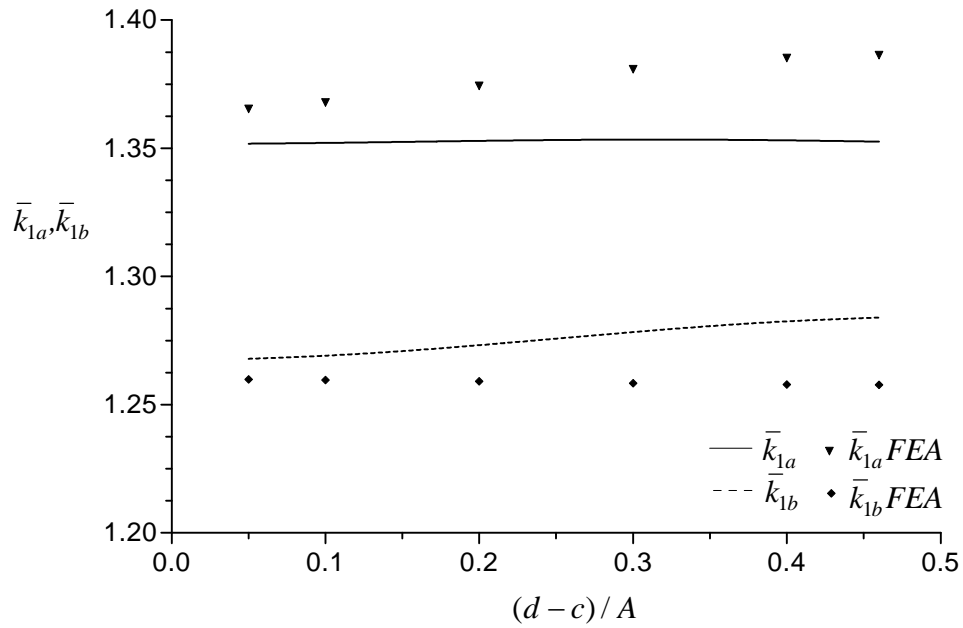
Figure 6.12. Variation of Normalized Stress Intensity Factors $\bar{k}_{1a}$, $\bar{k}_{1b}$ when B =1.5A, L = 0.5A, b - a = 0.3A, a + b = c + d = 2.5A, ν = 0.3.
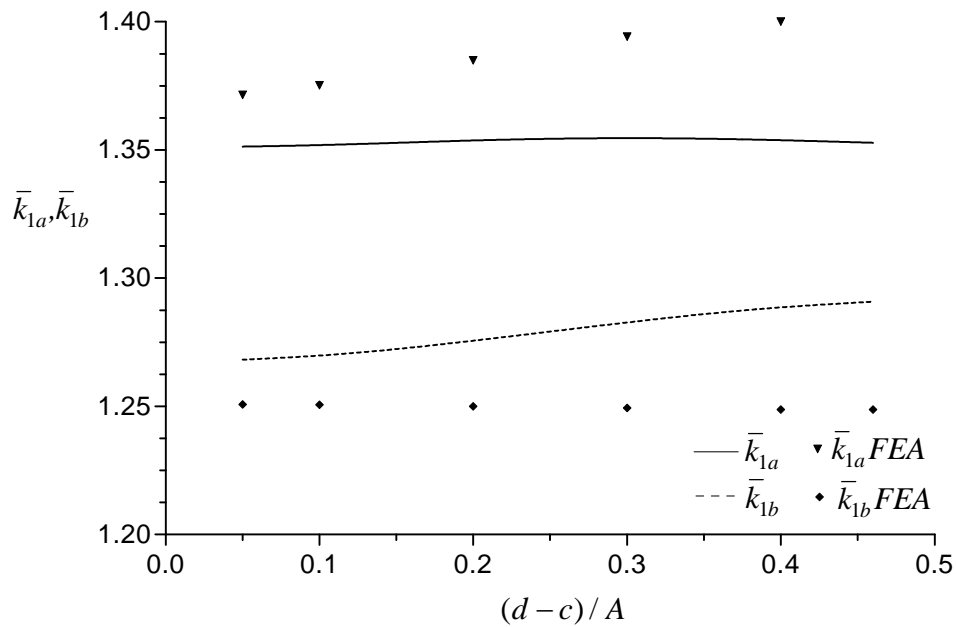
Figure 6.13. Variation of Normalized Stress Intensity Factors $\bar{k}_{1a}$, $\bar{k}_{1b}$ when B =1.5A, L = 0.5A, b - a = 0.3A, a + b = c + d = 2.5A, ν = 0.4.

In Figures 6.14-6.16, variations of normalized stress intensity factors $\bar{k}_{1a}$ and $\bar{k}_{1b}$ with $(d - c)/A$ when $L = 4.0A$ and $b - a = 0.15A$ for different ν values; 0.2, 0.3, 0.4 are shown respectively. The rigid inclusions and the crack are far away from each others. The difference between these figures and Figures 6.8-6.10 is the thickness of the hollow cylinder. In these figures, $\bar{k}_{1a}$ and $\bar{k}_{1b}$ remains constant with increasing inclusion widths, the analytical and numerical values coincide well with each other.
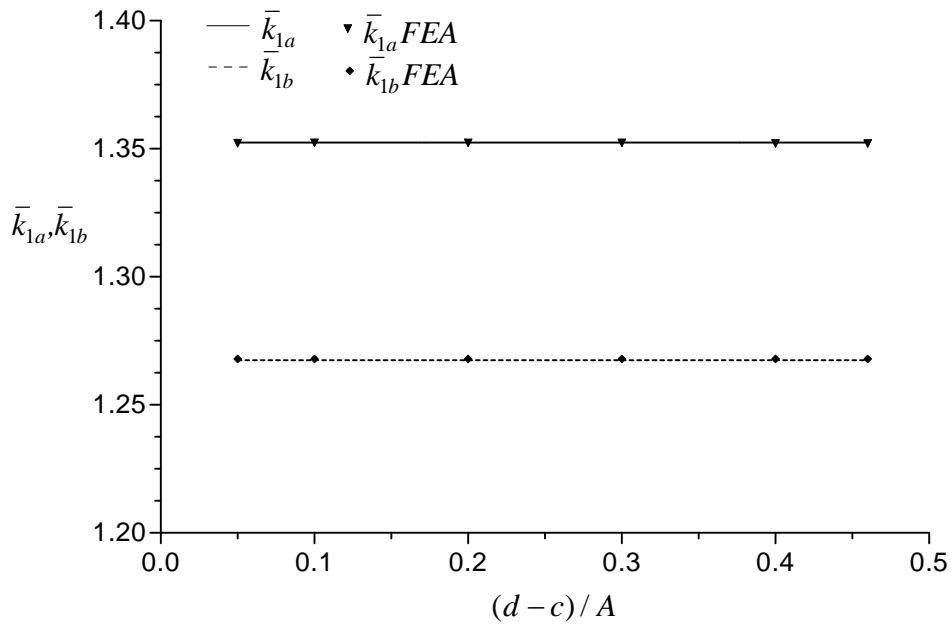
Figure 6.14. Variation of Normalized Stress Intensity Factors $\bar{k}_{1a}$, $\bar{k}_{1b}$ when B =1.5A,

L = 4.0A, b - a = 0.3A, a + b = c + d = 2.5A, $\nu = 0.2$.
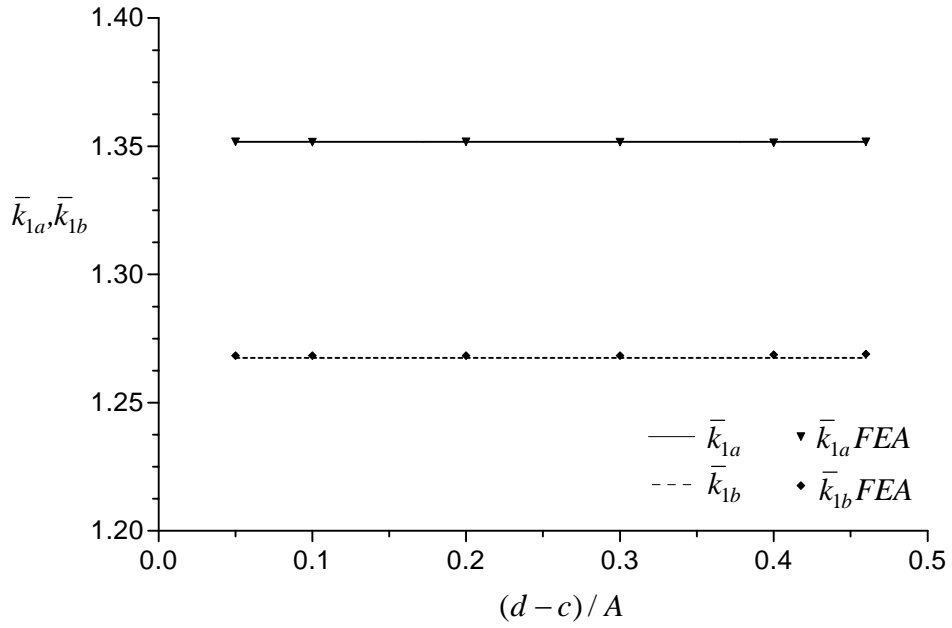
Figure 6.15. Variation of Normalized Stress Intensity Factors $\bar{k}_{1a}$, $\bar{k}_{1b}$ when B =1.5A, L = 4.0A, b - a = 0.3A, a + b = c + d = 2.5A, ν = 0.3.
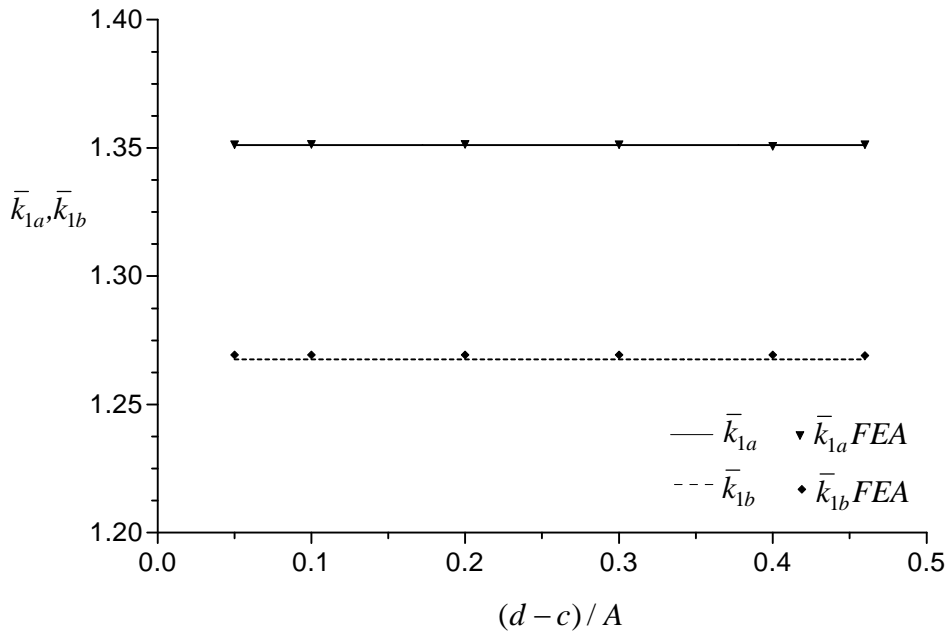
Figure 6.16. Variation of Normalized Stress Intensity Factors $\bar{k}_{1a}$, $\bar{k}_{1b}$ when B =1.5A, L = 4.0A, b - a = 0.3A, a + b = c + d = 2.5A, ν = 0.4.

Figures 6.17-6.19 show variations of normalized stress intensity factors $\bar{k}_{1a}$, $\bar{k}_{1b}$ with L/A when b – a = 0.15A and different d - c values; 0.09, 0.15 and 0.21, respectively.
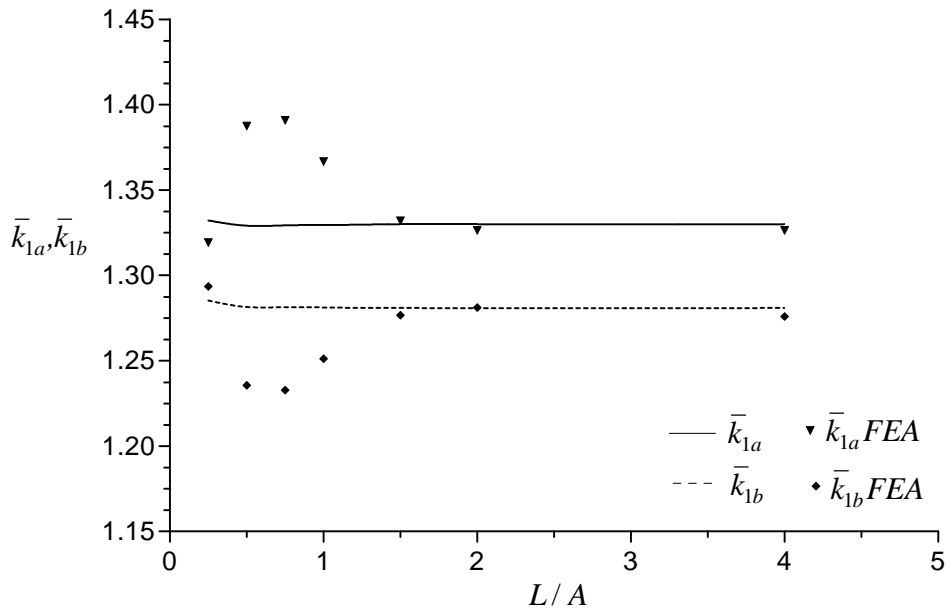
Figure 6.17. Variation of Normalized Stress Intensity Factors $\bar{k}_{1a}$, $\bar{k}_{1b}$ when B =1.25A, b - a = 0.15A, d – c = 0.09A, a + b = c + d = 2.25A, ν = 0.3.
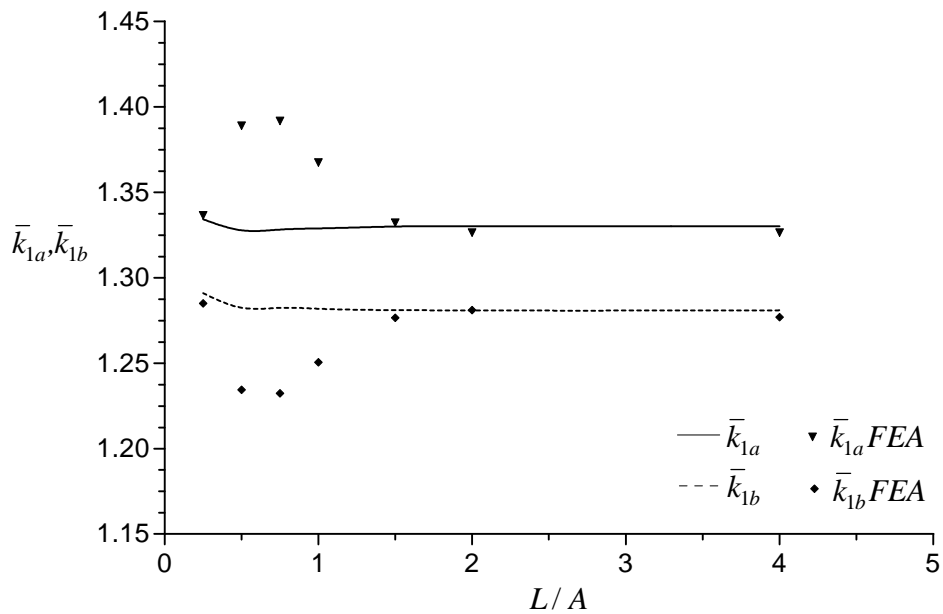
Figure 6.18. Variation of Normalized Stress Intensity Factors $\bar{k}_{1a}$, $\bar{k}_{1b}$ when B =1.25A, b - a = 0.15A, d - c = 0.15A, a + b = c + d = 2.25A, ν = 0.3.

According to analytical results, with increasing L/A, both $\bar{k}_{1a}$ and $\bar{k}_{1b}$ tend to asymptotic values when L/A>~1.5. When the L/A values are 0.25 and >=1.5, the analytical and numerical results are in good agreement. There are acceptable differences when the L/A values are between 0.5 and 1.5.
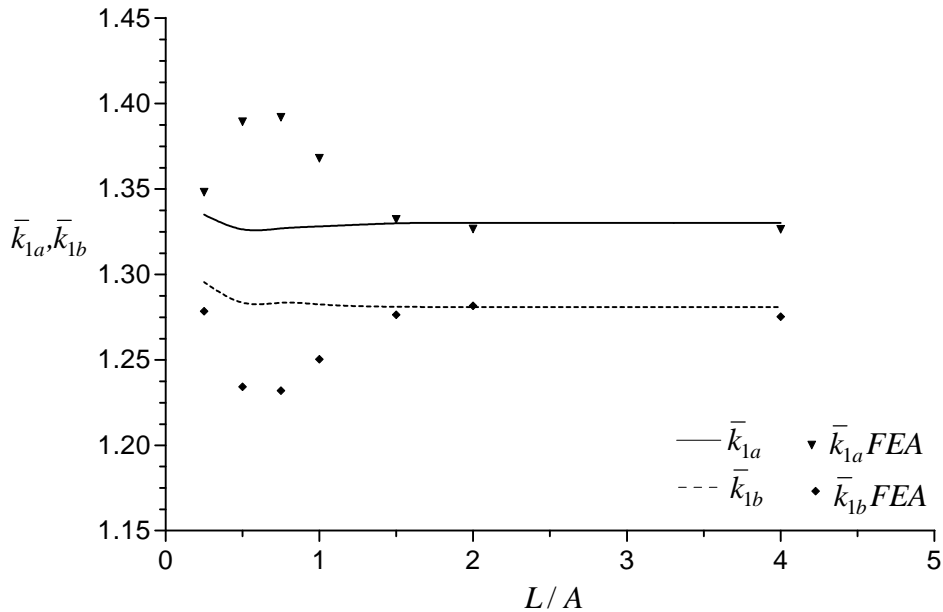
Figure 6.19. Variation of Normalized Stress Intensity Factors $\bar{k}_{1a}$, $\bar{k}_{1b}$ when B =1.25A,

b - a = 0.15A, d - c = 0.21A, a + b = c + d = 2.25A, ν = 0.3.

Figures 6.20-6.22 show variations of normalized stress intensity factors $\bar{k}_{1a}$ and $\bar{k}_{1b}$ with L/A when b – a = 0.3A and different d-c values; 0.18, 0.3 and 0.42,respectively. The difference between these figures and Figures 6.17-6.19 is the thickness of the hollow cylinder.When the L/A values are >=2, the analytical and numerical results are in good agreement. There are acceptable differences when the L/A values are between 0.25 and 2.
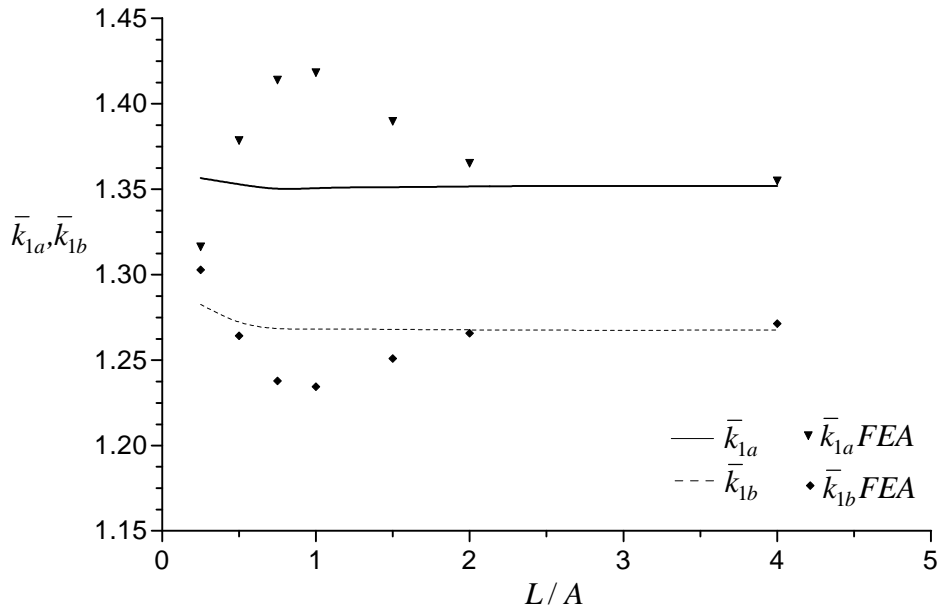
Figure 6.20. Variation of Normalized Stress Intensity Factors $\bar{k}_{1a}$, $\bar{k}_{1b}$ when B =1.5A, b - a = 0.3A, d - c = 0.18A, a + b = c + d = 2.5A, ν = 0.3.
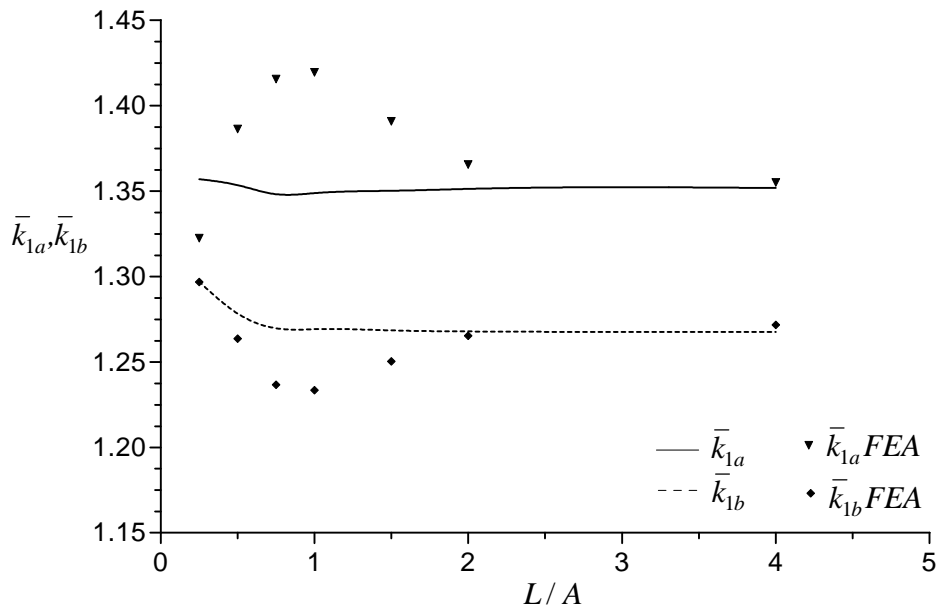
Figure 6.21. Variation of Normalized Stress Intensity Factors $\bar{k}_{1a}$, $\bar{k}_{1b}$ when B =1.5A, b - a = 0.3A, d - c = 0.3A, a + b = c + d = 2.5A, ν = 0.3.
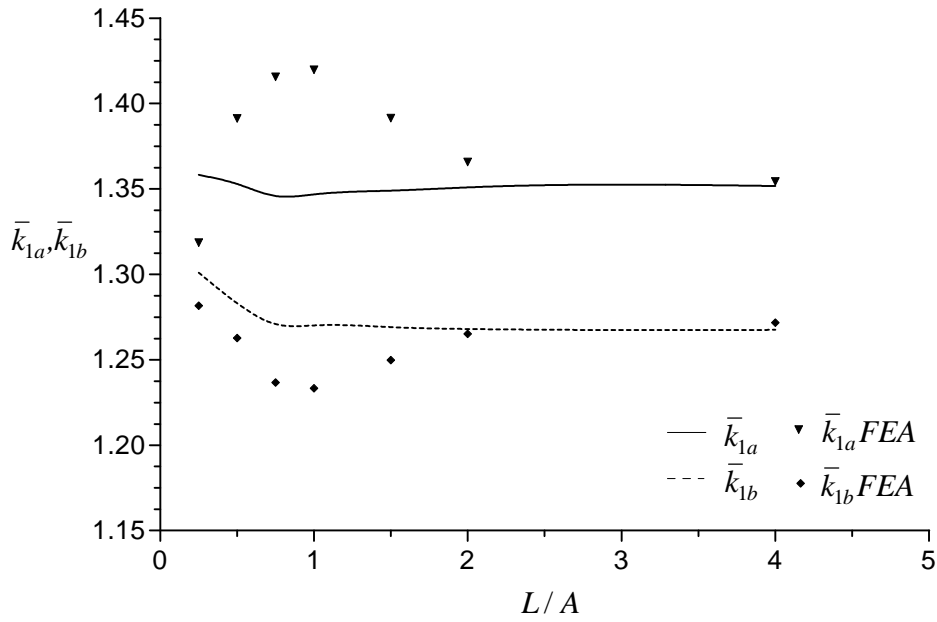
**Figure 6.22.** Variation of Normalized Stress Intensity Factors $\bar{k}_{1a}$, $\bar{k}_{1b}$ when B =1.5A, b - a = 0.3A, d - c = 0.42A, a + b = c + d = 2.5A, ν = 0.3.

Figure 6.23 shows variations of normalized stress intensity factors $\bar{k}_{1a}$, $\bar{k}_{1b}$ with L/A when b – a = 0.15A and d –c =0.05A. When the L/A values are >=1.5, the analytical and numerical results coincide well with each other.
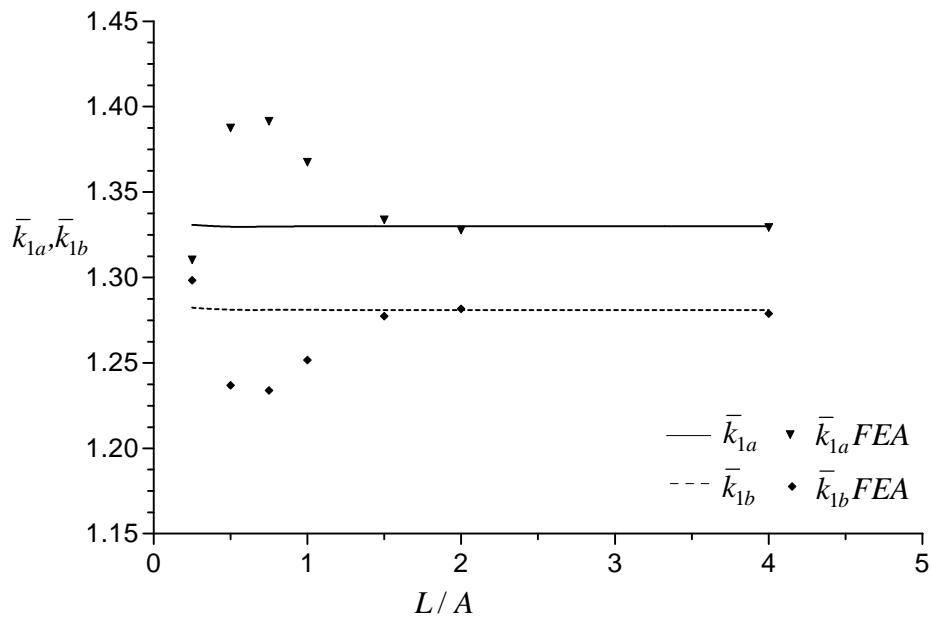

Figure 6.23. Variation of Normalized Stress Intensity Factors $\bar{k}_{1a}$, $\bar{k}_{1b}$ when B =1.25A, b - a = 0.15A, d - c = 0.05A, a + b = c + d = 2.25A, ν = 0.3.

Figures 6.24-6.26 show variations of normalized stress intensity factors $\bar{k}_{1a}$ and $\bar{k}_{1b}$ with L/A when b – a = 0.15A and d – c =0.23A for different ν values.
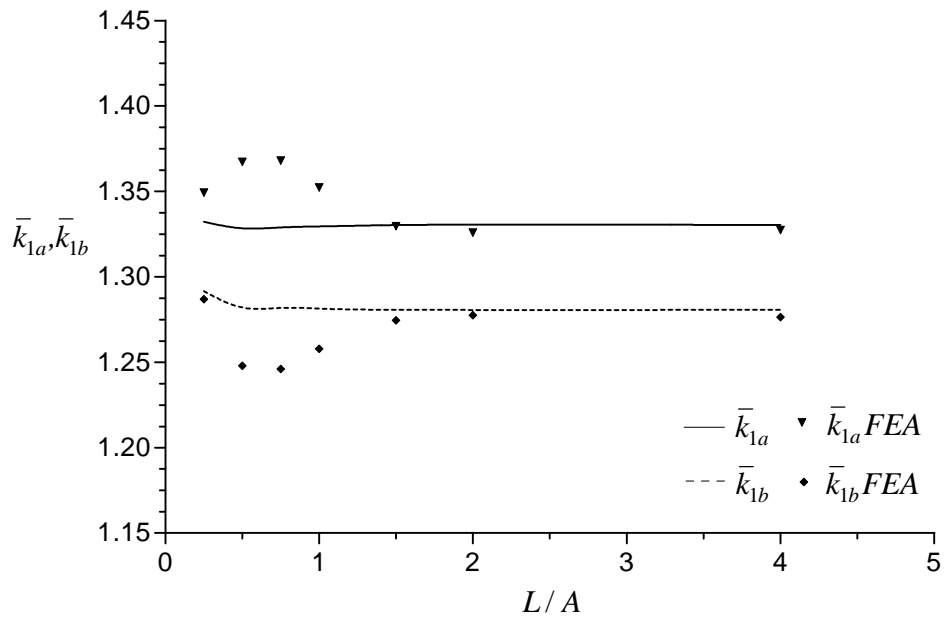

Figure 6.24. Variation of Normalized Stress Intensity Factors $\bar{k}_{1a}$, $\bar{k}_{1b}$ when B =1.5A,

b - a = 0.15A, d - c = 0.23A, a + b = c + d = 2.25A, ν = 0.2.
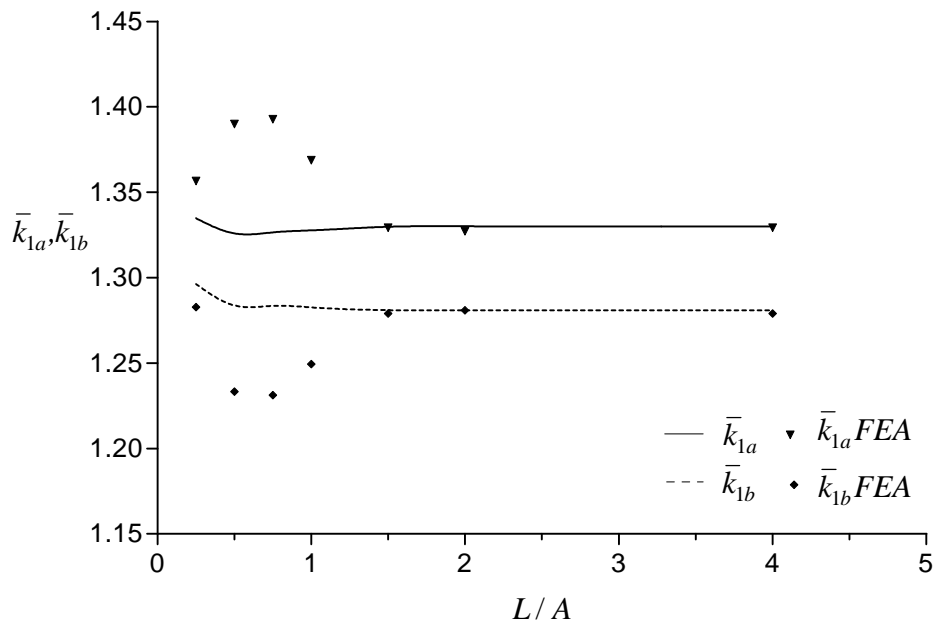

Figure 6.25. Variation of Normalized Stress Intensity Factors $\bar{k}_{1a}$, $\bar{k}_{1b}$ when B =1.5A,

b - a = 0.15A, d - c = 0.23A, a + b = c + d = 2.25A, ν = 0.3.

When the L/A values are 0.25 and >=1.5, the analytical and numerical results coincide well with each other. There are acceptable differences when the L/A values are between 0.5 and 1.5. The differences increase with increasing ν values.
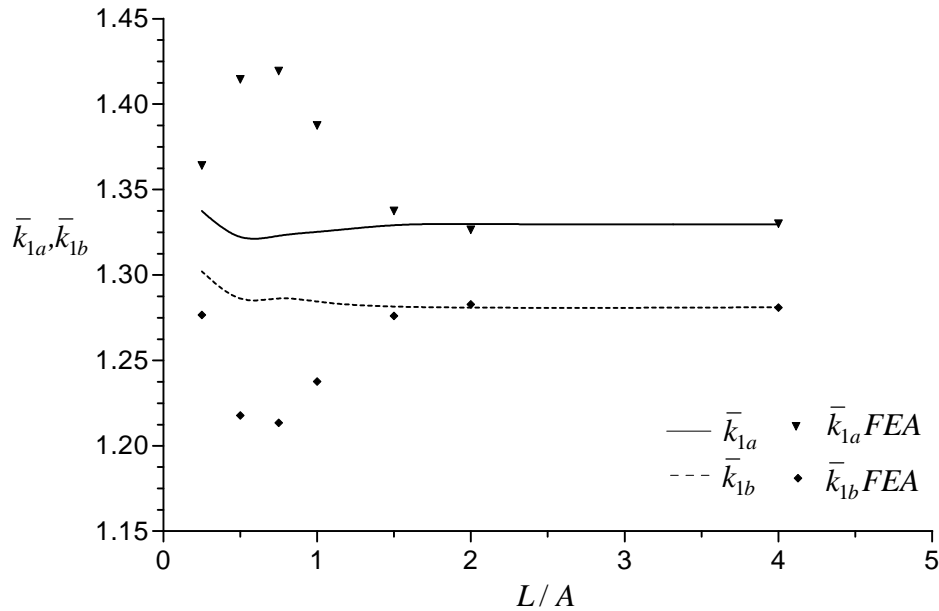
Figure 6.26. Variation of Normalized Stress Intensity Factors $\bar{k}_{1a}$, $\bar{k}_{1b}$ when B =1.5A, b - a = 0.15A, d - c = 0.23A, a + b = c + d = 2.25A, ν = 0.4.

Figures 6.27-6.29 show variations of normalized stress intensity factors $\bar{k}_{1a}$ and $\bar{k}_{1b}$ with L/A when d - c = 0.3A and for different b - a values; 0.18, 0.3 and 0.42,respectively. According to analytical results, both $\bar{k}_{1a}$ and $\bar{k}_{1b}$ become independent of L/A when L/A>~1. When the L/A values are 0.25 and >=2, the numerical results are in good agreement with the analytical ones. There are acceptable differences when L/A values are between 0.5 and 2.
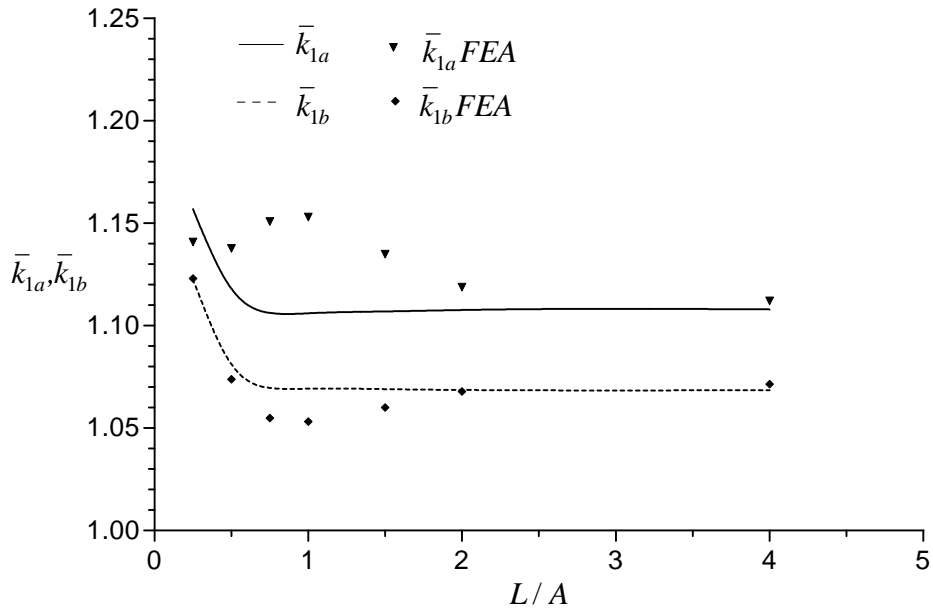
Figure 6.27. Variation of Normalized Stress Intensity Factors $\bar{k}_{1a}$, $\bar{k}_{1b}$ when B =1.5A,

b - a = 0.18A, d - c = 0.3A, a + b = c + d = 2.5A, ν = 0.3.
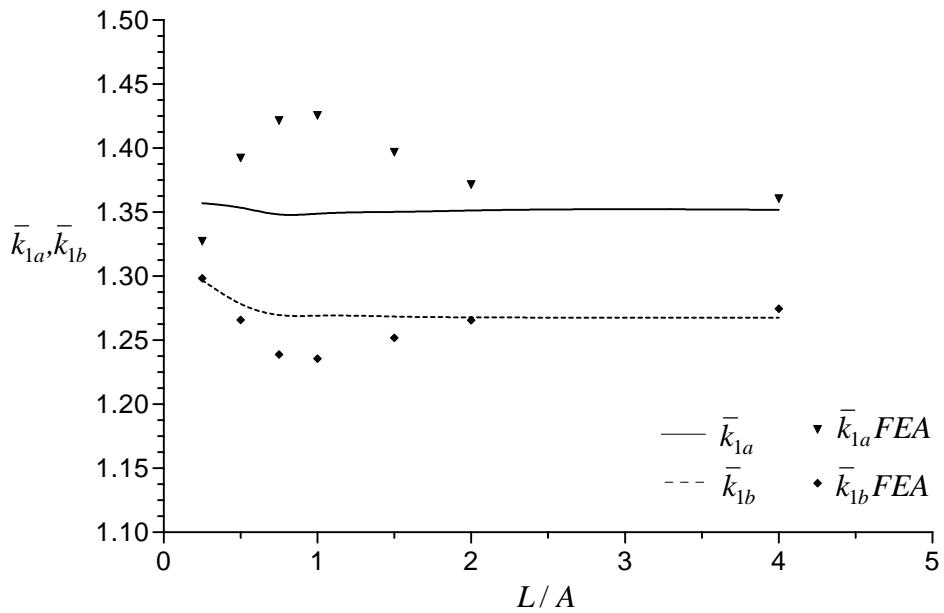
Figure 6.28. Variation of Normalized Stress Intensity Factors $\bar{k}_{1a}$, $\bar{k}_{1b}$ when B =1.5A,

b - a = 0.3A, d - c = 0.3A, a + b = c + d = 2.5A, ν = 0.3.
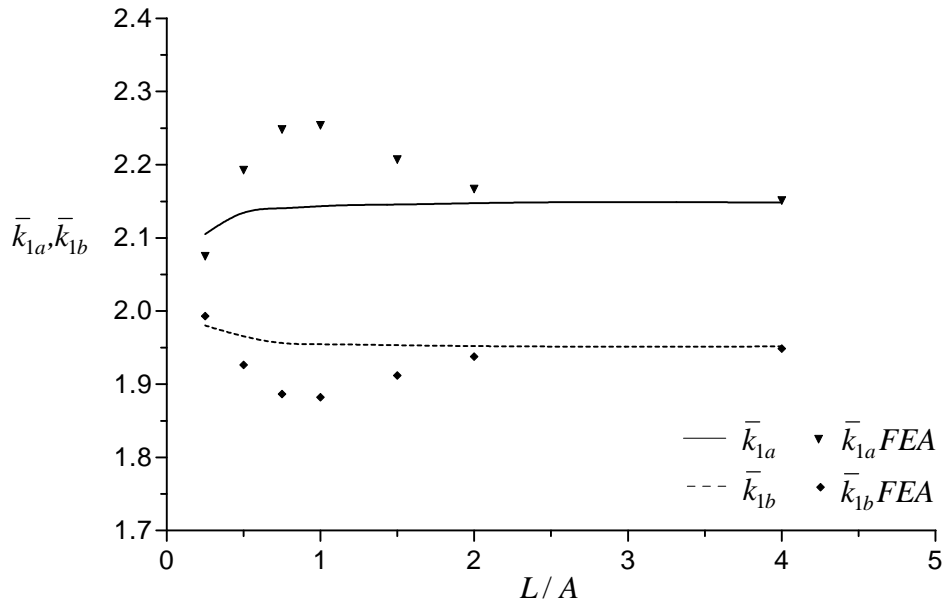
Figure 6.29. Variation of Normalized Stress Intensity Factors $\bar{k}_{1a}$, $\bar{k}_{1b}$ when B =1.5A, b - a = 0.42A, d - c = 0.3A, a + b = c + d = 2.5A, $\nu = 0.3$.

Figures 6.30-6.32 show variations of normalized stress intensity factors $\bar{k}_{1a}$ and $\bar{k}_{1b}$ with L/A when b – a = 0.1A and d – c =0.21A. In these figures, the crack is located closer to the inner surface, at the center and closer to the outer surface of the infinite hollow cylinder,respectively. According to analytical results, with increasing L/A, especially when L/A>~1.5, $\bar{k}_{1a}$ and $\bar{k}_{1b}$ both tend to approach a constant value. When the L/A values are 0.25 and >=1.5, the analytical and numerical results coincide well with each other. As from the viewpoint of the finite element analysis, there are acceptable differences when L/A<~1.5.
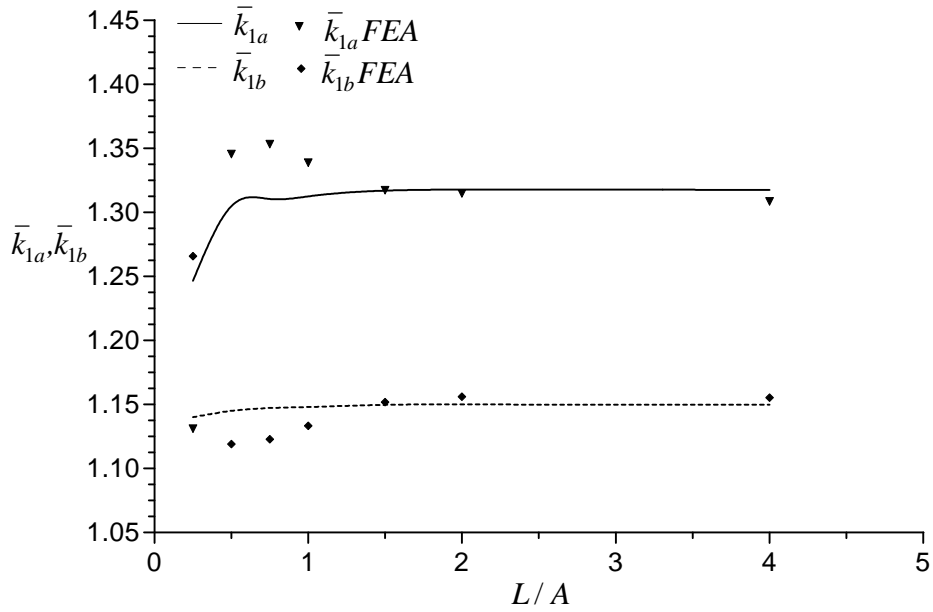
Figure 6.30. Variation of Normalized Stress Intensity Factors $\bar{k}_{1a}$, $\bar{k}_{1b}$ when B =1.25A, b - a = 0.1A, d - c = 0.21A, a + b = 2.15A, c + d = 2.25A, ν = 0.3.
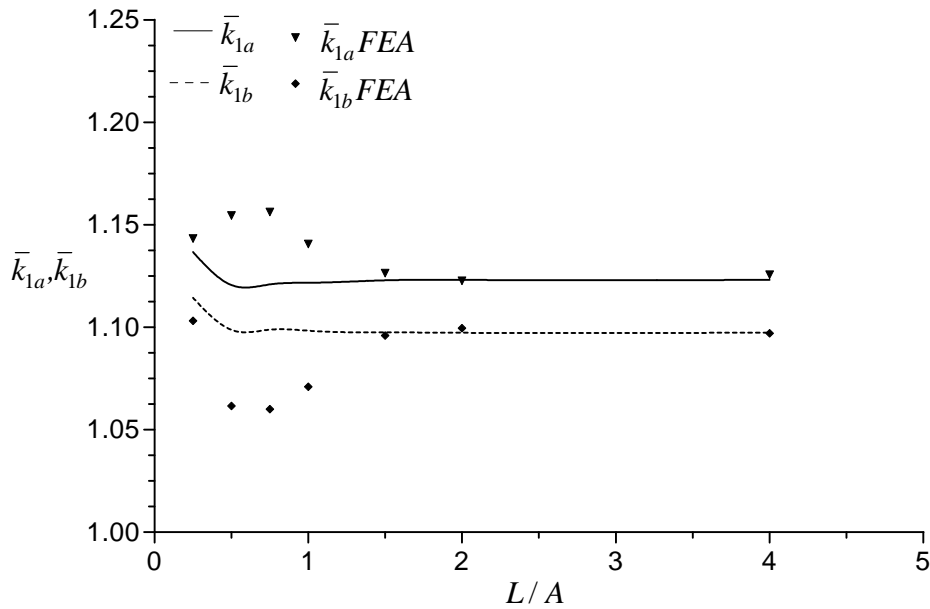

Figure 6.31. Variation of Normalized Stress Intensity Factors $\bar{k}_{1a}$, $\bar{k}_{1b}$ when B =1.25A, b - a = 0.1A, d - c = 0.21A, a + b = 2.25A, c + d = 2.25A, ν = 0.3.
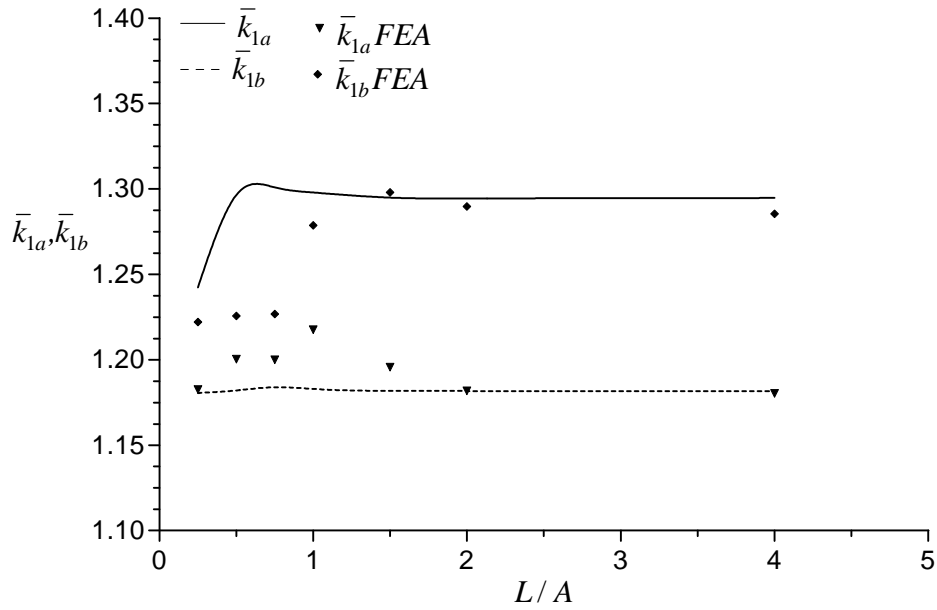
Figure 6.32. Variation of Normalized Stress Intensity Factors $\bar{k}_{1a}$, $\bar{k}_{1b}$ when B =1.25A, b - a = 0.1A, d - c = 0.21A, a + b = 2.35A, c + d = 2.25A, ν = 0.3.

Figures 6.33-6.35 show variations of normalized stress intensity factors $\bar{k}_{1a}$ and $\bar{k}_{1b}$ with L/A when b – a = 0.21A and d – c = 0.1A. In these figures, the rigid inclusions are located closer to the inner surface, at the center and closer to the outer surface.
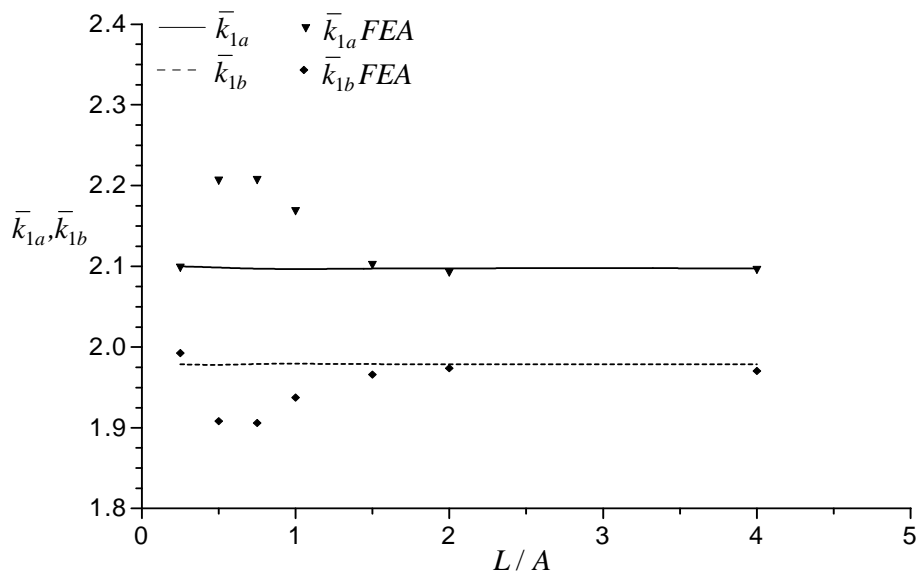
Figure 6.33. Variation of Normalized Stress Intensity Factors $\bar{k}_{1a}$, $\bar{k}_{1b}$ when B =1.25A, b - a = 0.21A, d - c = 0.1A, a + b = 2.25A, c + d = 2.15A, ν = 0.3.
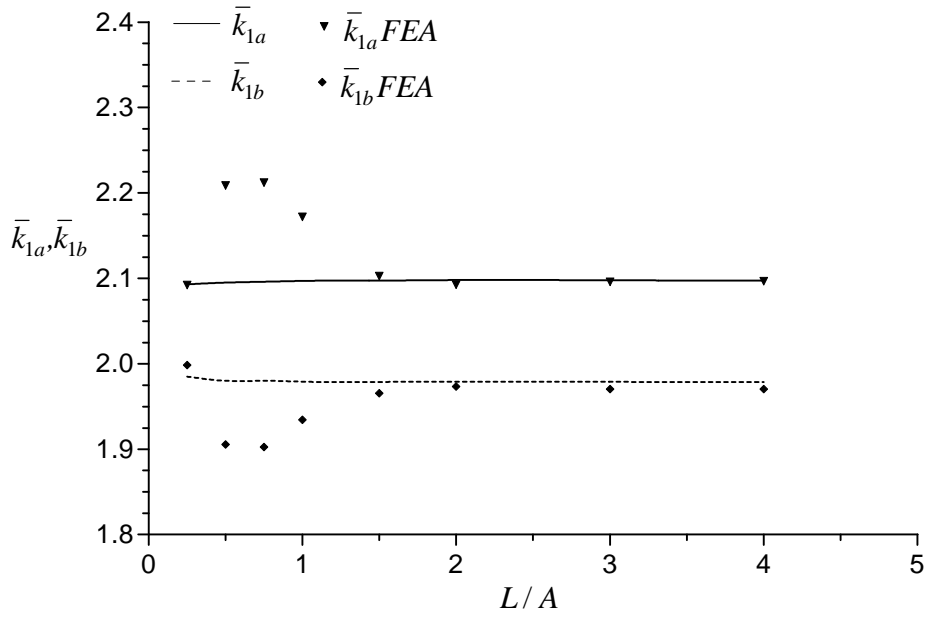
Figure 6.34. Variation of Normalized Stress Intensity Factors $\bar{k}_{1a}$, $\bar{k}_{1b}$ when B =1.25A, b - a = 0.21A, d - c = 0.1A, a + b = 2.25A, c + d = 2.25A, ν = 0.3.
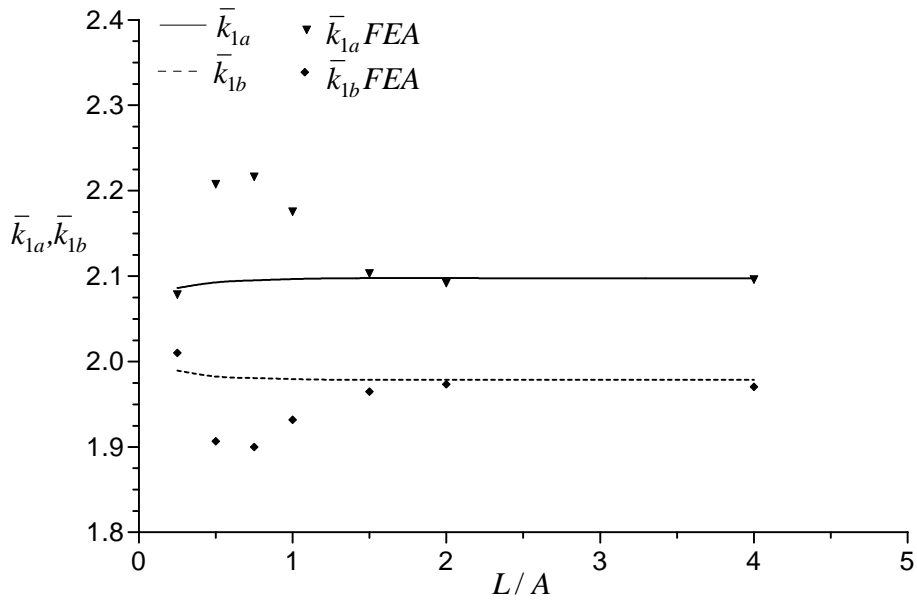
Figure 6.35. Variation of Normalized Stress Intensity Factors $\bar{k}_{1a}$, $\bar{k}_{1b}$ when B =1.25A, b - a = 0.21A, d - c = 0.1A, a + b = 2.25A, c + d = 2.35A, ν = 0.3.

Figures 6.36-6.38 show variations of normalized stress intensity factors $\bar{k}_{1a}$ and $\bar{k}_{1b}$ with L/A when b – a = 0.2A and d – c =0.42A. In these figures, the crack is located closer to the inner surface, at the center and closer to the outer surface, respectively. When the L/A values are >=2, the analytical and numerical results coincide well with each other. There are acceptable differences when the L/A values are between 0.25 and 2.
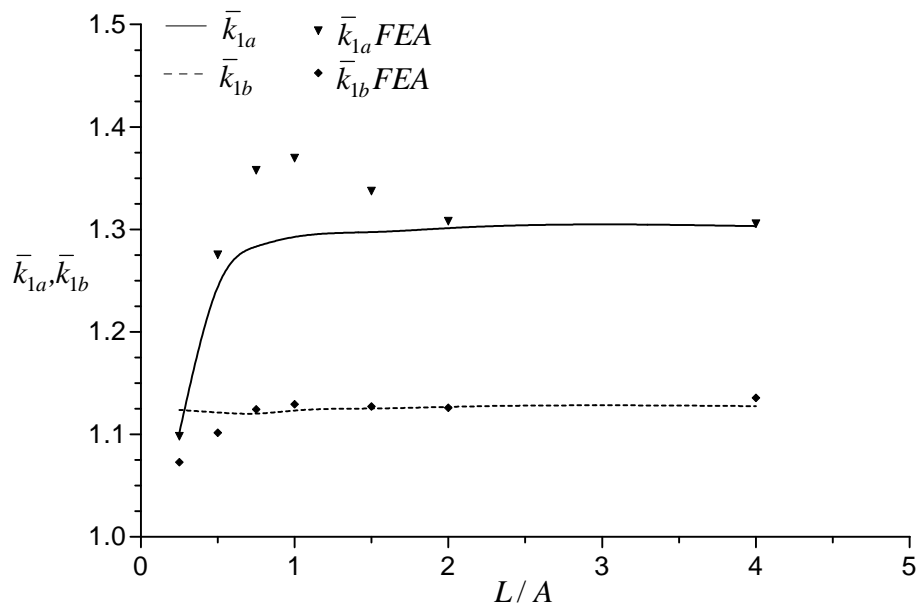
Figure 6.36. Variation of Normalized Stress Intensity Factors $\bar{k}_{1a}$, $\bar{k}_{1b}$ when B =1.5A, b - a = 0.2A, d - c = 0.42A, a + b = 2.3A, c + d = 2.5A, ν = 0.3.
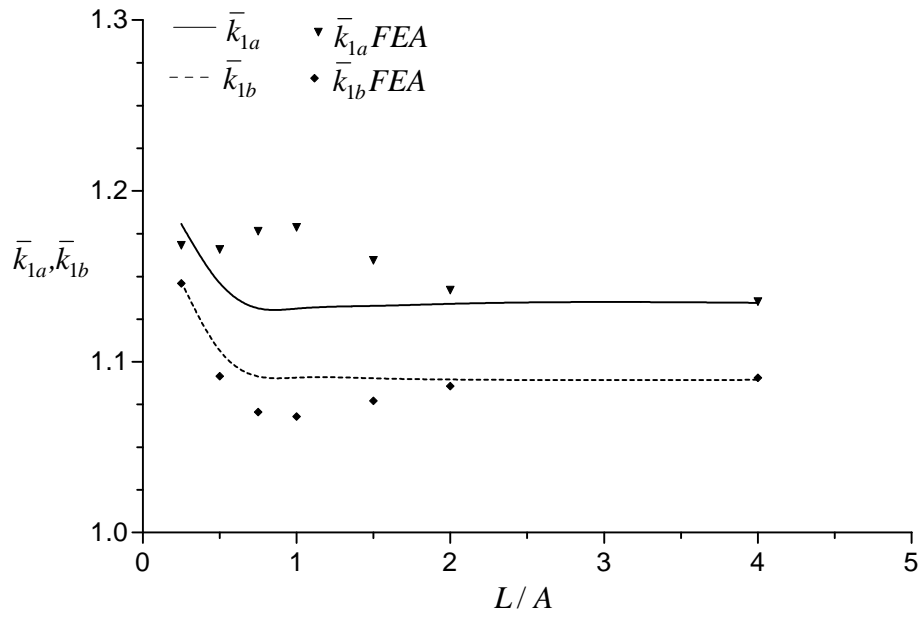
**Figure 6.37..** Variation of Normalized Stress Intensity Factors $\bar{k}_{1a}$, $\bar{k}_{1b}$ when B =1.5A,

b - a = 0.2A, d - c = 0.42A, a + b = 2.5A, c + d = 2.5A, ν = 0.3.
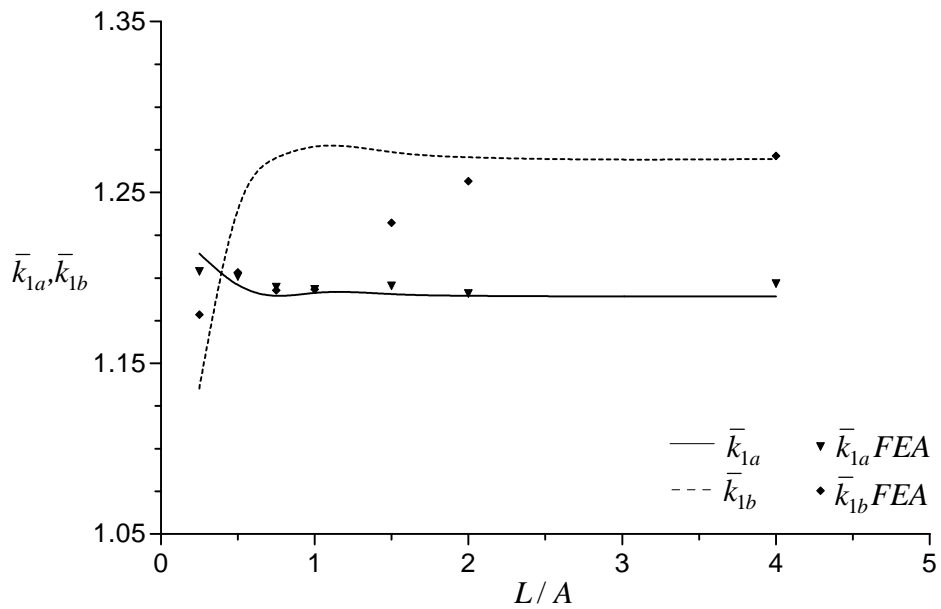
Figure 6.38.. Variation of Normalized Stress Intensity Factors $\bar{k}_{1a}$, $\bar{k}_{1b}$ when B =1.5A,

b - a = 0.2A, d - c = 0.42A, a + b = 2.7A, c + d = 2.5A, ν = 0.3.

The variation of normalized stress intensity factors $\bar{k}_{1a}$ and $\bar{k}_{1b}$ at the tips of the cracks are presented in graphical form by Figures 6.1-6.38. As it is seen from these figures, when the inclusions are far away from the crack, the interaction among them vanishes. In this case, the numerical and analytical results are in good agreement. When the inclusions approach the crack, a discrepancy has been occurred, but in the acceptable limits. There may be several reasons related to this case. In the analytical work, the stress distributions along the rigid inclusions may be neglected due to negligible thickness of the rigid inclusions. But in the finite element analysis, this case is not valid. Also, the rigid inclusions having negligible thickness may not be modelled properly. Add to these, the accurcy of analytical and numerical solutions may be affected when the inclusions get too close to each other.

Related data and % differences between numerical and analytical results for each figure are tabulated and given in Appendix A. The stress distributions for a sample case are given in Appendix B.

CHAPTER 7

CONCLUSIONS

A numerical implementation based on the finite element method for an elastic hollow cylinder under axial tension containing a crack and two rigid inclusions of ring-shape is presented in this study. The proposed model uses efficiently the capabilities of a commercially available finite element program, ANSYS, to determine the stress intensity factors at the crack tips. The numerical results illustrated for various crack and inclusion configurations are presented in Chapter 6. Stress intensity factors at the tips of the crack are investigated numerically and compared for accuracy with those studied by Artem [12] and Erdol [13].

At the beginning, in order to verify the finite element model built for the problem investigated in this study, a similar problem without rigid inclusions has been analyzed. When the results obtained from finite element analysis compared with the analytical ones [13], it is seen that the results coincide well with each other. Thus, it can be mentioned that the model used in this study is suitable and can be relied on for further analyses. Then, the rigid inclusions have been included in the model as in [12]. The results obtained by using this model are compared with the analytical ones [12]. When the inclusions are far away from the crack, the interaction among them vanishes. In this case, the numerical and analytical results are in good agreement. When the inclusions approach the crack, a discrepancy has been occurred, but in the acceptable limits. There may be several reasons related to this situation:

1) In the analytical work, the inclusions are assumed to be sufficiently thin (having negligible thickness) so that the thickness distribution of the stresses in the inclusions may be neglected. But, in the finite element analysis this assumption is not valid.

2) The rigid inclusions with negligible thicknesses are modelled with a small size compared with the height of the hollow cylinder. But, the condition of negligibility may not be obtained properly.

3) The distance between the rigid inclusions tends to affect the accuracy of the solutions (analytical or numerical) so much that the solutions may fail to converge as the inclusions get too close to each other.

REFERENCES

[1]   N. K. Anifantis, "Crack surface interference: a finite element analysis," *Engineering Fracture Mechanics* **68**, (2001), 1403-1415.

[2]   M. Tarafder, S. Tarafder, V. R. Ranganath and R. N. Ghosh, "Finite element solutions for stress intensity factors in longitudinally cracked cylindirical components," *International Journal of Pressure Vessels & Piping* **70**, (1997), 127-133.

[3]   Y. Shih and J. Chen, "The stress intensity factor study of an elliptical cracked shaft," *Nuclear Engineering and Design* **214**, (2002), 137-145.

[4]   K. Shankar and W. Wu, " Effect of welding and weld repair on crack propagation behaviour in aluminium alloy 5083 plates," *Materials & Design* **23**, (2002), 201-208.

[5]   N. Pan and S. D. Sheppard, "Stress intensity factors in spot welds," *Engineering Fracture Mechanics* **xxx**, (2002), xxx-xxx.

[6]   L. Banks-Sills and R. Eliasi, "Fatigue analysis of a cannon barrel," *Engineering Failure Analysis* **6**, (1999), 371-385.

[7]   B. Sergeev, E. Madenci and D. R. Ambur, "Stress intensity factors for an arbitrarily oriented crack near a hole in longeron web," *Theoretical and Applied Fracture Mechanics* **31**, (1999), 213-222.

[8]   Z. M. Xiao, J. Y. Guo and S. Yi, "Stress intensity factors for ring-shaped crack sorrounded by spherical inclusions," *Theoretical and Applied Fracture Mechanics* **32**, (1999), 147-155.

[9]   Z. M. Xiao and J. Bai, "On piezoelectric inhomogeneity related problems-part II: a circular piezoelectric inhomogeneity interacting with a nearby crack," *International Journal of Engineering Science* **37**, (1999), 961-976.

[10]   Z. M. Xiao and J. Bai, "Numerical simulation on a coated piezoelectric sensor interacting with a crack," *Finite Elements in Analysis and Design* **38**, (2002), 691-706.

[11]   Z. M. Xiao and B. J. Chen, "Stress intensity factor for a Griffith crack interacting with a coated inclusion," *International Journal of Fracture* **108**, (2001), 193-205.

[12]   H. S. A. Artem, *Problem of Cracked Infinite Hollow Cylinder with Two Rigid Inclusions*, Ph.D. Thesis, Middle East Technical University, Ankara, Turkey, 1999.

[13]   R. Erdol and F. Erdogan, "A thick-walled cylinder with an axisymmetric internal or edge crack," *Journal of Applied Mechanics* **45**, (1978), 281-286.

 [14]   T. L. Anderson, *Fracture Mechanics : Fundamental and Applications*, Second Edition, 1995, by CRC Press, Inc.

[15]   F. Erdogan, "Stress intensiy factors," *Journal of Applied Mechanics* **50**, (1983), 992-1002.

[16]   A. P. Boresi, R. J. Schmidt, O. M. Sidebottom, *Advanced Mechanics of Materials*, Fifth Edition, 1993, by John Wiley and Sons, Inc.

[17]   F. Erdogan, "Fracture Mechanics," *International Journal of Solids and Structures* **37**, (2000), 171-183.

[18]   S. Moaveni, *Finite Element Analysis Theory and Application with ANSYS*, First Edition, 1999, by Prentice-Hall, Inc.

[19]   R. D. Cook, D. S. Malkus, M. E. Plesha, *Concepts and Applications of Finite Element Analysis*, Third Edition, 1989, by John Wiley and Sons, Inc.

[20]   J. N. Reddy, An Introduction to The Finite Element Method, Second Edition, 1993, by McGraw-Hill, Inc.

[21]   *ANSYS Modeling and Meshing Guide*, Second Edition, SAS IP Inc.

[22]   G. Gendron, "A review of four PC packages for FE structural analysis," *Finite Elements in Analysis and Design* **28**, (1997), 105-114.

[23]   *ANSYS Elements Reference*, Eight Edition, SAS IP Inc.

[24]   T. R. Chandrupatla and A. D. Belegundu, *Introduction to Finite Elements in Engineering*, Second Edition, 1997, by Prentice-Hall, Inc.

[25]   S. H. Ahn, T. H. Kim, B. M. Kim and J. C. Choi, "A study on prediction of fatigue life in an axi-symmetric extrusion die," *Journal of Materials Processing Technology* **71**, (1997), 343-349.

[26]   R. L. Williamson, J. K. Wright, E. D. Steffler and R. M. Cannon, "Numerical analysis of surface cracks at regions of curvature in oxide scales," *Materias Science & Engineering* **A00**, (2002), 1-11.

[27]   B. B. Bouiadjra, M. Belhouari and B. Serier, "Computation of the stress intensity factors for repaired cracks with bonded composite patch in mode I and mixed mode," *Composite Structures* **56**, (2002), 401-406.

[28]   *ANSYS Theory Reference*, Eight Edition, SAS IP Inc.

APPENDICES

APPENDIX-A

DATA AND % DIFFERENCES BETWEEN NUMERICAL AND ANALYTICAL RESULTS FOR FIGURES IN CHAPTER 6

Table A-1 Data and % differences between analytical and numerical results for Figure 6.1.

b/B(A/B=0.2,a/B=0.4)	k'(1b)	k' (1a)	k'(1b)FEA	%dif.	k'(1a)FEA	%dif.
0.4	1	1				
0.5	0.9864	1.0405	0.9864	0.0000	1.0418	0.1249
0.6	0.9963	1.1017	0.9936	-0.2710	1.1019	0.0182
0.7	1.0345	1.19	1.0294	-0.4930	1.1877	-0.1933
0.8	1.1262	1.3252	1.1216	-0.4085	1.3245	-0.0528
0.9	1.3726	1.5644	1.3682	-0.3206	1.5681	0.2365
1						

Table A-2 Data and % differences between analytical and numerical results for Figure 6.2.

b/B(A/B=0.3,a/B=0.4)	k'(1b)	k' (1a)	k'(1b)FEA	%dif.	k'(1a)FEA	%dif.
0.4	1	1				
0.5	0.9973	1.0591	1.0074	1.0127	1.0724	1.2558
0.6	1.0167	1.1493	1.0251	0.8262	1.1611	1.0267
0.7	1.0626	1.269	1.069	0.6023	1.2788	0.7723
0.8	1.1645	1.4416	1.1674	0.2490	1.4478	0.4301
0.9	1.4361	1.7374	1.434	-0.1462	1.7408	0.1957
1						

Table A-3 Data and % differences between analytical and numerical results for Figure 6.3.

b/B(A/B=0.3,a/B=0.5)	k'(1b)	k' (1a)	k'(1b)FEA	%dif.	k'(1a)FEA	%dif.
0.4						
0.5	1	1				
0.6	0.9931	1.0377	0.9961	0.3021	1.0424	0.4529
0.7	1.015	1.1035	1.016	0.0985	1.1071	0.3262
0.8	1.0833	1.2098	1.0814	-0.1754	1.2111	0.1075
0.9	1.287	1.4022	1.282	-0.3885	1.4037	0.1070
1						

k' in all tables defines the normalized stress intensity factor.

Table A-4 Data and % differences between analytical and numerical results for Figure 6.4.

(b-a)/A	k'(1a)	k'(1b)	k'(1a)FEA	%dif.	k'(1b)FEA	%dif
0.025	1.0238	1.0184	1.0299	0.5958	1.0225	0.4026
0.05	1.0445	1.0336	1.0513	0.6510	1.0382	0.4450
0.1	1.1355	1.1107	1.1394	0.3435	1.1112	0.0450
0.15	1.3342	1.2909	1.337	0.2099	1.2852	-0.4416
0.2	1.8654	1.7823	1.8694	0.2144	1.7662	-0.9033
0.23	2.9746	2.824	2.9568	-0.5984	2.7748	-1.7422

Table A-5 Data and % differences between analytical and numerical results for Figure 6.5.

(d-c)/A	k'(1a)	k'(1b)	k'(1a)FEA	%dif.	k'(1b)FEA	%dif.
0.025	1.3304	1.2807	1.3563	1.9468	1.244	-2.8656
0.05	1.3303	1.2808	1.3571	2.0146	1.2433	-2.9279
0.1	1.3299	1.281	1.3582	2.1280	1.2425	-3.0055
0.15	1.3293	1.2814	1.359	2.2343	1.2419	-3.0826
0.2	1.3287	1.2818	1.3592	2.2955	1.2416	-3.1362
0.23	1.3284	1.282	1.3591	2.3111	1.2417	-3.1435

Table A-6 Data and % differences between analytical and numerical results for Figure 6.6.

(d-c)/A	k'(1a)	k'(1b)	k'(1a)FEA	%dif.	k'(1b)FEA	%dif.
0.025	1.33	1.281	1.3843	4.0827	1.2371	-3.4270
0.05	1.3297	1.2811	1.3855	4.1964	1.2362	-3.5048
0.1	1.329	1.282	1.3872	4.3792	1.2348	-3.6817
0.15	1.3277	1.2824	1.3884	4.5718	1.2339	-3.7820
0.2	1.326	1.283	1.3888	4.7360	1.2336	-3.8504
0.23	1.3256	1.2837	1.3885	4.7450	1.2338	-3.8872

Table A-7 Data and % differences between analytical and numerical results for Figure 6.7

(d-c)/A	k'(1a)	k'(1b)	k'(1a)FEA	%dif.	k'(1b)FEA	%dif.
0.025	1.3295	1.2812	1.4023	5.4757	1.2178	-4.9485
0.05	1.3291	1.2814	1.4037	5.6128	1.2167	-5.0492
0.1	1.3277	1.2824	1.4062	5.9125	1.2147	-5.2792
0.15	1.3256	1.2838	1.4077	6.1934	1.2133	-5.4915
0.2	1.3234	1.2854	1.4081	6.4002	1.2131	-5.6247
0.23	1.3223	1.2862	1.4078	6.4660	1.2132	-5.6756

Table A-8 Data and % differences between analytical and numerical results for Figure 6.8.

(d-c)/A	k'(1a)	k'(1b)	k'(1a)FEA	%dif.	k'(1b)FEA	%dif.
0.025	1.3304	1.2807	1.3292	-0.0902	1.2764	-0.3358
0.05	1.3304	1.2807	1.3287	-0.1278	1.2765	-0.3279
0.1	1.3304	1.2807	1.3287	-0.1278	1.2766	-0.3201
0.15	1.3304	1.2807	1.3287	-0.1278	1.2765	-0.3279
0.2	1.3304	1.2807	1.3287	-0.1278	1.2765	-0.3279
0.23	1.3304	1.2807	1.3287	-0.1278	1.2765	-0.3279

Table A-9 Data and % differences between analytical and numerical results for Figure 6.9.

(d-c)/A	k'(1a)	k'(1b)	k'(1a)FEA	%dif.	k'(1b)FEA	%dif.
0.025	1.33	1.2809	1.3315	0.1128	1.2807	-0.0156
0.05	1.33	1.2809	1.3315	0.1128	1.2807	-0.0156
0.1	1.33	1.2809	1.3316	0.1203	1.2803	-0.0468
0.15	1.33	1.2809	1.3316	0.1203	1.2802	-0.0546
0.2	1.33	1.2809	1.3316	0.1203	1.2802	-0.0546
0.23	1.33	1.2809	1.3316	0.1203	1.2802	-0.0546

Table A-10 Data and % differences between analytical and numerical results for Figure 6.10.

(d-c)/A	k'(1a)	k'(1b)	k'(1a)FEA	%dif.	k'(1b)FEA	%dif.
0.025	1.3296	1.2811	1.3274	-0.1655	1.2797	-0.1093
0.05	1.3296	1.2811	1.3272	-0.1805	1.2797	-0.1093
0.1	1.3296	1.2811	1.3272	-0.1805	1.2797	-0.1093
0.15	1.3296	1.2811	1.3272	-0.1805	1.2797	-0.1093
0.2	1.3296	1.2811	1.328	-0.1203	1.2785	-0.2030
0.23	1.3296	1.2811	1.328	-0.1203	1.2785	-0.2030

Table A-11 Data and % differences between analytical and numerical results for Figure 6.11.

(d-c)/A	k'(1a)	k'(1b)	k'(1a)FEA	%dif.	k'(1b)FEA	%dif.
0.05	1.3524	1.2677	1.3605	0.5989	1.265	-0.2130
0.1	1.3524	1.2685	1.3619	0.7025	1.2649	-0.2838
0.2	1.3524	1.2714	1.3656	0.9760	1.2645	-0.5427
0.3	1.3522	1.2749	1.3694	1.2720	1.2642	-0.8393
0.4	1.3518	1.2778	1.3719	1.4869	1.2639	-1.0878
0.46	1.3516	1.2787	1.3726	1.5537	1.2638	-1.1652

Table A-12 Data and % differences between analytical and numerical results for Figure 6.12.

(d-c)/A	k'(1a)	k'(1b)	k'(1a)FEA	%dif.	k'(1b)FEA	%dif.
0.05	1.3518	1.2679	1.3653	0.9987	1.2599	-0.6310
0.1	1.3521	1.2691	1.3678	1.1612	1.2596	-0.7486
0.2	1.3529	1.2732	1.3743	1.5818	1.2591	-1.1074
0.3	1.3534	1.2783	1.3808	2.0245	1.2584	-1.5568
0.4	1.3531	1.2825	1.3852	2.3723	1.2579	-1.9181
0.46	1.3526	1.284	1.3863	2.4915	1.2577	-2.0483

Table A-13 Data and % differences between analytical and numerical results for Figure 6.13.

(d-c)/A	k'(1a)	k'(1b)	k'(1a)FEA	%dif.	k'(1b)FEA	%dif.
0.05	1.3513	1.2682	1.3715	1.4949	1.2508	-1.3720
0.1	1.3519	1.2698	1.3752	1.7235	1.2506	-1.5120
0.2	1.3537	1.2756	1.3849	2.3048	1.25	-2.0069
0.3	1.3546	1.2827	1.3942	2.9234	1.2494	-2.5961
0.4	1.3538	1.2886	1.4	3.4126	1.2488	-3.0886
0.46	1.3528	1.2908	1.4013	3.5852	1.2487	-3.2615

Table A-14 Data and % differences between analytical and numerical results for Figure 6.14.

(d-c)/A	k'(1a)	k'(1b)	k'(1a)FEA	%dif.	k'(1b)FEA	%dif.
0.05	1.3524	1.2674	1.3522	-0.0148	1.2679	0.0395
0.1	1.3524	1.2674	1.3523	-0.0074	1.2679	0.0395
0.2	1.3524	1.2674	1.3523	-0.0074	1.2679	0.0395
0.3	1.3524	1.2674	1.3523	-0.0074	1.268	0.0473
0.4	1.3524	1.2674	1.352	-0.0296	1.268	0.0473
0.46	1.3524	1.2674	1.352	-0.0296	1.268	0.0473

Table A-15 Data and % differences between analytical and numerical results for Figure 6.15.

(d-c)/A	k'(1a)	k'(1b)	k'(1a)FEA	%dif.	k'(1b)FEA	%dif.
0.05	1.3517	1.2675	1.3517	0.0000	1.2683	0.0631
0.1	1.3517	1.2675	1.3516	-0.0074	1.2683	0.0631
0.2	1.3517	1.2675	1.3517	0.0000	1.2683	0.0631
0.3	1.3517	1.2675	1.3516	-0.0074	1.2683	0.0631
0.4	1.3517	1.2675	1.3514	-0.0222	1.2687	0.0947
0.46	1.3517	1.2675	1.3517	0.0000	1.269	0.1183

Table A-16 Data and % differences between analytical and numerical results for Figure 6.16.

(d-c)/A	k'(1a)	k'(1b)	k'(1a)FEA	%dif.	k'(1b)FEA	%dif.
0.05	1.3511	1.2676	1.3512	0.0074	1.2693	0.1341
0.1	1.3511	1.2676	1.3514	0.0222	1.2693	0.1341
0.2	1.3511	1.2676	1.3514	0.0222	1.2694	0.1420
0.3	1.3511	1.2676	1.3513	0.0148	1.2694	0.1420
0.4	1.3511	1.2676	1.3506	-0.0370	1.2693	0.1341
0.46	1.3511	1.2676	1.3512	0.0074	1.2691	0.1183

Table A-17 Data and % differences between analytical and numerical results for Figure 6.17.

L/A	k'(1a)	k'(1b)	k'(1a)FEA	%dif.	k'(1b)FEA	%dif.
0.25	1.3322	1.2852	1.3193	-0.9683	1.2936	0.6536
0.5	1.3291	1.2815	1.3875	4.3940	1.2356	-3.5817
0.75	1.3293	1.2814	1.3908	4.6265	1.2328	-3.7927
1	1.3295	1.2812	1.3666	2.7905	1.2511	-2.3494
1.5	1.33	1.2809	1.3323	0.1729	1.277	-0.3045
2	1.33	1.2808	1.3263	-0.2782	1.2812	0.0312
4	1.33	1.2809	1.3264	-0.2707	1.2759	-0.3904

Table A-18 Data and % differences between analytical and numerical results for Figure 6.18.

L/A	k'(1a)	k'(1b)	k'(1a)FEA	%dif.	k'(1b)FEA	%dif.
0.25	1.3342	1.2909	1.3365	0.1724	1.2849	-0.4648
0.5	1.3277	1.2824	1.3889	4.6095	1.2344	-3.7430
0.75	1.3281	1.2823	1.3916	4.7813	1.2323	-3.8992
1	1.3288	1.2818	1.3673	2.8974	1.2505	-2.4419
1.5	1.3299	1.281	1.3324	0.1880	1.2769	-0.3201
2	1.3301	1.2808	1.3264	-0.2782	1.281	0.0156
4	1.33	1.2809	1.3264	-0.2707	1.2769	-0.3123

Table A-19 Data and % differences between analytical and numerical results for Figure 6.19.

L/A	k'(1a)	k'(1b)	k'(1a)FEA	%dif.	k'(1b)FEA	%dif.
0.25	1.3349	1.2955	1.348	0.9813	1.2784	-1.3200
0.5	1.3263	1.2834	1.3893	4.7501	1.2341	-3.8414
0.75	1.3268	1.2833	1.3919	4.9065	1.232	-3.9975
1	1.328	1.2824	1.3679	3.0045	1.2502	-2.5109
1.5	1.3298	1.281	1.3326	0.2106	1.2768	-0.3279
2	1.3301	1.2808	1.3265	-0.2707	1.2815	0.0547
4	1.33	1.2809	1.3264	-0.2707	1.2752	-0.4450

Table A-20 Data and % differences between analytical and numerical results for Figure 6.20.

L/A	k'(1a)	k'(1b)	k'(1a)FEA	%dif.	k'(1b)FEA	%dif.
0.25	1.3564	1.2825	1.3162	-2.9637	1.3027	1.5750
0.5	1.3528	1.2722	1.3784	1.8924	1.2642	-0.6288
0.75	1.3502	1.2684	1.4138	4.7104	1.2377	-2.4204
1	1.3505	1.2681	1.418	4.9981	1.2344	-2.6575
1.5	1.3511	1.2679	1.3896	2.8495	1.2509	-1.3408
2	1.3515	1.2676	1.3651	1.0063	1.2656	-0.1578
4	1.3517	1.2675	1.3549	0.2367	1.272	0.3550

Table A-21 Data and % differences between analytical and numerical results for Figure 6.21.

L/A	k'(1a)	k'(1b)	k'(1a)FEA	%dif.	k'(1b)FEA	%dif.
0.25	1.3569	1.2969	1.3224	-2.5426	1.2967	-0.0154
0.5	1.3534	1.2783	1.3863	2.4309	1.2635	-1.1578
0.75	1.3481	1.2696	1.4154	4.9922	1.2366	-2.5992
1	1.3487	1.2691	1.4194	5.2421	1.2334	-2.8130
1.5	1.3501	1.2684	1.3907	3.0072	1.2502	-1.4349
2	1.3512	1.2678	1.3655	1.0583	1.2653	-0.1972
4	1.3517	1.2675	1.3549	0.2367	1.2721	0.3629

Table A-22 Data and % differences between analytical and numerical results for Figure 6.22.

L/A	k'(1a)	k'(1b)	k'(1a)FEA	%dif.	k'(1b)FEA	%dif.
0.25	1.3582	1.301	1.3186	-2.9156	1.2816	-1.4912
0.5	1.3529	1.2831	1.3912	2.8310	1.2628	-1.5821
0.75	1.3459	1.2709	1.4157	5.1861	1.2366	-2.6989
1	1.3468	1.2701	1.4197	5.4128	1.2332	-2.9053
1.5	1.349	1.2691	1.3914	3.1431	1.2498	-1.5208
2	1.3509	1.268	1.3658	1.1030	1.2652	-0.2208
4	1.3517	1.2675	1.3549	0.2367	1.2721	0.3629

Table A-23 Data and % differences between analytical and numerical results for Figure 6.23.

L/A	k'(1a)	k'(1b)	k'(1a)FEA	%dif.	k'(1b)FEA	%dif.
0.25	1.3308	1.2823	1.3103	-1.5404	1.2984	1.2556
0.5	1.3297	1.2811	1.3875	4.3468	1.2368	-3.4580
0.75	1.3298	1.281	1.3914	4.6323	1.2338	-3.6846
1	1.3299	1.281	1.3674	2.8198	1.2516	-2.2951
1.5	1.33	1.2809	1.3337	0.2782	1.2774	-0.2732
2	1.33	1.2809	1.3278	-0.1654	1.2817	0.0625
4	1.33	1.2809	1.3293	-0.0526	1.2789	-0.1561

Table A-24 Data and % differences between analytical and numerical results for Figure 6.24.

L/A	k'(1a)	k'(1b)	k'(1a)FEA	%dif.	k'(1b)FEA	%dif.
0.25	1.3322	1.2916	1.3493	1.2836	1.2869	-0.3639
0.5	1.3284	1.282	1.3672	2.9208	1.248	-2.6521
0.75	1.3289	1.2818	1.3681	2.9498	1.246	-2.7929
1	1.3295	1.2814	1.3522	1.7074	1.2579	-1.8339
1.5	1.3303	1.2807	1.3296	-0.0526	1.2746	-0.4763
2	1.3305	1.2806	1.3259	-0.3457	1.2776	-0.2343
4	1.3304	1.2807	1.3273	-0.2330	1.2763	-0.3436

Table A-25 Data and % differences between analytical and numerical results for Figure 6.25.

L/A	k'(1a)	k'(1b)	k'(1a)FEA	%dif.	k'(1b)FEA	%dif.
0.25	1.3348	1.2963	1.3566	1.6332	1.2827	-1.0491
0.5	1.3259	1.2837	1.3899	4.8269	1.2332	-3.9339
0.75	1.3265	1.2835	1.3928	4.9981	1.2313	-4.0670
1	1.3277	1.2826	1.3687	3.0880	1.2494	-2.5885
1.5	1.3298	1.281	1.3293	-0.0376	1.279	-0.1561
2	1.3301	1.2808	1.3271	-0.2255	1.2809	0.0078
4	1.33	1.2809	1.3293	-0.0526	1.279	-0.1483

Table A-26 Data and % differences between analytical and numerical results for Figure 6.26.

L/A	k'(1a)	k'(1b)	k'(1a)FEA	%dif.	k'(1b)FEA	%dif.
0.25	1.3374	1.302	1.3641	1.9964	1.2765	-1.9585
0.5	1.3223	1.2862	1.4144	6.9651	1.2177	-5.3258
0.75	1.3229	1.2862	1.4194	7.2946	1.2135	-5.6523
1	1.3252	1.2844	1.3875	4.7012	1.2376	-3.6437
1.5	1.3291	1.2815	1.3374	0.6245	1.276	-0.4292
2	1.3298	1.2809	1.3265	-0.2482	1.2828	0.1483
4	1.3296	1.2811	1.33	0.0301	1.2809	-0.0156

Table A-27 Data and % differences between analytical and numerical results for Figure 6.27.

L/A	k'(1a)	k'(1b)	k'(1a)FEA	%dif.	k'(1b)FEA	%dif.
0.25	1.1568	1.1226	1.1408	-1.3831	1.1229	0.0267
0.5	1.118	1.0812	1.1377	1.7621	1.0738	-0.6844
0.75	1.1062	1.0696	1.1507	4.0228	1.0549	-1.3743
1	1.106	1.0692	1.1529	4.2405	1.0532	-1.4964
1.5	1.1069	1.069	1.1348	2.5206	1.06	-0.8419
2	1.1076	1.0686	1.1188	1.0112	1.0679	-0.0655
4	1.1079	1.0685	1.112	0.3701	1.0714	0.2714

Table A-28 Data and % differences between analytical and numerical results for Figure 6.28.

L/A	k'(1a)	k'(1b)	k'(1a)FEA	%dif.	k'(1b)FEA	%dif.
0.25	1.3569	1.2969	1.3273	-2.1814	1.2982	0.1002
0.5	1.3534	1.2783	1.3921	2.8595	1.2657	-0.9857
0.75	1.3481	1.2696	1.4215	5.4447	1.2388	-2.4260
1	1.3487	1.2691	1.4254	5.6870	1.2356	-2.6397
1.5	1.3501	1.2684	1.3967	3.4516	1.2519	-1.3009
2	1.3512	1.2678	1.3715	1.5024	1.2655	-0.1814
4	1.3517	1.2675	1.3605	0.6510	1.2744	0.5444

Table A-29 Data and % differences between analytical and numerical results for Figure 6.29.

L/A	k'(1a)	k'(1b)	k'(1a)FEA	%dif.	k'(1b)FEA	%dif.
0.25	2.105	1.9803	2.0749	-1.4299	1.993	0.6413
0.5	2.1343	1.9655	2.1924	2.7222	1.9263	-1.9944
0.75	2.1405	1.9562	2.2479	5.0175	1.8865	-3.5630
1	2.1433	1.9545	2.2539	5.1603	1.8823	-3.6940
1.5	2.1456	1.9532	2.207	2.8617	1.9119	-2.1145
2	2.1474	1.952	2.1669	0.9081	1.9378	-0.7275
4	2.1482	1.9515	2.1509	0.1257	1.9485	-0.1537

Table A-30 Data and % differences between analytical and numerical results for Figure 6.30.

L/A	k'(1a)	k'(1b)	k'(1a)FEA	%dif.	k'(1b)FEA	%dif.
0.25	1.2464	1.14	1.131	-9.2587	1.2657	11.0263
0.5	1.3047	1.1449	1.3454	3.1195	1.1191	-2.2535
0.75	1.3104	1.1472	1.3533	3.2738	1.1229	-2.1182
1	1.3124	1.148	1.3388	2.0116	1.1332	-1.2892
1.5	1.3169	1.1497	1.3193	0.1822	1.1517	0.1740
2	1.3177	1.15	1.3162	-0.1138	1.1556	0.4870
4	1.3174	1.1499	1.3192	0.1366	1.1574	0.6522

Table A-31 Data and % differences between analytical and numerical results for Figure 6.31.

L/A	k'(1a)	k'(1b)	k'(1a)FEA	%dif.	k'(1b)FEA	%dif.
0.25	1.1367	1.1144	1.1432	0.5718	1.1031	-1.0140
0.5	1.1206	1.0987	1.1545	3.0252	1.0616	-3.3767
0.75	1.1209	1.0988	1.1563	3.1582	1.06	-3.5311
1	1.1217	1.0983	1.1406	1.6849	1.0709	-2.4948
1.5	1.1229	1.0975	1.1261	0.2850	1.0958	-0.1549
2	1.1231	1.0973	1.1222	-0.0801	1.0989	0.1458
4	1.1231	1.0974	1.1241	0.0890	1.0985	0.1002

Table A-32 Data and % differences between analytical and numerical results for Figure 6.32.

L/A	k'(1a)	k'(1b)	k'(1a)FEA	%dif.	k'(1b)FEA	%dif.
0.25	1.1805	1.2423	1.1826	0.1779	1.222	-1.6341
0.5	1.182	1.2964	1.2004	1.5567	1.2256	-5.4613
0.75	1.1839	1.3009	1.2	1.3599	1.2268	-5.6961
1	1.1829	1.2979	1.2176	2.9335	1.2787	-1.4793
1.5	1.1818	1.2949	1.1958	1.1846	1.3009	0.4634
2	1.1817	1.2944	1.1814	-0.0254	1.2926	-0.1391
4	1.1817	1.2947	1.1802	-0.1269	1.2854	-0.7183

Table A-33 Data and % differences between analytical and numerical results for Figure 6.33.

L/A	k'(1a)	k'(1b)	k'(1a)FEA	%dif.	k'(1b)FEA	%dif.
0.25	2.1	1.9786	2.098	-0.0952	1.9924	0.6975
0.5	2.0984	1.9779	2.2059	5.1230	1.908	-3.5341
0.75	2.0971	1.9789	2.2069	5.2358	1.9057	-3.6990
1	2.0967	1.9792	2.1682	3.4101	1.9374	-2.1120
1.5	2.0972	1.9788	2.1015	0.2050	1.9658	-0.6570
2	2.0975	1.9786	2.092	-0.2622	1.9736	-0.2527
4	2.0975	1.9786	2.0955	-0.0954	1.9703	-0.4195

Table A-34 Data and % differences between analytical and numerical results for Figure 6.34.

L/A	k'(1a)	k'(1b)	k'(1a)FEA	%dif.	k'(1b)FEA	%dif.
0.25	2.093	1.985	2.092	-0.0478	1.9983	0.6700
0.5	2.095	1.98	2.2088	5.4320	1.9056	-3.7576
0.75	2.096	1.98	2.2121	5.5391	1.9025	-3.9141
1	2.097	1.979	2.1719	3.5718	1.9344	-2.2537
1.5	2.0974	1.9787	2.1027	0.2527	1.9656	-0.6621
2	2.098	1.979	2.0926	-0.2574	1.9732	-0.2931
3	2.0977	1.9788	2.0959	-0.0858	1.9705	-0.4194
4	2.0975	1.9786	2.0965	-0.0477	1.9703	-0.4195

Table A-35 Data and % differences between analytical and numerical results for Figure 6.35.

L/A	k'(1a)	k'(1b)	k'(1a)FEA	%dif.	k'(1b)FEA	%dif.
0.25	2.086	1.9895	2.0782	-0.3739	2.0101	1.0354
0.5	2.0926	1.9824	2.2075	5.4908	1.9066	-3.8236
0.75	2.095	1.9806	2.2162	5.7852	1.8998	-4.0796
1	2.0965	1.9794	2.1752	3.7539	1.9318	-2.4048
1.5	2.0976	1.9785	2.1031	0.2622	1.9648	-0.6924
2	2.0976	1.9785	2.0916	-0.2860	1.9732	-0.2679
4	2.0975	1.9786	2.0959	-0.0763	1.9703	-0.4195

Table A-36 Data and % differences between analytical and numerical results for Figure 6.36.

| L/A	k'(1a)	k'(1b)	k'(1a)FEA	%dif.	k'(1b)FEA	%dif.
0.25	1.1013	1.1239	1.0983	-0.2724	1.0729	-4.5378
0.5	1.2438	1.1214	1.2753	2.5326	1.1018	-1.7478
0.75	1.2833	1.1203	1.3577	5.7976	1.1245	0.3749
1	1.2927	1.1233	1.3697	5.9565	1.1294	0.5430
1.5	1.2974	1.1253	1.3373	3.0754	1.1274	0.1866
2	1.3013	1.1269	1.3082	0.5302	1.126	-0.0799
4	1.3032	1.1276	1.3069	0.2839	1.1352	0.6740

Table A-37 Data and % differences between analytical and numerical results for Figure 6.37.

L/A	k'(1a)	k'(1b)	k'(1a)FEA	%dif.	k'(1b)FEA	%dif.
0.25	1.1807	1.1469	1.1681	-1.0672	1.1459	-0.0872
0.5	1.1461	1.1066	1.1658	1.7189	1.0916	-1.3555
0.75	1.1313	1.0914	1.1764	3.9866	1.0706	-1.9058
1	1.1311	1.0907	1.1787	4.2083	1.0679	-2.0904
1.5	1.1327	1.0903	1.1594	2.3572	1.0771	-1.2107
2	1.1339	1.0896	1.1419	0.7055	1.0858	-0.3488
4	1.1345	1.0894	1.1347	0.0176	1.09	0.0551

**Table A-38** Data and % differences between analytical and numerical results for Figure 6.38.

| L/A	k'(1a)	k'(1b)	k'(1a)FEA	%dif.	k'(1b)FEA	%dif.
0.25	1.2142	1.1352	1.2038	-0.8565	1.1784	3.8055
0.5	1.1959	1.2394	1.2008	0.4097	1.2031	-2.9288
0.75	1.1895	1.2701	1.1946	0.4288	1.1926	-6.1019
1	1.1912	1.2768	1.1932	0.1679	1.1933	-6.5398
1.5	1.1905	1.2736	1.1954	0.4116	1.2323	-3.2428
2	1.1895	1.2706	1.1909	0.1177	1.2565	-1.1097
4	1.1892	1.2696	1.1971	0.6643	1.2747	0.4017

APPENDIX-B

## STRESS DISTRIBUTIONS FOR A SAMPLE CASE
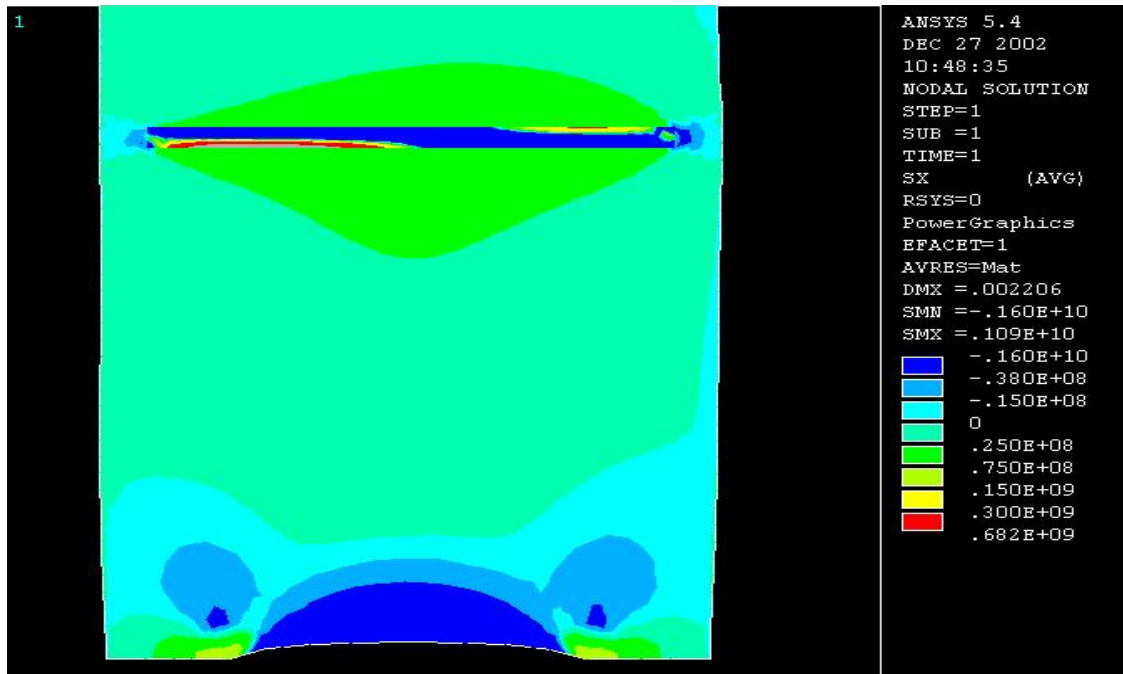
Figure B1. σ_x distribution when B = 1.25A, L = 0.25A, b – a = 0.15A, d – c = 0.21A, a + b = c + d = 2.25A, ν = 0.3.
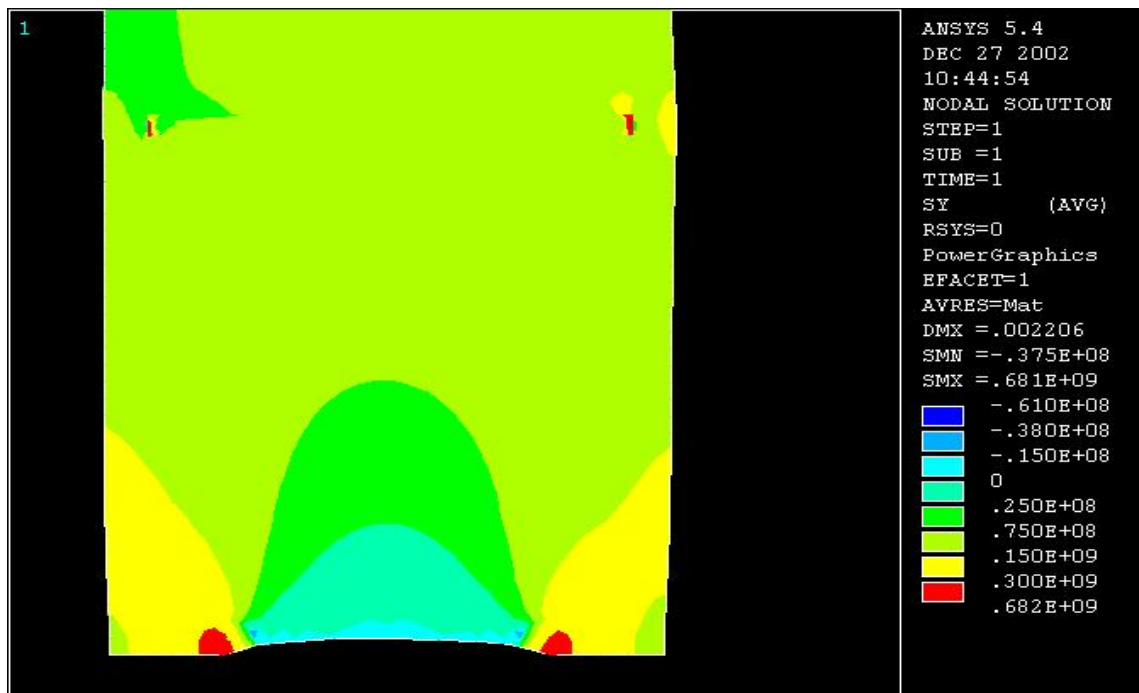
Figure B2. σ_Y distribution when B = 1.25A, L = 0.25A, b – a = 0.15A, d – c = 0.21A, a + b = c + d = 2.25A, ν = 0.3.
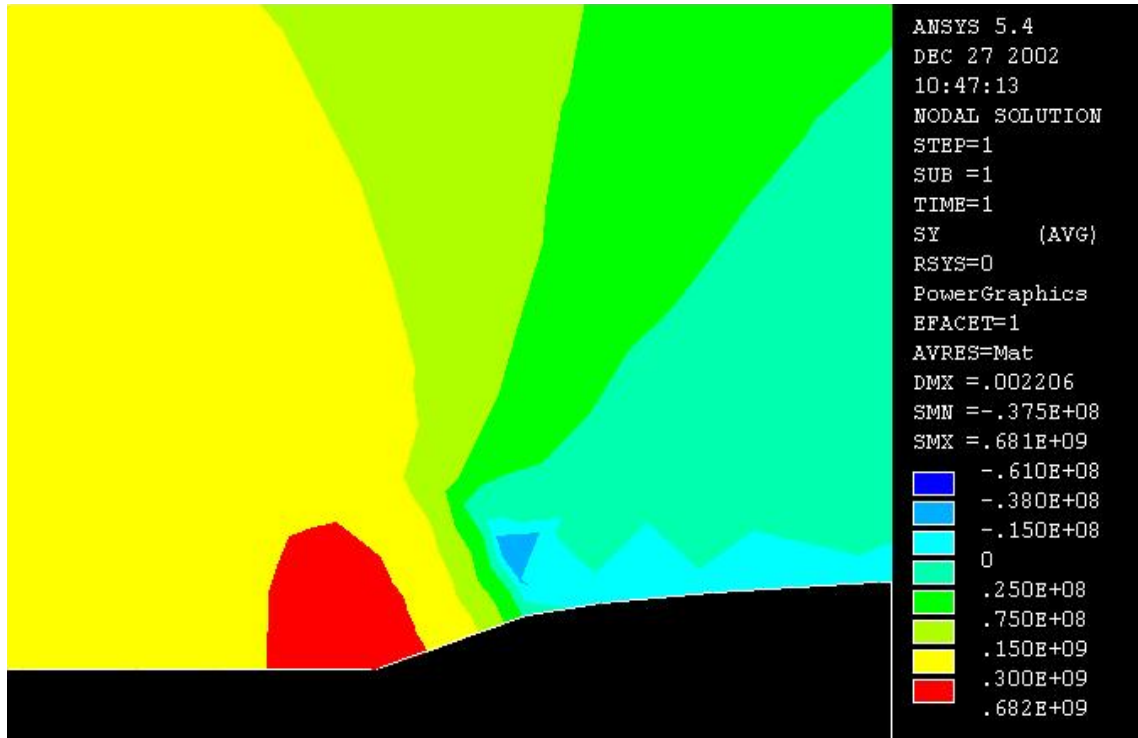
Figure B3. A zoomed view of σ_Y distribution at the left crack tip when B = 1.25A, L = 0.25A, b – a = 0.15A, d – c = 0.21A, a + b = c + d = 2.5A, ν = 0.3.
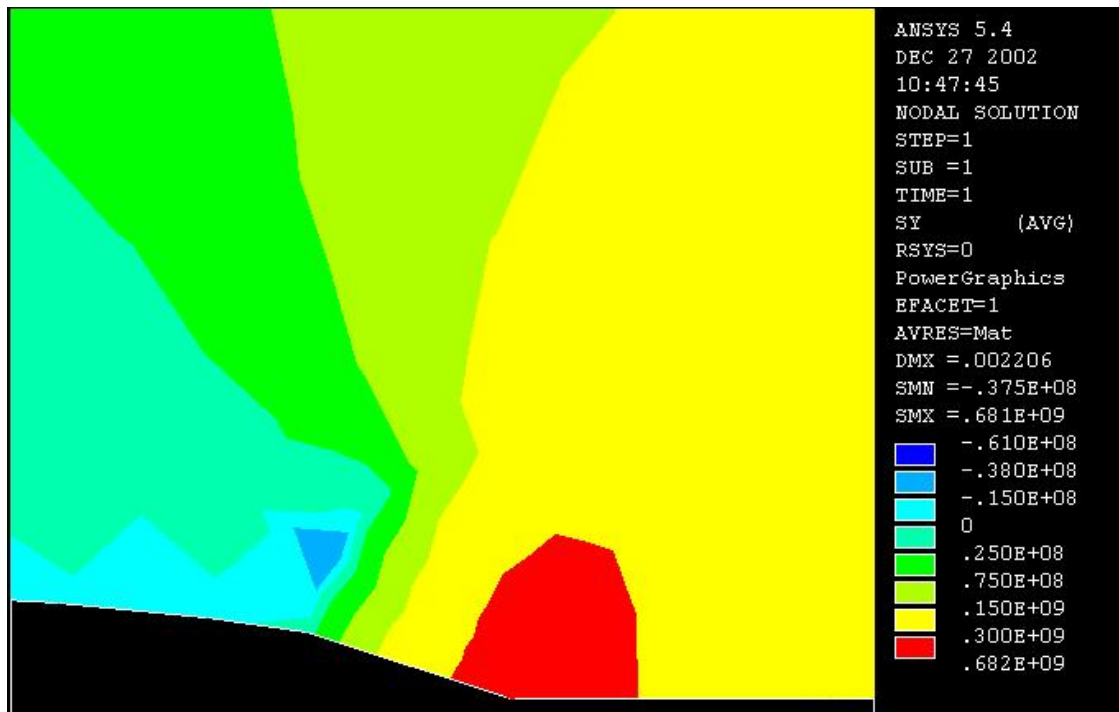
Figure B4. A zoomed view of σ_Y distribution at the right crack tip when B = 1.25A, L = 0.25A, b – a = 0.15A, d – c = 0.21A, a + b = c + d = 2.25A, ν = 0.3.

APPENDIX-C

A SAMPLE LOG FILE IN APDL LANGUAGE

```
/UNITS,SI
/PREP7
ET,1,PLANE2
KEYOPT,1,3,1
MP,EX,1,200E9
MP,NUXY,1,0.3
MP,EX,2,2E18
MP,NUXY,2,1E-9
ba=0.6275/0.5
ka=1.1*ba
kb=1.4*ba
bb=1.5*ba
cn=(ka+kb)/2
cc=1.1*ba
dd=1.4*ba
kh=0.495*ba
bh=0.505*ba
K,1,ba,0,0
K,2,ka,0,0
K,3,cn,0,0
K,4,cn,kh,0
K,5,cc,kh,0
K,6,cc,bh,0
K,7,cn,bh,0
K,8,cn,2,0
K,9,ba,2,0
K,10,kb,0,0
K,11,bb,0,0
```

K,12,bb,2,0

K,13,dd,bh,0

K,14,dd,kh,0

K,15,ba,2.25,0

K,16,bb,2.25,0

A,1,2,3,4,5,6,7,8,9,1

A,3,10,11,12,8,7,13,14,4,3

A,5,6,7,13,14,4,5

A,9,8,12,16,15,9

AGLUE,ALL

KSCON,2,(kb-ka)/10,0,16,0.5

KSCON,10,(kb-ka)/10,0,16,0.5

FINISH